

DOKUZ EYLÜL UNIVERSITY
GRADUATE SCHOOL OF NATURAL AND APPLIED
SCIENCES

THE CRYSTAL STRUCTURE ANALYSIS OF A
DINUCLEAR Rh(I) N-HETEROCYCLIC
CARBENE COMPLEX

by

Şeyma ORTATATLI

September, 2013

İZMİR

**THE CRYSTAL STRUCTURE ANALYSIS OF A
DINUCLEAR Rh(I) N-HETEROCYCLIC
CARBENE COMPLEX**

**A Thesis Submitted to the
Graduate School of Natural and Applied Sciences of Dokuz Eylül University
In Partial Fulfillment of the Requirements for the Degree of Master of
Science in Physics**

by

Şeyma ORTATATLI

September, 2013

İZMİR

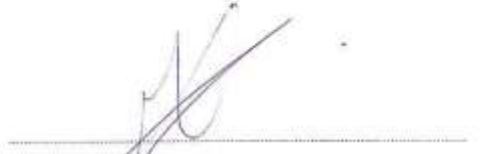
M.Sc THESIS EXAMINATION RESULT FORM

We have read the thesis entitled “**THE CRYSTAL STRUCTURE ANALYSIS OF A DINUCLEAR Rh(I) N-HETEROCYCLIC CARBENE COMPLEX**” completed by **ŞEYMA ORTATATLI** under supervision of **Assist. Prof. AYTAÇ GÜRHAN GÖKÇE** and we certify that in our opinion it is fully adequate, in scope and in quality, as a thesis for the degree of Master of Science.



Assist. Prof. Aytaç Gürhan GÖKÇE

Supervisor



Assoc. Prof. Dr. İlhan KARAKILIÇ
(Jury member)



Assoc. Prof. Dr. Hasan KARABIYIK
(Jury member)



Prof. Dr. Ayşe OKUR

Director

Graduate School of Natural and Applied Sciences

ACKNOWLEDGEMENTS

I would like to express my gratitude to my supervisor Assist. Prof. Aytaç Gürhan GÖKÇE for his valuable suggestions and guidance throughout the preparation of this thesis.

My grateful thanks to Assoc. Prof. Hasan KARABIYIK for his help and patience and I also would like to thank to Duygu BARUT and Gül ÖZKAN YAKALI for their precious suggestions.

Finally, I would like to express my deepest gratitude to my family, especially to my mother, for their continual support made me keep going.

Şeyma ORTATATLI

THE CRYSTAL STRUCTURE ANALYSIS OF A DINUCLEAR Rh(I) N-HETEROCYCLIC CARBENE COMPLEX

ABSTRACT

N-heterocyclic carbene (NHC) complexes, bound to a transition metal atom, bearing benzimidazole, imidazole and imidazoline rings that possess various biological activities have remarkable importance in organometallic chemistry and homogeneous catalysis. After the first reports about the stability of the transition metal complexes of NHCs by H. -W. Wanzlick and K. Öfele independently from each other, the studies focused on these important type of carbene complexes.

In the scope of this study, the molecular and crystal structure of Rh(I) N-heterocyclic carbene complex bearing 2,6-bis(1-pentamethylbenzyl-1-H-benzimidazole-2-yl) pyridine have been determined by using single crystal X-ray diffraction technique. The title compound crystallizes in the monoclinic cell setting with space group *C12/c1*. The coordination geometry around the Rh atom is slightly distorted square-planar. The terdentate units act as bis-monodentate ligands resulting from the connection between the benzimidazole and [Rh(COD)Cl] units through the nitrogen atoms. There exist inter- and intra-molecular interactions of different types in the title compound. The effects of these interactions on the geometry of the complex and their consequences are investigated and discussed in detail.

Keywords: N-heterocyclic carbene complexes, benzimidazole, crystal structure.

İKİ ÇEKİRDEKLİ Rh(I) N-HETEROSİKLİK KARBEN KOMPLEKSİNİN KRİSTAL YAPI ANALİZİ

ÖZ

Pek çok biyolojik aktiviteye sahip benzimidazol, imidazol ve imidazolin halkaları içeren, bir geçiş metaline bağlı bulunan N-heterosiklik karben (NHK) kompleksleri, organometalik kimya ve homojen katalizde büyük bir öneme sahiptir. NHK'ler'in geçiş metali komplekslerinin kararlılığı ile ilgili H. -W. Wanzlick ve K. Öfele tarafından birbirlerinden bağımsız olarak yayınlanan ilk bildirilerin ardından, çalışmalar karben komplekslerinin bu önemli türü üzerinde yoğunlaşmaya başlamıştır.

Bu çalışma kapsamında, 2,6-bis(1-pentametilbenzil-1-H-benzimidazol-2-yl) piridin taşıyan Rh(I) N-heterosiklik karben kompleksinin moleküler ve kristal yapısı, tek kristal X-ışını kırınımı yöntemi kullanılarak belirlenmiştir. Söz konusu bileşik monoklinik hücre yapısında C12/c1 uzay grubuna sahip olarak kristallenmiştir. Bileşikte Rh atomu etrafındaki koordinasyon geometrisi hafifçe bozulmuş kare düzlemseldir. Terdentat birimleri, benzimidazol ve [Rh(COD)Cl] birimleri arasındaki bağdan dolayı bis-monodentat ligandları gibi davranırlar. Söz konusu bileşikte farklı türlerde molekül içi ve moleküller arası etkileşimler bulunmaktadır. Bu etkileşimlerin kompleksin tamamı üzerindeki etkileri ve bu etkilerin sonuçları detaylı bir şekilde incelenmiş ve tartışılmıştır.

Anahtar kelimeler: N-heterosiklik karben kompleksleri, benzimidazol, kristal yapı.

CONTENTS

	Page
THESIS EXAMINATION RESULT FORM	ii
ACKNOWLEDGEMENTS	iii
ABSTRACT.....	iv
ÖZ	v
LIST OF FIGURES	ix
LIST OF TABLES	xi
CHAPTER ONE – INTRODUCTION	1
1.1 Introduction	1
CHAPTER TWO – X-RAY CRYSTALLOGRAPHY	3
2.1 X-Ray Diffraction.....	3
2.2 Diffraction Geometry	7
2.3 Single Crystal X-Ray Diffraction.....	12
2.3.1 Introduction: Diffraction Methods	12
2.3.2 Crystal Selection for Single Crystal XRD.....	14
2.3.3 Technical Equipment for Single Crystal XRD.....	16
2.3.4 Measurement of Intensity: Scanning Angles of Diffractometer	20
CHAPTER THREE – CRYSTAL STRUCTURE ANALYSIS	21
3.1 Introduction	21
3.2 Structure Factor	21
3.3 Data Reduction Process: Corrections to Intensity.....	26
3.3.1 Scale Factor	26
3.3.2 Lorentz Factor	27

3.3.3 Temperature Factor	27
3.3.4 Polarisation Factor	29
3.3.5 Absorption Factor	32
3.3.6 Extinction Factor	32
3.4 Phase Problem	34
3.4.1 Patterson Method	36
3.4.2 Direct Methods	36
3.4.2.1 Normalized Structure Factors	38
3.4.2.2 Fundamental Inequalities	43
3.4.2.3 Structure Invariants and Semi-invariants	45
3.4.2.4 Three-Phase Invariant	47
3.4.2.5 The Sayre Equation and Tangent Formula	48
3.4.2.6 Figures of Merit	51
3.4.2.7 Combined Figures of Merit (CFOM)	53
3.5 Electron Density Map (E-map)	53
CHAPTER FOUR – CRYSTAL STRUCTURE REFINEMENT	55
4.1 Introduction	55
4.2 Difference Fourier Method	56
4.3 The Method of Least-Squares	58
4.3.1 Refinement Against F^2	60
4.4 Constraints and Restraints	61
4.4.1 Constraints	61
4.4.2 Restraints	62
4.5 The Quality of a Refinement: Residual Parameters	63
4.6 Problems in Refinement	64
4.6.1 Disorder	65
4.6.2 Twinning	66
CHAPTER FIVE – RESULTS & DISCUSSION	68

REFERENCES	79
-------------------------	-----------

APPENDICES	87
-------------------------	-----------

1. The Fractional Coordinates & Equivalent Isotropic Temperature Parameters .	87
2. The Anisotropic Displacement Parameters	88
3. Bond Distances	90
4. Bond Angles	90
5. Torsion Angles	92

LIST OF FIGURES

	Page
Figure 1.1 Chemical diagram of the title compound	1
Figure 2.1 First diffraction pattern	4
Figure 2.2 The historical experimental setup	4
Figure 2.3 First specialist diffraction patterns	5
Figure 2.4 The Laue method	5
Figure 2.5 The Bragg reflection	6
Figure 2.6 A basic schema of single crystal X-ray diffraction	8
Figure 2.7 Diffraction patterns depend on unit cell dimensions	9
Figure 2.8 Diffraction pattern depend on crystal lattice	9
Figure 2.9 The Ewald sphere	10
Figure 2.10 The limiting sphere	12
Figure 2.11 Atomic arrangements in solids	14
Figure 2.12 Reciprocal lattice plots of twin crystals	15
Figure 2.13 Devices of a single crystal diffractometer	17
Figure 2.14 Crystal mounting techniques	18
Figure 2.15 Four circle diffractometer	19
Figure 3.1 Geometrical presentation of structure factor	22
Figure 3.2 Argand diagram	24
Figure 3.3 The polarization of X-rays	30
Figure 3.4 Diffraction without a monochromator	30
Figure 3.5 Diffraction with a monochromator	31
Figure 3.6 Primary extinction	33
Figure 3.7 Secondary extinction	34
Figure 3.8 The probabilistic density function	43
Figure 3.9 The similarity between $d(x)$ and $d^2(x)$	49
Figure 3.10 E-map presentation	54
Figure 4.1 Diffraction peaks of real and model crystal structures	58
Figure 4.2 The method of least-squares	59
Figure 4.3 Disorder in a crystal structure	66

Figure 4.4 Twin crystal and twinning plane.....	67
Figure 5.1 ORTEP-3 view of the title compound	71
Figure 5.2 The complete view of the title compound	72
Figure 5.3 Intra-molecular interactions within the structure.....	75
Figure 5.4 Inter-molecular interactions of type C–H··· π	76
Figure 5.5 Inter-molecular interactions of type C–H··· π	77
Figure 5.6 Inter-molecular interactions of type C–H···Cl.....	78

LIST OF TABLES

	Page
Table 3.1 Various $ E $ values depend on crystal structures	43
Table 3.2 Some structure invariants	47
Table 5.1 Crystallographic data, details of data collection and refinement	70
Table 5.2 Selected bond distances and angles	73
Table 5.3 The intra- and inter-molecular interactions within the structure.....	74

CHAPTER ONE

INTRODUCTION

1.1 Introduction

Before the discovery of X rays by Wilhelm Conrad Röntgen (1845-1923) in 1895, the structure determination studies of crystal samples were limited with the prediction of atomic arrangements by looking the appearance of crystals. But shortly after the discovery of X-rays, Max von Laue (1879-1960) and his colleagues W. Friedrich and P. Knipping observed a pioneering diffraction between X-rays and the electrons of crystal atoms. Thus, an exciting and a fascinating journey into the crystals' unknown world, *crystallography* by name, started.

X-ray crystallography or in other words, single crystal X-ray diffraction is an analytical and nondestructive technique for single crystal determination processes.

In the scope of this thesis, the crystal structure of Rh(I) N-heterocyclic carbene complex bearing 2,6-bis(1-pentamethylbenzyl-1-H-benzimidazole-2-yl)pyridine abbreviated as $[\{\text{Rh}(\text{COD})\text{Cl}\}_2\text{L}]$ where L is 2,6-bis(1-pentamethylbenzyl-1-H-benzimidazole-2-yl) pyridine, has been determined by using single crystal X-ray diffraction technique. One of the chemical diagrams of the title compound is given in Figure 1.1.

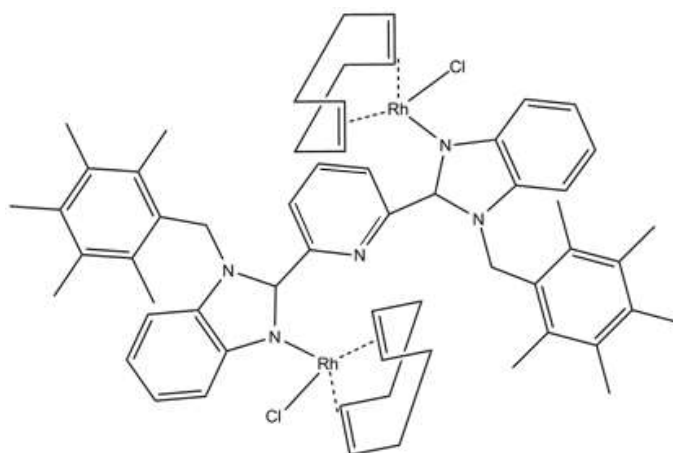


Figure 1.1 A chemical diagram of the title compound.

NHC ligands were first reported by Wanzlick & Schönher (1968) and Öfele (1968) independently from each other. The complexes that are formed by N-heterocyclic carbene ligands abbreviated as NHCs, binding to a transition metal atom and bearing a benzimidazole framework take an important place in homogeneous catalysis and organometallic chemistry.

Strong σ -bonding between the NHC and the metal atom is observed in the metal complexes including NHCs as ligands. Because while binding to a metal complex, NHCs act as strong σ -donors or on the contrary, they act as weak π -acceptors. NHCs have manifold catalytic applications as activators in carbon-carbon coupling reactions, formation of furans, cyclopropanation, olefin metathesis, etc.

Benzimidazole is a bicyclic compound containing one imidazole ring bearing two lone electron pairs on each nitrogen atom and one benzene ring that is bridged to that imidazole ring. Benzimidazoles are used in manifold medicinal applications due to their various biological activities such as anti-inflammatory (Leonard et al., 2007), anti-oxidant (Kuş, Ayhan-Kılıçgil, Can-Eke & İşcan, 2004, Ateş-Alagöz, Kuş & Çoban, 2005), anti-viral (Devivar et al., 1994), anti-tumor (Gellis, Kovacic, Boufatah & Vanelle, 2008), anti-ulcer (Bariwal et al., 2008), anti-microbial activity (Leonard et al., 2007, M. B. Deshmukh, Suryavanshi, S. A. Deshmukh, Jagtap, 2009, Ansari & Lal, 2009).

In this study, the crystallographic data of the title compound was collected by Agilent XCalibur X-ray Diffractometer with EOS CCD detector at X-Ray Crystallography Laboratory in the Department of Physics, Faculty of Science, Dokuz Eylül University. The structure of the title compound was solved by using SHELXS-97 (Sheldrick, 1998) software with direct methods and refined by SHELXL-97 (Sheldrick, 1998) software. All geometrical calculations and molecular graphics were created by WINGX (Farrugia, 1999), ORTEP-3 (Farrugia, 1997) and PLATON (Spek, 1990) programs.

CHAPTER TWO

X-RAY CRYSTALLOGRAPHY

2.1 X-Ray Diffraction

A pioneering discovery by W. C. Röntgen in 1895 showed that when the electrons emitted from a heated filament (cathode) in a vacuum tube were accelerated by a large external potential which was approximately $10^8 - 10^9$ eV, towards a metallic target (anode) inside of the tube, there appeared an interaction between the accelerated electrons and the target. As a result, a new radiation type called X-rays was emerged from the tube. The wavelengths of X-rays have different values in the interval varying from 0.1 Å to 100 Å.

In 1912, Max von Laue put forward that crystal planes could be used as diffraction gratings by taking advantage of the fact that the magnitude of the interplanar distances in a crystal is in the order of angstroms (Å) as the order of the wavelength of X-ray beams. This hypothesis was demonstrated by an experiment which was carried out by the students of W. C. Röntgen, W. Friedrich and P. Knipping under the guidance of von Laue in 1912. At the first attempt, they put the photographic film between the radiation source and crystal sample assuming the crystal would act like a mirror and reflect the incident beam (Ewald, 1962). However, there was nothing that could be observed on the film. Upon this failure, they decided to rerun the experiment by placing the film behind the crystal and here the legendary success came. According to the results of this precious study, when X-rays were diffracted from crystal atoms, each diffracted beam left a black spot on the photographic film behind the crystal sample and thus, a characteristic diffraction pattern was obtained.

The first diffraction pattern obtained and the experimental setup used by these two young scientists are given in Fig. (2.1) and (2.2), respectively. The diffraction patterns of zincblende were also obtained by Friedrich and Knipping that are given in Fig. (2.3).

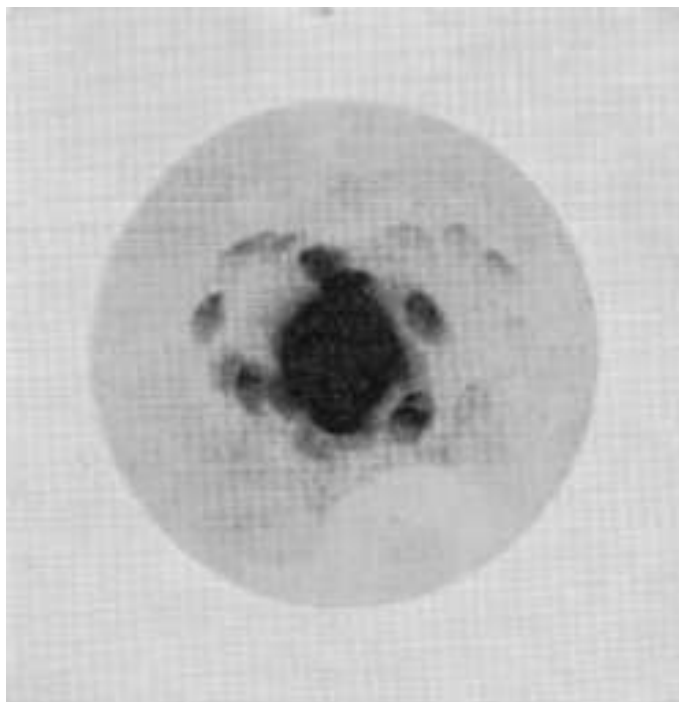


Figure 2.1 First diffraction pattern obtained by Friedrich and Knipping. (Ewald, 1962, chap. 4)

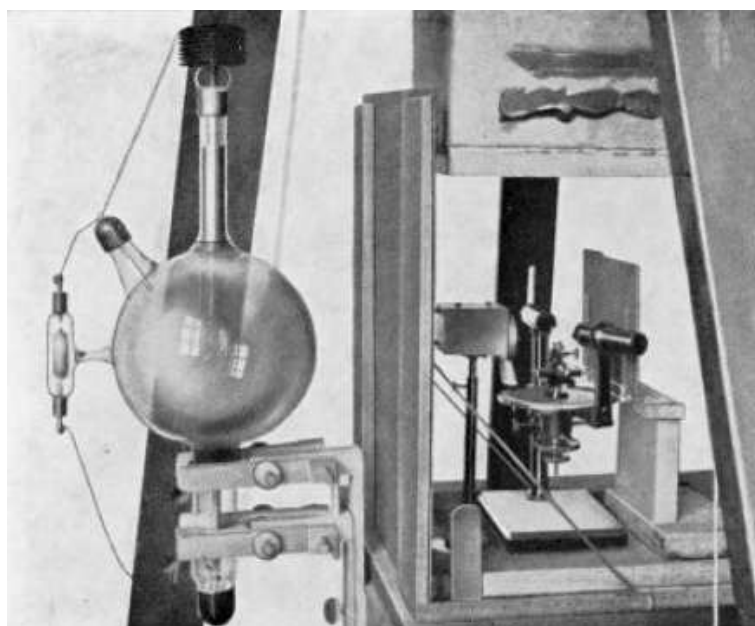


Figure 2.2 The experimental setup used by the young scientists. (Ewald, 1962, chap. 4)

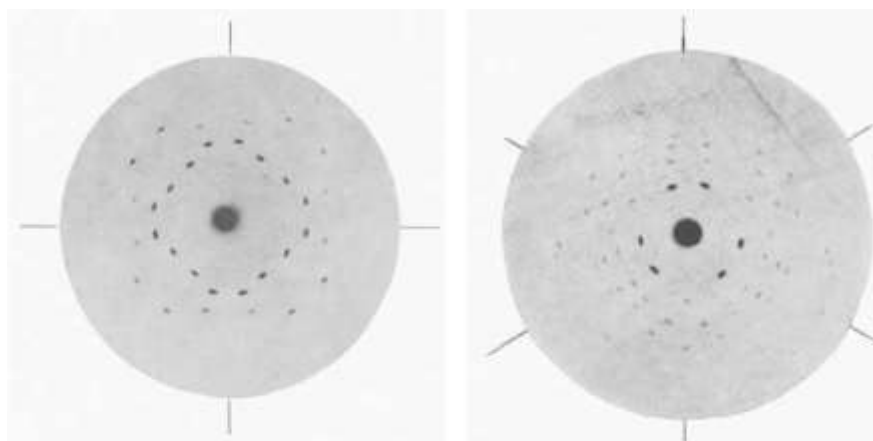


Figure 2.3 The diffraction patterns of Zincblende along four-fold (a) and three-fold (b) axes. (Ewald, 1962, chap. 4)

The method that was created by von Laue and his group is referred to as *Laue Method* in general which is illustrated simply in Fig. (2.4).

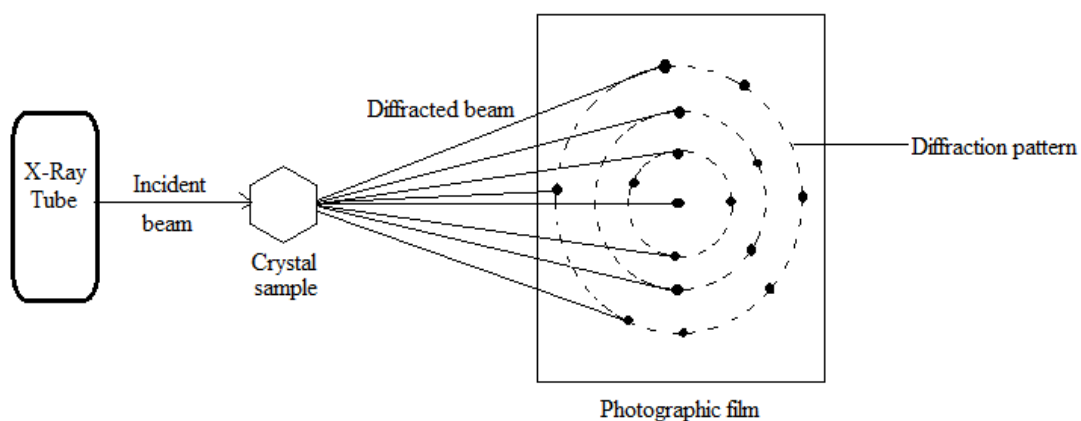


Figure 2.4 A basic schema for Laue Method.

Once the diffraction pattern is obtained, one can reach the information about the unknown structure of a crystal sample such as inter-atomic distances, bond angles, bond lengths.

The Laue Method was inspirational for many scientists. The first crystal structure determined using X-ray diffraction was sodium chloride (NaCl) which was performed by W. H. Bragg (1862-1942) and his son W. L. Bragg (1890-1971) in

1913. The father-son Braggs showed that X-rays diffracted from crystal lattice planes would be in phase and diffraction could be observed if and only if the following conditions were satisfied (Bragg & Bragg, 1913):

- *The angles of the incident and diffracted (or scattered) beams must be equal to each other in magnitude.*
- *The path difference ($2d\sin\theta$) between the incident and diffracted beams must be an integral multiple of the wavelength.*

The conditions given above are referred to as *Bragg Conditions* and they were successfully expressed in Eq. (2.1) which is known as the *Bragg Equation*.

$$n\lambda = 2d \sin \theta \quad (2.1)$$

In this equation n is an integer, λ is the wavelength of radiation, d is the inter-atomic distance in the lattice and θ is the angle of incidence. A diffraction satisfying the Bragg Conditions is called the *Bragg reflection* and a representing picture is given in Fig. (2.5).

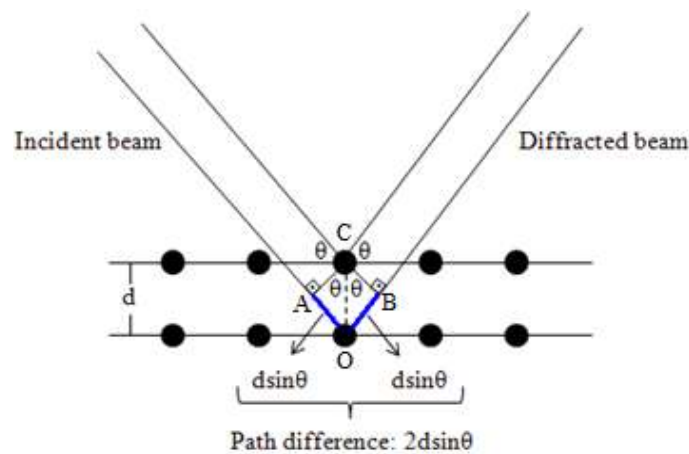


Figure 2.5 The Bragg reflection.

One can derive Eq. (2.1) simply using the geometry and trigonometry. According to the second Bragg Condition given above, to observe diffraction, the total path

difference ($|AO + OB|$) in Fig. (2.5), must be equal to an integral multiple of the wavelength. Then, one can write the following equation:

$$n\lambda = |AO + OB| \quad (2.2)$$

When the basic trigonometry rule for sinus is applied in the triangles CAO and CBO to define the lengths of AO and OB line segments ($|AO|$ and $|OB|$) in terms of θ ,

$$\sin\theta = \frac{|AO|}{|OC|} = \frac{|OB|}{|OC|} \quad (2.3)$$

is obtained. It is obvious in Fig. (2.5) that the inter-planar distance d is equal to $|OC|$, hence

$$|AO| = |OB| = d\sin\theta \quad (2.4)$$

is obtained and when the relations given in Eq. (2.4) are substituted in Eq. (2.2), the gorgeous Bragg formula occurs:

$$\boxed{n\lambda = 2d\sin\theta}$$

2.2 Diffraction Geometry

A basic schema for a single crystal X-ray diffraction experiment is illustrated in Fig. (2.6) that is very similar to that explained in Section 2.1.

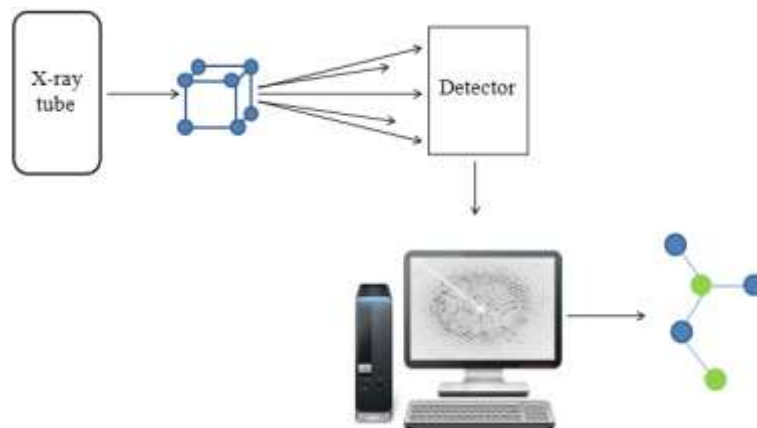


Figure 2.6 A simple schema showing a single crystal X-ray diffraction experiment: X-rays generated by the X-ray tube impact on the crystal sample and diffraction occurs. The diffracted (or scattered) X-rays are collected and processed by the detector. The processed data are sent to computer and the characteristic diffraction pattern is obtained.

X-rays diffracted from the crystal atoms satisfying the Bragg Conditions, leave black spots on the film that stands behind the crystal sample and these spots generate a diffraction pattern which varies from crystal to crystal (characteristic diffraction pattern). These diffraction spots are arranged on a lattice that is *reciprocal* to the crystal lattice. Each of the spots on the diffraction pattern represents atomic positions in the crystal sample, thus by measuring the distances between these spots, unit cell dimensions can be obtained. The unit cell is the smallest unit of a crystal lattice that possesses all of the features of the crystal and is defined by the geometrical properties of its shape such as the lengths of the edges (a , b , c) and angles between these edges of the unit cell (α , β , γ). Those parameters are known as unit cell dimensions.

Positions of the spots in a diffraction pattern are dependent on the size of the unit cell. When the unit cell grows, the spots approach each other. According to Fig. (2.7), it is obvious to realize the difference between the two diffraction patterns resulting from the different unit cell dimensions.

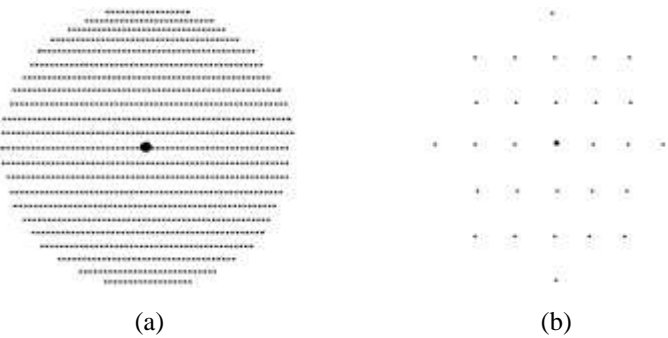


Figure 2.7 A comparison of diagrams of the diffraction patterns with different unit cell dimensions. The larger the unit cell, the closer the diffraction spots (a). The picture on the right (b) is the diffraction pattern of a smaller unit cell. (Pickworth-Glusker & Trueblood, 2010, chap. 3)

Shape of the spots in a diffraction pattern is related with the number and arrangements of the unit cells within the crystal (Fig. 2.8).

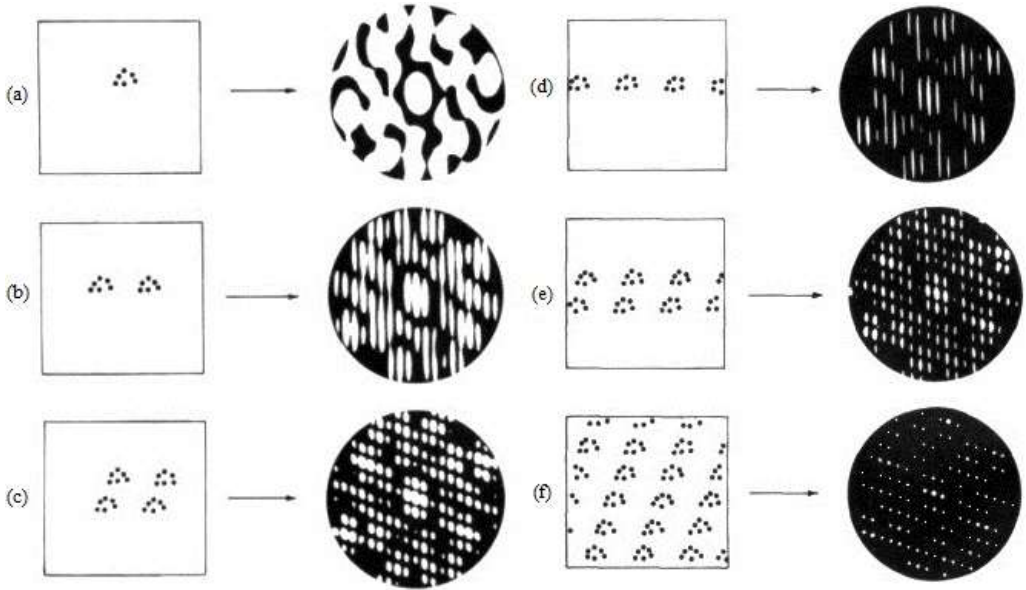


Figure 2.8 The effect of different crystal lattices on the diffraction patterns. The number of the molecules and their arrangements affect the patterns (Pickworth-Glusker & Trueblood, 2010, chap. 3).

As discussed in the previous section, diffraction process will occur if and only if the Bragg conditions are satisfied. Thus, from a geometric point of view, it will be possible to observe the diffracted beams or in other words Bragg reflections on the film as diffraction spots, in case the reciprocal lattice points lie on the surface of a sphere with radius $\frac{1}{\lambda}$ which was first described by Paul Peter Ewald in 1913 (Ewald,

1913). This construction is known as the *Ewald sphere* and a representing drawing is given in Fig. (2.9).

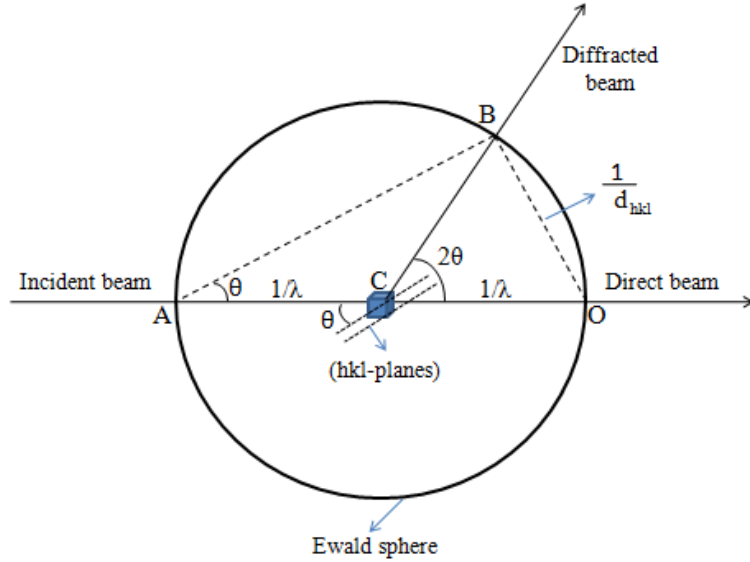


Figure 2.9 The Ewald sphere.

The reciprocal lattice is defined by applying Fourier transform to real space. Crystals consist of a large number of planes parallel to each other generating crystal lattices. These planes correspond to points that are arranged periodically in reciprocal space thereby reciprocal lattice occurs. Hence, these geometric points are called reciprocal lattice points. It is clear in Fig. (2.9) that the origin of the reciprocal lattice is located at the point O at which the incident beam emerges from the Ewald sphere and we assume that the crystal lies on the center of the sphere (Pickworth-Glusker & Trueblood, 2010).

During data collection process, the crystal is rotated around its center to scan all of the surfaces or in other words crystal planes. At each rotation, some of the reciprocal lattice points hit the surface of the Ewald sphere and the Bragg conditions are then satisfied. As a result, a characteristic diffraction pattern is obtained.

Now let us have a closer look into the geometry of the Ewald construction. According to Fig. (2.9), A is the point on the surface from where the incident beam enters into the sphere, B is the reciprocal lattice point and $|BO|$ is the norm of the

diffraction vector (\mathbf{r}^*). The length of the line segment BO equals to $\frac{1}{d_{hkl}}$ where d_{hkl} is the lattice constant (or inter-planar distance). We can prove that equality by doing some mathematical operations on the angles of the triangle ABO in Fig. (2.9). Then,

$$\sin \theta = \frac{|BO|}{|AO|} \quad (2.5)$$

can be written. $|AO|$ is the diameter, hence

$$\sin \theta = \frac{|BO|}{|AO|} = \frac{|BO|}{\frac{2}{\lambda}} \quad (2.6)$$

$$2 \left(\frac{1}{|BO|} \right) \sin \theta = \lambda \quad (2.7)$$

For $n = 1$, the Bragg equation that is given by Eq. (2.1) takes the following form:

$$\lambda = 2d_{hkl} \sin \theta \quad (2.8)$$

When Eq. (2.7) is substituted in Eq. (2.8), we have

$$2 \left(\frac{1}{|BO|} \right) \sin \theta = 2d_{hkl} \sin \theta \quad (2.9)$$

and we obtain the last equation for the lattice constant:

$$d_{hkl} = \frac{1}{|BO|} \quad (2.10)$$

If the inter-atomic distance in a crystal lattice (d_{hkl}) is smaller than $\lambda/2$ or the diffraction vector \mathbf{r}^* is larger than $2/\lambda$, then it cannot be possible to observe diffraction (Giacovazzo et. al., 2002). The reason is that there isn't any reciprocal lattice point intersecting the Ewald sphere in that case and thus, Bragg conditions are not satisfied. When the Ewald sphere is rotated around O_2 -origin (Fig. 2.10), a new

construction occurs called *limiting sphere* with radius $2/\lambda$ which is a limit to observe a diffraction as mentioned above.

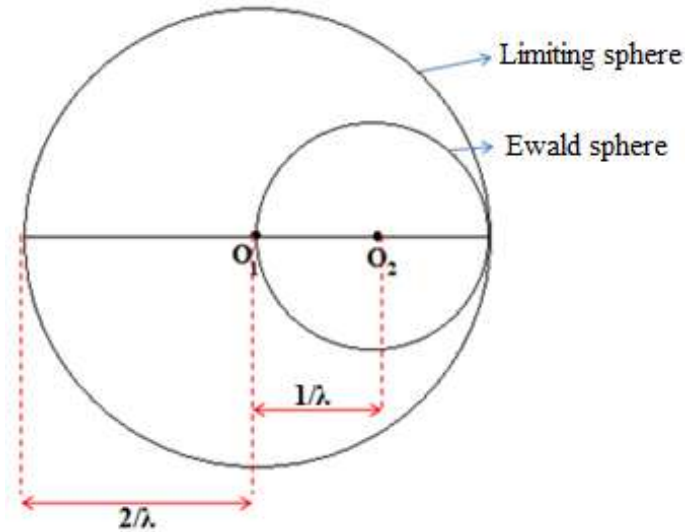


Figure 2.10 The limiting sphere surrounding the Ewald sphere.

2.3 Single Crystal X-ray Diffraction

2.3.1 Introduction: Diffraction Methods

The first discovery of X-ray diffraction from crystal atoms in 1912 by Max von Laue, opened a new gate to microstructures world. *Laue Method* which is the simplest, but adopted as a milestone of crystallography divided into different branches over time by transforming its form in terms of application. Experimental techniques that have been inspired by Laue Method are summarized as follows:

- I. *Rotating Crystal Method*: A crystal sample is rotated around one axis under a monochromatic beam. The photographic film and rotation axes are in cylindrical form. This method provides convenience to determine the unit cell dimensions of a single crystal.

- II. Debye-Scherrer Method: Polycrystalline samples that are quite small and randomly oriented crystallites are used in this technique. Crystalline sample in powder form is put in a sample holder and placed on the center of a powder diffractometer. A monochromatic beam impinges on the powder and then diffracted beams are recorded on a cylindrical film. The method was first created by P. J. W. Debye and P. Scherrer in 1916.

There is a third method known as *single crystal X-ray diffraction* which will be explained in detail. But first, mentioning about different radiation sources that are used in diffraction experiments would not be irrelevant.

The type of a radiation used in experiment varies according to the unit cell dimensions of sample. To observe the molecular structure, the order of the wavelength of a radiation must be similar to that of the inter-atomic distance of the sample (Pickworth-Glusker & Trueblood, 2010). X-rays produced by sealed tubes also known as the *brehmsstrahlung radiation* that has a continuous spectrum which occurs when a charged particle often an electron is accelerated by an electric field of another charged particle. Besides this, synchrotron radiation that is approximately 10^{13} times stronger than the brehmsstrahlung radiation, and neutrons from a nuclear reactor are used in structure analysis. The principle of the neutron diffraction is based on the nuclear interactions between the sample and neutrons.

In the first diffraction experiments, polychromatic radiation that consists of various wavelengths, was used which caused an obscuration in the diffraction patterns resulting from overlaps of the reflections from various single crystal planes. This is the disadvantage of the Laue Method, thus it can just be used to determine the crystal axes in general. But it is possible to analyze a single crystal structure using a monochromatic radiation of X-rays which is known as *single crystal X-ray diffraction* or *X-ray crystallography* shortly, and the method has a crucial importance mainly in materials science, chemistry and condensed matter physics.

2.3.2 Crystal Selection for Single Crystal XRD

A crystal is a solid in which all of the atoms, molecules or ions have a regular and periodic arrangement. This periodicity is observed perfectly in single crystals (Fig. 2.11).

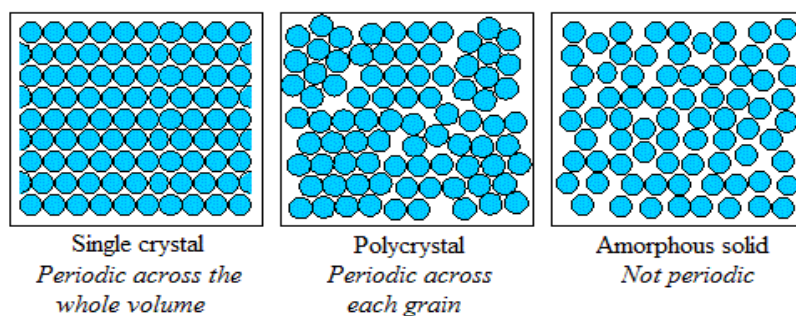


Figure 2.11 Difference between the atomic arrangements in solids (Barber & Best, n. d.).

The primary and the most important step for diffraction experiment is obtaining a suitable crystal or crystalline sample. Thus, a great care must be taken while selecting a single crystal. The reason is that almost all of the crystals have impurities, disorders or defects naturally. *Crystal twinning* is one of them.

Sometimes two or more crystals grow together sharing the same symmetry element which is called twin planes. The crystals that have such formation are called *twin crystals*. In a more explanatory fashion, according to Giacovazzo et. al. (2002), “Twins are regular aggregates consisting of individual crystals of the same species joined together in some definite mutual orientation” (chap. 2). The diffraction pattern of a twin crystal is a superposition of two symmetrical patterns as can be seen from Fig. (2.12).

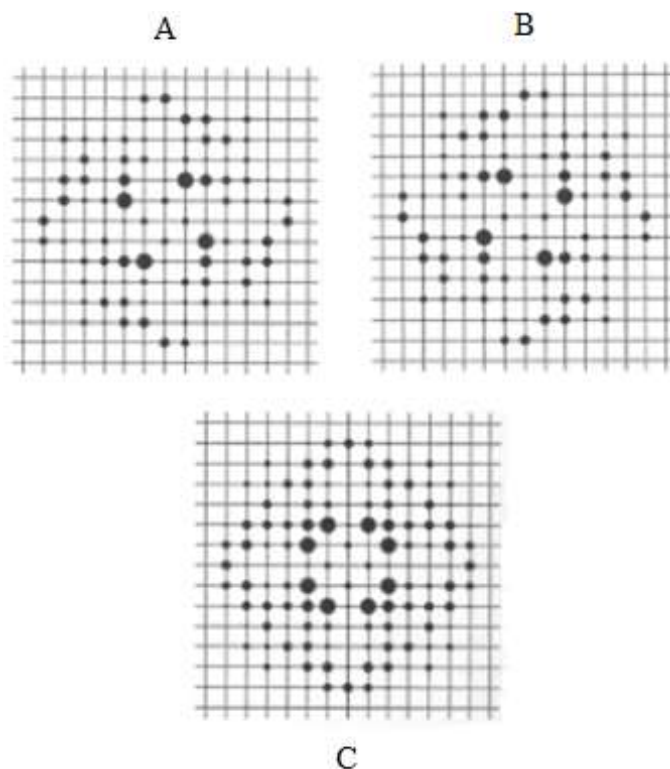


Figure 2.12 Reciprocal lattice plots of twin crystals (A and B). C shows the superposition of these two symmetrical crystals (Müller, Herbst-Irmer, Spek, Schneider & Sawaya, 2006, chap. 7).

Crystal twinning and structural distortions reduce the quality of crystals and may change their electrical, optical or magnetic properties. Thus, a crystal can be examined under a microscope by using polarized light where the waves vibrate along one direction. In addition, some single crystals are susceptible to humidity, air, high and/or low temperature or pressure, etc. resulting with a negative change in the structure that are the disadvantages of the single crystal X-ray diffraction. On the other hand, the method has many advantages that cannot be ignored. It is an analytical and nondestructive technique, and detailed information about the molecular structures of single crystals can be obtained examining the three-dimensional picture of the crystal sample.

As explained by Pickworth-Glusker and Trueblood (2010), “Once this information is available, and the positions of the individual atoms are therefore known precisely, one can calculate inter-atomic distances, bond angles, and other features of the molecular geometry that are of interest” (chap. 1).

Another important point that should be addressed in this section is the importance of the geometrical dimensions of a crystal sample for a diffraction experiment. When the dimensions of a sample is larger than the diameter of the collimator located at the tip of the X-ray tube, then some surfaces of the sample cannot be detected and this will cause regular decreases in the intensity data, for this reason, one may need to cut the crystal (Karabiyik, 2008).

2.3.3 Technical Equipment for Single Crystal XRD

Crystal structure determination experiments by X-rays or other radiation sources that we discussed briefly in the Subsection 2.3.1, can be grouped under three stages:

- 1. Data collection*
- 2. Diffraction pattern analysis*
- 3. Data refinement*

The first stage *data collection* involves experimental measurement of the directions of diffracted beams, hence a unit cell can be selected and its dimensions are measured (Pickworth-Glusker & Trueblood, 2010). The beams diffracted by single crystal atoms are collected, recorded, and then converted into an electrical signal by a detector. The diffraction pattern that is a sum of all of the electrical signals reveals the positions of atoms within the unit cell. At the second stage, a model structure is suggested which calculated by the crystallographer. The observed intensities of diffracted beams are compared with the calculated model in order to obtain a molecular structure that is closest to the real one. At the last stage, errors that occur between the calculated and observed models are tried to be minimized by use of refinement methods in order to obtain the crystal structure in three-dimension correctly.

Above all of these stages, selection of a suitable single crystal sample has priority as we discussed in the previous section. Besides this, technical equipment that is used during data collection has a crucial importance.

Crystal symmetry, crystal lattice parameters and diffraction data are collected and measured with a diffractometer which varies according to whether the sample that will be analyzed is polycrystalline or a single crystal. The operation principles of these machines are very similar to those used in 1912 (Fig. 2.2). A diffractometer consists of a radiation source (X-ray tube, synchrotron radiation or neutrons), goniometer and a detector basically (Fig. 2.13).

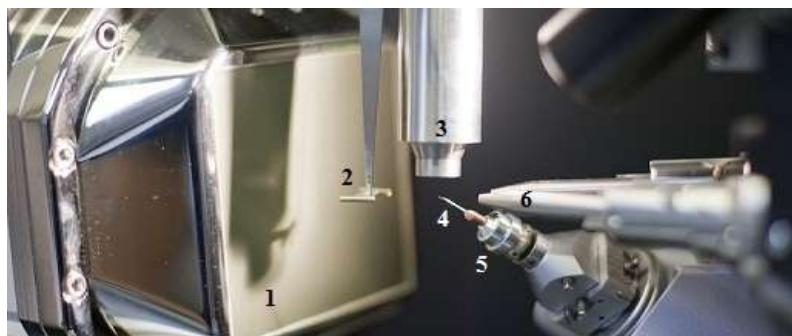


Figure 2.13 Devices of a single crystal X-ray diffractometer. (1) CCD-detector, (2) beamstop, (3) cooling device, (4) glass fibre, (5) goniometer head, (6) collimator of radiation beam.

A very thin glass fiber lies on the top of the goniometer on which the crystal sample is placed. The detection system can be an image plate, a charge-coupled device (CCD) or a photographic film. When the X-rays are impinged on the crystal atoms, scattered beams are collected and then processed by a detector. The most common one of them is CCD detectors. These detectors can collect lots of Bragg reflections at one time. A CCD detector consists of two radiation sensitive metal-oxide semiconductor (abbreviated as MOS) capacitors that store and transport the charge. According to Rivas et al. (2013), “To operate the CCDs, digital pulses are applied to the top plates of the MOS structures. The charge packets can be transported from one capacitor to its neighbour capacitor” (chap. 16). The beamstop collects the beam that has passed the crystal atoms directly without interaction, to prevent superpositions of spots on the diffraction pattern. The collimator aligns the rays in one direction to block scatterings out.

Before the technological improvements of these devices, it had been a problem to center the crystal in the diffractometer. The reason is that if the crystal does not take

place in the center, some crystal surfaces cannot be detected and some of the atomic positions are lost resulting with an incorrect diffraction pattern. In addition, a great care must be taken when aligning the crystal on the goniometer head, otherwise insecure mounting cause noise to occur on the diffraction pattern and/or poor data about the crystal structure (Blake et. al., 2009). Thus, there are some different techniques used to mount the sample (Fig. 2.14). Glass fibre must be thick enough not to allow the crystal to vibrate and must be thin enough not to cause extra diffraction spots appear on the pattern.

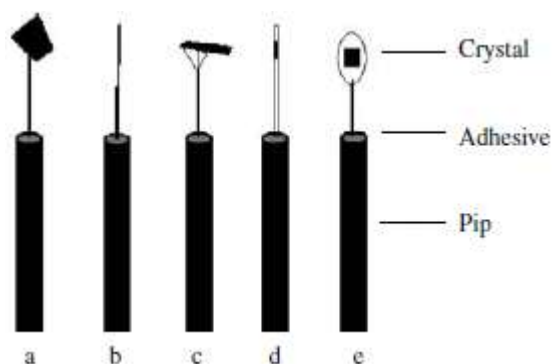


Figure 2.14 Crystal mounting techniques. The crystal is on a glass fibre (a), on a two-stage fibre (b), mounted on a fibre with some glass wool (c), within a capillary tube (d), in a solvent loop (e) (Blake et. al., 2009, chap. 3).

It is now possible to analyze every kind of crystal structure by new generations of diffractometers. One of them is the *four-circle diffractometer* that allows us to determine all the unit cell dimensions and to measure the Bragg reflections definitely (Shmueli, 2007). The diffraction data are collected by rotating the crystal at four different angles (χ , 2θ , ϕ , ω) by using these diffractometers that are illustrated in Fig. (2.15).

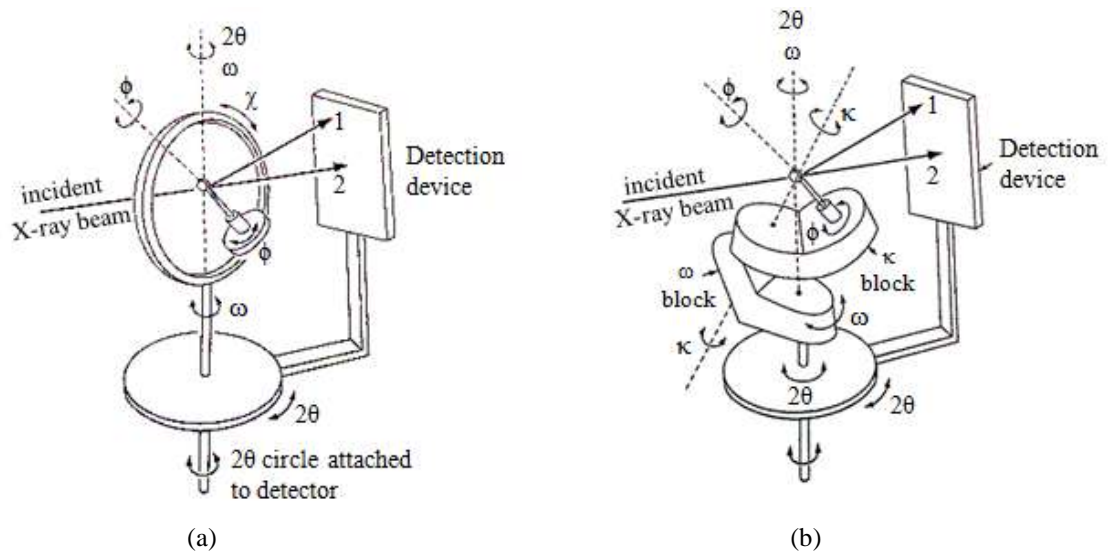


Figure 2.15 A four circle diffractometer with Eulerian (a) and Kappa (b) geometries. In both pictures, the beams numbered with 1 and 2 represent diffracted and direct beams, respectively (Pickworth-Glusker & Trueblood, 2010, chap. 4).

Let us have a deeper look into the two different geometries of a four-circle diffractometer:

- a. **Eulerian Geometry:** According to Fig. 2.15 (a), crystal, radiation source and detector lie on the same plane which is called the diffraction plane and it is horizontal with respect to the main axis that passes through the crystal. Thus, the detector is constrained to rotate about the main axis (Shmueli, 2007, chap. 4). It is clear in the Fig. 2.15 (a) that the crystal is rotated around three axes ϕ , χ , and ω . The rotation axes and their roles in the machine can be summarized as follows:
 - **Phi (ϕ) axis:** The rotation axis around the goniometer head where the crystal is mounted.
 - **Chi (χ) axis:** Passes through the center of the crystal and the crystal rolls over the closed circle that is called χ circle.
 - **Omega (ω) axis:** This is the axis that allows the χ circle to rotate around it, or in other words the whole goniometer moves around ω axis.
 - **2-Theta (2θ) axis:** The detector rotates around 2θ axis that is coaxial with ω axis.

- b. Kappa Geometry: It is an alternative geometry that does not have a χ circle, but ϕ and 2θ axes are identical to those in Eulerian geometry (Ripoll & Cano, n. d.) and there are two new axes, κ and ω_κ , instead of χ axis. According to Fig. 2.15 (b), the first (*kappa*) block rotates around the base plate of the diffractometer whilst the second (*omega*) block rotates around the first one. These movements of the blocks do not cause any coincidence between the axes during the experiment which cannot be observed for the diffractometers designed to operate on the principle of Eulerian geometry.

2.3.4 Measurement of Intensity: Scanning Angles of Diffractometer

There are three methods in order to measure the diffraction intensity depending on the movements of crystal and detector:

- Rotating crystal - Rotating detector: This method corresponds to the $\omega/2\theta$ -scan of the diffractometer. The crystal rotates around ω -axis while the detector rotates in the 2θ -circle. The equation below shows the relation between the angular velocities of detector and crystal. ω_d and ω_c indicate the velocities of detector and crystal, respectively.

$$\omega_d = 2\omega_c$$

- Rotating crystal - Fixed detector: This method corresponds to the ω -scan of the diffractometer. The detector is fixed at 2θ position, while the crystal rotates around ω -axis.
- Fixed crystal - Fixed detector: The detector and crystal are stationary at 2θ and reflection position, respectively.

CHAPTER THREE

CRYSTAL STRUCTURE SOLUTION

3.1 Introduction

The aim of a diffraction experiment is to obtain the intensities of Bragg reflections to calculate the electron density maps and therefore obtaining a three-dimensional image of the crystal sample.

The intensities of Bragg reflections are mainly depend on the atomic arrangements within the unit cell and interference of X-rays scattered by crystal atoms. In addition, the intensity of diffracted beams is proportional to the square of the amplitude of the structure factor.

In a diffraction experiment one can observe the intensity and therefore the amplitude of the structure factor directly. But the electrons of a crystal atom form a charge cloud around the nucleus and they scatter the incident beam in all directions, thus, phase differences occurring between the scattered rays must be taken into account (Omar, 1975). But it is not possible to observe the phases directly during an experiment. This annoying situation is known as the *phase problem* in crystallography.

In this chapter, the structure factor and its relation with the intensity of diffracted rays, correction factors that have to be calculated during the data reduction process, phase problem and different methods (*Direct Methods and Patterson Method*) in order to cope with the problem will be discussed in detail.

3.2 Structure Factor

A measure of the power of scattering electrons of an atom in a crystal lattice is known as the *atomic scattering (or form) factor*- f_j where j represents the j th atom in the crystal lattice. The ratio of the amplitude of X-rays scattered from the electrons of

a single atom to that scattered from a single electron gives the magnitude of the atomic scattering factor- $|f_j|$. The wave scattered by all of the atoms in a unit cell is known as the *structure factor-F* and it carries information about where the atoms sit in unit cells, and describes how atomic arrangements influence the intensities of diffracted beams.

The structure factor F is obtained by the summation of all the waves diffracted from the individual atoms, but scattering by the atom at the origin also must be added (Weaver, n. d.). Thus, a complex exponential function is used in order to express the scattered waves. Then, the structure factor is said to be a composition of real and imaginary components as given below:

$$F(hkl) = A(hkl) + iB(hkl) \quad (3.1)$$

In Eq. (3.1), A is the atom at origin $(0, 0, 0)$, B is the atom at any (x, y, z) position in the crystal and (hkl) is a crystal plane from where the incident beam scatters. This relation is depicted with a simple graphic (Fig. 3.1).

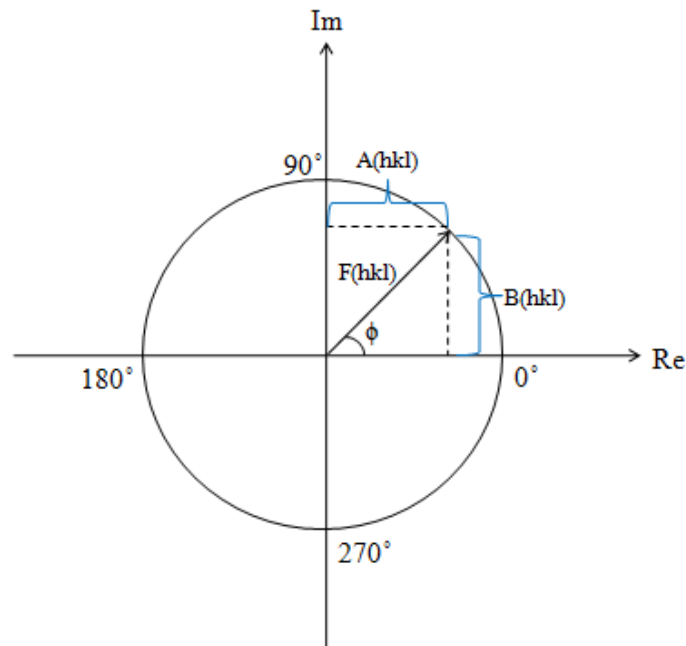


Figure 3.1 Graphical representation of the structure factor. ϕ is the phase difference occurring by the shifts between the scattered rays. $F(hkl)$ has two components on real and imaginary axes.

Now consider a crystal including N atoms. The total ray scattered by the entire material is the sum of each ray scattered from all the unit cells in a crystal lattice. According to Fig. (3.1), A and B are given as follows:

$$A(hkl) = \sum_{j=1}^N f_j \cos\phi_j \quad (3.2)$$

$$B(hkl) = \sum_{j=1}^N f_j \sin\phi_j \quad (3.3)$$

When Eqns. (3.2) and (3.3) are substituted in Eq. (3.1), the general formula for structure factor is obtained:

$$F(hkl) = A(hkl) + iB(hkl)$$

$$= \sum_{j=1}^N f_j (\cos\phi_j + i\sin\phi_j)$$

$$\boxed{F_{hkl} = \sum_{j=1}^N f_j e^{i\phi_j}} \quad (3.4)$$

A useful representation of Eq. (3.4) is given with the Argand diagram which is a diagram of complex numbers that are plotted as points in a two-dimensional plane that is composed of real and imaginary axes (Fig. 3.2).

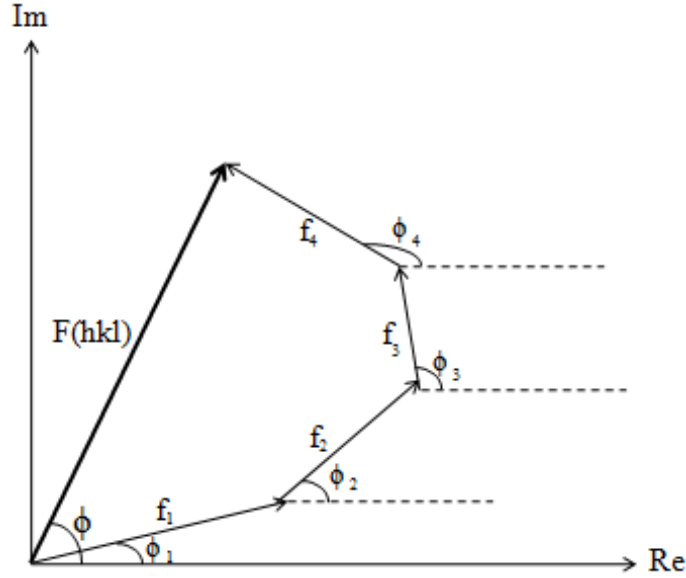


Figure 3.2 Argand diagram of the structure factor $F(hkl)$ that is a sum of all the waves scattered from the whole crystal.

In Eq. (3.4), ϕ_j is the phase difference resulting from the shift between the scattered rays. The phase difference depends on the arrangements of atoms in a crystal and it can be expressed by using the dot product of the reciprocal lattice vector \mathbf{G} ($\mathbf{G} = h\mathbf{x}_j + k\mathbf{y}_j + l\mathbf{z}_j$) with the real lattice vector \mathbf{r}_j ($\mathbf{r}_j = a\mathbf{x}_j + b\mathbf{y}_j + c\mathbf{z}_j$). Hence,

$$\phi_j = 2\pi\mathbf{G} \cdot \mathbf{r}_j \quad (3.5)$$

$$\phi_j = 2\pi(hx_j + ky_j + lz_j) \quad (3.6)$$

$$\phi_j = 2\pi[\underbrace{(h \cdot a)}_1 x_j + \underbrace{(k \cdot b)}_2 y_j + \underbrace{(l \cdot c)}_3 z_j] \quad (3.7)$$

$$\phi_j = 2\pi(hx_j + ky_j + lz_j) \quad (3.8)$$

In Eq. (3.7), the numbers **1**, **2**, and **3** represent the Laue equations (Kittel, 2005). Eq. (3.8) is the general formula for the phase angle of a hkl -reflection at (x_j, y_j, z_j) position. When the Eq. (3.8) is substituted in Eq. (3.4), then the following expression for the structure factor is obtained:

$$F_{hkl} = \sum_{j=1}^N f_j e^{i2\pi(hx_j + ky_j + lz_j)} \quad (3.9)$$

The last equation provides information about which reflections are expected in a diffraction pattern obtained from a given crystal structure with atoms located at positions (x, y, z) , (Weaver, n. d.).

The amplitude of the structure factor- $|F(hkl)|$ is the ratio of the amplitude of the rays scattered from the whole atoms in a unit cell to that scattered from a single electron. $|F(hkl)|$ is calculated multiplying $F(hkl)$ by its complex conjugate $F^*(hkl)$ and taking the square root of the result. By doing some mathematical operations,

$$\begin{aligned} |F(hkl)| &= \sqrt{F \cdot F^*} \\ &= \sqrt{(A + iB) \cdot (A - iB)} \end{aligned}$$

$$|F(hkl)| = \sqrt{A^2 + B^2} \quad (3.10)$$

is obtained. A and B have been described by the Eqns. (3.2) and (3.3), thus when they are substituted, the amplitude of the structure factor is calculated as follows:

$$|F(hkl)| = \sqrt{\left(\sum_{j=1}^N f_j\right)^2} = \sum_{j=1}^N f_j \quad (3.11)$$

The intensities of diffracted beams are proportional to the square of the amplitude of the structure factor (Eq. (3.12)) and are independent of h , k , and l values whilst they are dependent on the atomic arrangements and weights. In a diffraction pattern, the spots of the beams diffracted from heavier atoms are brighter and larger than others.

$$I(hkl) \propto |F(hkl)|^2 \quad (3.12)$$

3.3 Data Reduction Process: Corrections to Intensity

Crystal structure analysis requires definite and accurate determination of the diffraction pattern both in terms of the positions of spots and intensities in order to comment the crystal structure correctly (Connolly, 2012). The occurrence of the systematic errors during a diffraction experiment is a major problem and it must be handled before crystal structure solution and refinement processes (Bennett, 2010). Thus, data reduction process holds a great importance because of providing consistency between the calculated and observed data.

It had been a problem to bring the experimental results to the same scale with the calculated model until a method was introduced by A. J. C. Wilson (Wilson, 1942). According to the method, it is possible to convert the proportion between the intensity- I and $|F(hkl)|^2$ into an equation by adding some factors which are called ‘*correction factors*’ (Eq. (3.13)).

$$I(hkl) = K L T P A E |F(hkl)|^2 \quad (3.13)$$

The letters K , L , T , P , A , and E in Eq. (3.13) are scale, Lorentz, temperature, polarisation, absorption, and extinction factors, respectively that are explained in detail in the following sections. The diffracted X-ray intensities scaled by these factors are called ‘*reduced intensities*’.

3.3.1 Scale Factor

In order to make a comparison between the observed and calculated models, they are brought to the same scale by the scale factor which is represented as K (Sevinçek, 2006). The scale factor is defined with the ratio given below:

$$K = \frac{\langle |F(hkl)_{\text{obs}}|^2 \rangle}{\langle |F(hkl)_{\text{cal}}|^2 \rangle} \quad (3.14)$$

3.3.2 Lorentz Factor

As the crystal rotates during the diffraction experiment, reciprocal lattice nodes rotate with different linear velocities, therefore the length of time that a crystal atom remains in diffraction position differs. The intensities obtained from the nodes with high velocities are smaller than those obtained from lower ones. As a result, the geometry of the diffraction pattern changes. Lorentz (or shortly, L-) factor is a geometrical correction factor that is used to reduce this difference between the intensities on the diffraction pattern.

If the diffractometer used in the experiment is a *four-circle diffractometer*, then the reciprocal lattice nodes lie on the equatorial plane where $\phi = 0$, therefore the following expression is used to perform the Lorentz correction (Gökçe, 2008),

$$L = \csc 2\theta \quad (3.14)$$

when using the diffractometers with area-detectors the above expression changes its form as follows (Lipson, Langford & Hu, 2004):

$$L = (\sin\theta)^{-1}(\cos^2\phi - \sin^2\theta)^{-1/2} \quad (3.15)$$

3.3.3 Temperature Factor

According to Tilley (2006), “The most important correction term applied to intensity calculations is the temperature factor” (chap. 6). The reason is that when deriving the expression for structure factor, all the atoms in a unit cell are treated as stationary (when the temperature is considered to be *absolute zero*). However, this is not the actual case. Every atom within a crystal vibrates about its lattice position by the influence of heat in three-dimensions x, y, and z. The electron cloud around the

nucleus of a crystal atom diffuses into a larger volume due to the thermal motion, thus the geometrical shape of the atom looks like an ellipsoid and the scattering power of the atom decreases exponentially (Eq. (3.16)). If the amplitude of vibration of an atom is the same in any direction within the crystal, then the atom is called *isotropic*, otherwise it is called *anisotropic*.

$$f = f_0 \exp\left(-B \frac{\sin^2 \theta}{\lambda^2}\right) \quad (3.16)$$

In Eq. (3.16), f and f_0 are the atomic scattering factors of thermally vibrating atom and stationary atom, respectively. The letter B represents the *atomic temperature factor* or rather known as the *Debye-Waller factor* (Eq. (3.17)), λ is the wavelength of radiation, and θ is the Bragg angle.

$$B = 8\pi \langle u \rangle^2 \quad (3.17)$$

In Eq. (3.17), $\langle u \rangle^2$ represents the square of the mean displacement from the equilibrium position and mostly given as U_{iso} which means *isotropic temperature factor*.

Now, let us consider the relation between the thermal motion and diffracted intensity. When the atomic scattering factor that is given by Eq. (3.16) is substituted into the structure factor (Eq. (3.9)),

$$F_{hkl} = \sum_{j=1}^N f_j e^{i2\pi(hx_j + ky_j + lz_j)} \quad (3.9)$$

$$F_{hkl} = \sum_{j=1}^N f_j \exp\left(-B \left(\frac{\sin \theta}{\lambda}\right)^2\right) \exp(i2\pi(hx_j + ky_j + lz_j))$$

$$F_{hkl} = \sum_{j=1}^N f_j \exp\left(-i2\pi B \frac{\sin^2 \theta}{\lambda^2} (hx_j + ky_j + lz_j)\right) \quad (3.18)$$

is obtained. The diffracted intensity is proportional to the square of the amplitude of the structure factor as we discussed before, then the following expression occurs:

$$|F_{hkl}|^2 = \left[\sum_{j=1}^N f_j \exp \left(-i2\pi B \frac{\sin^2\theta}{\lambda^2} (hx_j + ky_j + lz_j) \right) \right]^2 \propto I_{hkl} \quad (3.19)$$

Consequently, when temperature increases, the amplitude of the atomic scattering factor, therefore the amplitude of structure factor and the diffracted intensity decreases. Thus, it is needed to correct the intensity with the temperature factor.

3.3.4 Polarisation Factor

Although there had been many attempts to show the polarisation of X-rays, this was first demonstrated successfully by Charles G. Barkla (Barkla, 1905). The X-ray beam emerging from the monochromator is unpolarised but, after the beam diffracted from the crystal, resultant beam is polarised depending on the Bragg angle- θ (Fig. 3.3).

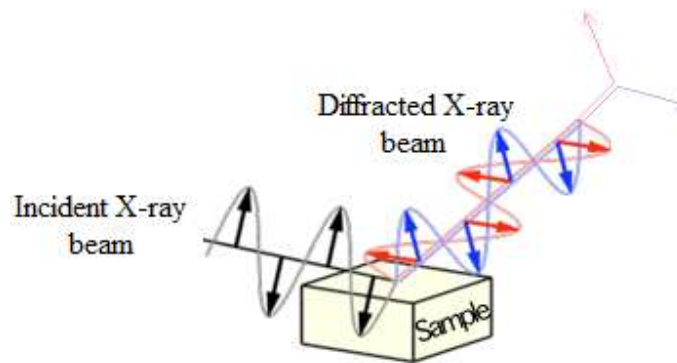


Figure 3.3 The polarisation of X-rays after diffraction.

The intensity of the diffracted rays decreases due to the polarisation, hence a correction have to be added into the intensity data which indicated as P in Eq. (3.13). Thus, if a monochromator isn't used during the experiment (Fig. 3.4), then the polarisation correction- P is given by Eq. (3.20).

$$P = \frac{1 + \cos^2 2\theta}{2} \quad (3.20)$$

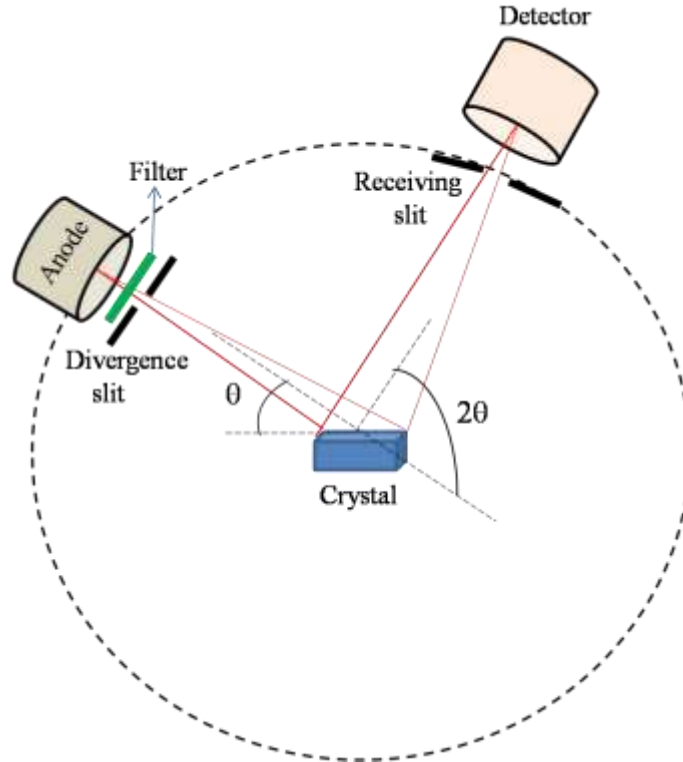


Figure 3.4 Diffraction process without a monochromator.

But, if a monochromator is used, we need to write Eq. (3.21).

$$P = \frac{1 + \cos^2 2\theta_M \cos^2 2\theta}{2} \quad (3.21)$$

In Eq. (3.21), θ_M is the Bragg angle of the monochromator which is a preset constant determined by the lattice constant (or inter-planar distance) d (Cockcroft, n. d.). Diffraction by a monochromator produces partial polarisation. In this study, graphite monochromator was used and a representing schema of the geometry of this setup is given by Fig. (3.5).

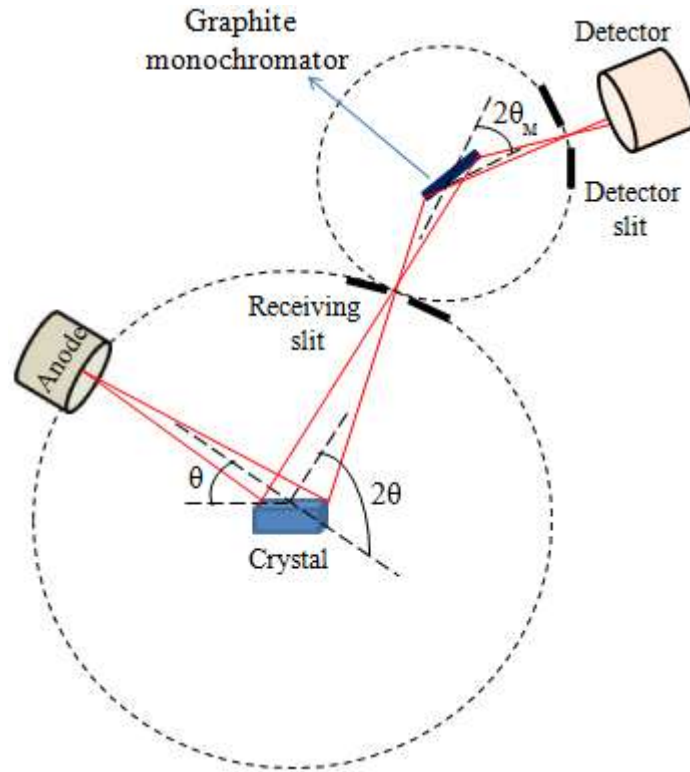


Figure 3.5 Diffraction process with a monochromator.

Before Barkla's successful experiments, in 1808, E. L. Malus observed polarisation using a calcite crystal, unlike other scientists, and he realized that when he rotated the crystal, the intensity of the reflected beam was changing depending on the reflection angle (that is Bragg angle)- θ . Therefore, he derived Eq. (3.22) to denote the effect of polarisation on the intensity by taking the square of the amplitude of the incident wave. This equation is known as *Malus' Law*.

$$I = I_0 \cos^2 2\theta \quad (3.22)$$

In the equation above, I_0 is the intensity of the incident beam. According to J. J. Thomson, the value of intensity of X-rays scattered by a single electron at a distance r from the electron is given with the equation below which is the advanced form of Eq. (3.22):

$$I = I_0 \frac{e^4}{m^2 r^2 c^2} \left(\frac{1 + \cos^2 2\theta}{2} \right) \quad (3.23)$$

Consequently, the intensity of the diffracted beam is dependent on the Bragg angle while independent from the diffraction technique used.

3.3.5 Absorption Factor

While passing through a crystal, some of the X-rays are absorbed by the crystal atoms. According to Lambert-Beer's Law, the intensity of X-rays travelling through an absorbing media depends on the thickness of the media (t) and linear absorption coefficient (μ) given with the expression below:

$$I = I_0 e^{-\mu t} \quad (3.24)$$

In Eq. (3.24) I_0 is the intensity of the incident beam while I is the intensity of the beam that is absorbed by the material. It is evident in the equation that the diffracted intensity is inversely proportional to μ thus, when analysing crystal structures including heavy atoms, absorption factor must be added in order to improve the quality of the collected data.

3.3.6 Extinction Factor

“Extinction is the increase in absorption that is to be expected when Bragg reflection of X-rays takes place in single crystals, and the corresponding decrease in intensity of reflection observed” (Lonsdale, 1947). Extinction correction has two components as *primary* and *secondary*. When the sample crystal used in diffraction experiment is very close to perfection which means a crystal bears the periodicity of its atomic arrangement from $-\infty$ to $+\infty$, almost each radiation beam transmitted on the crystal is reflected by different crystal planes. This situation is referred to as *multiple reflection* (Fig. 3.6). The phase difference between those undergoing multiple reflection is $\pi/2$ and in case the double reflection the difference becomes π . If the incident and reflected rays travel in the same direction, destructive interference

occurs due to their opposite phases. As a result, the intensity of the incident beam decreases. This type of extinction is known as *primary extinction* (Fig. 3.6).

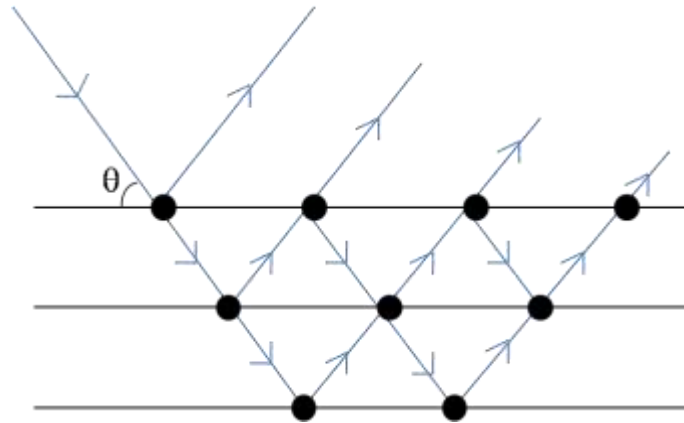


Figure 3.6 Primary extinction: Multiple reflection by the atoms sitting in different crystal planes.

Primary extinction becomes important when the thickness of the layers in crystal is larger than 10^{-4} cm that means there are small spacings within the structure. Otherwise the number of multiple reflections decrease and primary extinction becomes unimportant (Lonsdale, 1947). Besides the primary extinction, the important fraction of the incident beam is reflected by the crystal plane which first encounters with the beam. Hence, the lower planes in the crystal receive less radiation (Giacovazzo et. al., 2002). This type of extinction is known as *secondary extinction* and it causes a decrease in the intensity of the reflected beams (Fig. 3.7). We can compare the two extinctions briefly:

- *Primary extinction is independent from wavelength, but the secondary is not.*
- *Crystallite size is important for both primary and secondary extinctions, but the size of the entire crystal is also important for secondary extinction.*

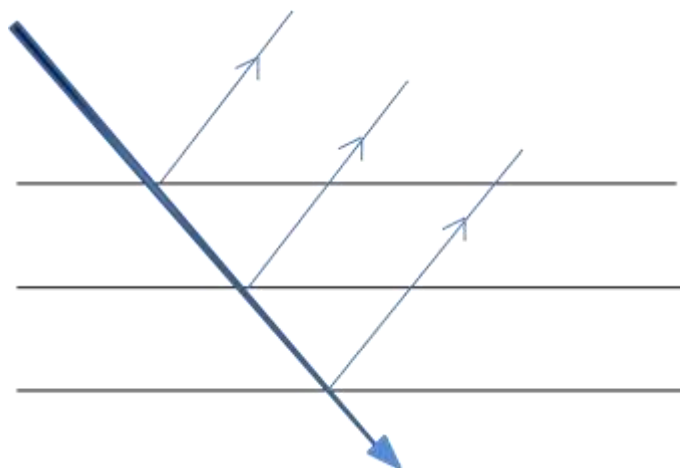


Figure 3.7 Secondary extinction.

3.4 Phase Problem

In order to obtain the electron density maps, shortly *e-maps*, one needs knowledge about not only the amplitudes of the structure factor, but also the phases of the diffracted waves. Unfortunately, as we discussed at the beginning of this chapter, it is not possible to recover the phases directly from a diffraction experiment, although the amplitude can be obtained directly by its relation with diffracted intensity. This trouble is referred to as *phase problem* that had been recognized presumably by Bragg in 1929 (Sayre, 2002). The *problem* preoccupied crystallographers for a long time and since the mid 1900s, some methods which will be described in the following sections were presented in order to solve the problem.

Crystals are solids that consist of periodic arrangements of atoms. Therefore, the electron density distribution is periodic or in other words, the distribution remains *invariant* under the translational symmetry operation. Hence, the electron density function $\rho(\mathbf{r})$ where \mathbf{r} is the lattice vector, is the same even if the position of the atom is translated by a vector \mathbf{T} (Eq. (3.25)).

$$\rho(\mathbf{r}) = \rho(\mathbf{r} + \mathbf{T}) \quad (3.25)$$

A mathematical representation of the three-dimensional electron density function of the lattice vector \mathbf{r} ($\mathbf{r} = \mathbf{a}x + \mathbf{b}y + \mathbf{c}z$) can be written as follows by means of

Fourier series that are used to decompose the periodic functions into complex exponentials:

$$\rho(\mathbf{r}) = \frac{1}{V} \sum_{h,k,l=-\infty}^{\infty} F_{hkl} \exp[-2\pi i(hx + ky + lz)] \quad (3.26)$$

where V is the volume of the unit cell and h, k, l are integers (Harker & Kasper, 1948). The structure factor can be expressed in terms of electron density function,

$$F_{hkl} = \int_V \rho(\mathbf{r}) \exp[2\pi i(hx + ky + lz)] dV \quad (3.27)$$

or can be expressed as a wave function which consists of amplitude and phase, hence

$$F_{hkl} = |F_{hkl}| e^{i\phi_{hkl}} \quad (3.28)$$

is obtained. If the exponential function is decomposed into its trigonometric functions, we obtain Eq. (3.29) for the structure factor.

$$F_{hkl} = |F_{hkl}| \cos \phi_{hkl} \quad (3.29)$$

In case the crystal lattice is centrosymmetric that means the crystal possesses an inversion symmetry as one of its symmetry elements, then ϕ_{hkl} must be 0° or 180° . Thus, the phase problem reduces to *selection of the correct sign problem* for the structure factor amplitudes, $F_{hkl} = \mp |F_{hkl}|$. The number of the possible phase combination for n independent reflections is 2^n , while it is 4^n for non-centrosymmetric structures. In addition, if the crystal lattice is non-centrosymmetric, then the phase may have a value from 0° to 360° by 45° increments.

In order to solve the phase problem, some methods are present such as *multiple isomorphous replacement*, *anomalous dispersion*, etc. But the most common ones which proposed depending on the atomic composition of a crystal are:

- *Patterson method*
- *Direct methods*

3.4.1 Patterson Method

A remediation to the phase problem was first suggested by Arthur L. Patterson (1934). The phase information leads us to determine the positions of atoms that are surrounded with electron densities higher than those on the Bragg planes. *Patterson method* does not provide accurate information about that type of atomic positions, nonetheless the inter-atomic distances can be obtained directly. In one-dimension Eq. (3.30) is written for Patterson function or the average electron density function,

$$P(t) = \frac{1}{d} \int_0^d \rho(x)\rho(x+t)dx \quad (3.30)$$

where d is the inter-planar distance and t is the amount of displacement (Patterson, 1934). In three-dimension, the Patterson function is given as follows:

$$P(t) = \frac{1}{V} \sum_{h,k,l} |F_{hkl}|^2 e^{-i\phi_{hkl}} \quad (3.31)$$

Two crystal atoms in real (or crystal) space correspond to *one peak* in Patterson space (shortly *P-space*) and the distance of the maximum peak from the origin (this is the case where $t = 0$) corresponds to the distance between two atoms in a unit cell.

Patterson method is not feasible for light atoms. The reason is that peaks of the heavy atoms possess higher intensities and their peaks are more visible than those of light ones in *P-space*.

3.4.2 Direct Methods

When determining a crystal structure by *Patterson method*, a previously known molecular geometry of the sample including heavy atoms is required. But according to a method which was first proposed by Harker and Kasper (1948), the phases of

structure factors and the signs of the amplitudes can be obtained *directly*, without any preliminary information about the structure, by applying the Cauchy-Schwarz inequalities to the formulas of the structure factors that include information about the atomic positions within a crystal structure. Hence, the method which leads us to obtain the missing phases directly from the observed amplitudes is referred to as *direct methods* in crystallography. Before the study of Harker and Kasper in 1948, some direct solutions to the phase problem had been discovered in 1920s by Ott (1927).

One can obtain very good results for small-sized molecules by direct methods. Although any preliminary information about the structure is not required when studying with direct methods, the size of the sample bears importance which is a limitation for the method. Thus, structure determination of macromolecules such as proteins, must be handled by Patterson method. Despite the fact that the first inequalities derived by Harker and Kasper (1948) that will be given in the later sections were convenient for determination of the phases of structure factors from the amplitudes of the reflected intensities (highest ones) of centrosymmetric crystal structures, they could not provide satisfactory results. Hence, Karle and Hauptman reconfigured these inequalities by transforming them into determinants. There are two assumptions in the basis of their study: *positiveness of the electron density and atomicity*.

- *Description 1- Positiveness*: The sum that is assigned for a Fourier series generates a function which is positive in everywhere in the space where it is described. The structure factor is expressed by means of Fourier series, therefore the electron density distribution has to be positive in everywhere in the unit cell ($\rho(\mathbf{r}) \geq 0$).

The determinants presented by Karle and Hauptman are given as follows:

$$D = \begin{vmatrix} F(\mathbf{0}) & F(-\mathbf{h}_1) & \cdots & F(-\mathbf{h}_n) \\ F(\mathbf{h}_1) & F(\mathbf{0}) & \cdots & F(\mathbf{h}_1 - \mathbf{h}_n) \\ \vdots & \vdots & \ddots & \vdots \\ F(\mathbf{h}_n) & F(\mathbf{h}_n - \mathbf{h}_1) & \cdots & F(\mathbf{0}) \end{vmatrix} \geq 0 \quad (3.32)$$

In Eq. (3.32), the vectors in parentheses represent (hkl) , while $\mathbf{0}$ corresponds to $h = k = l = 0$ and n is integer varies from 0 to ∞ . The determinant D which is known as *Karle-Hauptman determinant* belongs to a hermitian matrix which is a square matrix with a complex conjugate equals to its transpose, resulting from $F^*(\mathbf{h}) = F(-\mathbf{h})$ where F^* and F are the Fourier coefficients and it is non-negative if and only if the electron density is non-negative. The whole expression gives the set of *Karle-Hauptman inequalities* (Blake et. al., 2009) that are very feasible for every kind of reflected intensity, i.e. not only the highest ones and provide direct information about the phases.

In order to make Karle-Hauptman inequalities more useful, derivation of normalized structure factors that will be discussed in the following section, was required.

- *Description 2-Atomicity*: This condition assumes that the electron density around the atomic center are maximum and in the form of peaks showing spherical distribution. At the points further away from the center, the values of the peaks decrease, even they approach to zero.

3.4.2.1 Normalized Structure Factors

The expected value of a reflected intensity which is equal to $|F_h|^2$, is given by Eq. (3.33) assuming the displacements of each atom in a crystal lattice is *isotropic* that means, every atom in the lattice moves independently and equally (*equal atom structure*):

$$\langle |F_h|^2 \rangle = \sum_{j=1}^N f_j^2 \quad (3.33)$$

where h represents (hkl) . It is not possible to compare the intensities of the beams reflected at different θ -angles. For this reason, a new structure factor which called *normalized structure factor* that eliminates the dependence on θ of the structure factor, is defined by means of Eq. (3.33) as follows:

$$|E_h|^2 = \frac{|F_h|^2}{\sum_{j=1}^N f_j^2} \quad (3.34)$$

If we calculate the expected value of $|E_h|^2$ by using Eqns. (3.33) and (3.34), we obtain Eq. (3.35) which is true for all crystal structures and all values of θ .

$$\langle |E_h|^2 \rangle = \frac{\langle |F_h|^2 \rangle}{\sum_{j=1}^N f_j^2} = \frac{\sum_{j=1}^N f_j^2}{\sum_{j=1}^N f_j^2} = 1 \quad (3.35)$$

“If one replaces the real crystal, with continuous electron density $\rho(\mathbf{r})$, by an idealized one, the unit cell of which consists of N discrete, non-vibrating point atoms, then the structure factor F_h is replaced by the normalized structure factor E_h ” (Hauptman, 1986). Therefore, the general formula for the normalized structure factor is:

$$E_h = \frac{1}{[\sum_{j=1}^N f_j^2]^{1/2}} \sum_{j=1}^N f_j \exp[2\pi i(hx_j + ky_j + lz_j)] \quad (3.36)$$

Eq. (3.36) shows that the dependence on θ does not exist anymore. When the angle of scattering is equal to zero, the atomic scattering factor and therefore the structure factor reaches to its maximum value that is the atomic number Z ($F(000) = Z$). Hence, the maximum value of the amplitudes of the reflected waves cannot be larger than Z ($|F_{hkl}| \leq Z$). By taking into account this case, let us recall the definition of the atomic scattering factor (f_j);

$$|f_j| = \frac{\text{Amplitude of X-rays scattered by electrons of a single atom}}{\text{Amplitude of X-rays scattered by a single electron}} \quad (3.37)$$

Under the assumption of *equal atom structure*, we can say that $|f_j|$ is equal to Z ($f_j = Z$). Thus, it is easy to write the denominator of Eq. (3.36) in terms of N and Z .

$$\left[\sum_{j=1}^N f_j^2 \right]^{1/2} = [NZ^2]^{1/2} \quad (3.38)$$

When Eq. (3.38) is substituted in Eq. (3.36), we obtain:

$$E_h = \frac{Z}{[NZ^2]^{1/2}} \sum_{j=1}^N \exp[2\pi i(hx_j + ky_j + lz_j)]$$

$$E_h = \frac{1}{\sqrt{N}} \sum_{j=1}^N \exp[2\pi i(hx_j + ky_j + lz_j)] \quad (3.39)$$

The maximum possible value of E_h ($\langle E_h \rangle_{max}$) is equal to $\frac{N}{\sqrt{N}} = \sqrt{N}$ from Eq. (3.39). Before the normalized structure factors are defined, the unitary structure factors (U_h) were used in the direct methods. The relation between U_h and F_h is defined by Eq. (3.40).

$$U_h = \frac{F_h}{Z} \quad (3.40)$$

The magnitude of U_h is written by means of the equality between f_j and Z as follows:

$$|U_h| = \frac{|F_h|^2}{\sum_{j=1}^N f_j} \quad (3.41)$$

The denominator of Eq. (3.41) is the maximum possible value of the structure factor (F_h), then U_h varies between 0 and 1 (Eq. (3.42)).

$$0 \leq U_h \leq 1 \quad (3.42)$$

The first problem encountered when analysing a crystal structure is whether the structure is centrosymmetric or not. Because the distribution of the normalized structure factors varies depending on this criteria. According to *central limit theorem* (CLT) which was first introduced by A. J. C. Wilson (1949), if there exist n independent variables (x_1, x_2, \dots, x_n) distributed identically and randomly, the mean (μ) and variance (σ^2) are the same for each variable. Then, the sum of the variables is given as follows:

$$S_n = \sum_{j=1}^n x_j \quad (3.43)$$

When the mean and variance are considered as $\mu_n = n\mu$ and $\Sigma_n = n\sigma^2$ the *probabilistic distribution function* (abbreviated as *pdf*) of the sum S_n for $n \gg 1$,

$$p(S_n) \approx \frac{1}{\sqrt{2\pi\Sigma_n}} \exp\left[-\frac{S_n - \mu_n}{2\Sigma_n}\right] \quad (3.44)$$

The *pdf* of the structure factor F can be calculated by using the theorem. If a crystal structure is centrosymmetric and the origin is the center of symmetry then, the structure factor can be written as given in Eq. (3.45):

$$F = 2 \sum_{j=1}^{N/2} f_j \cos(2\pi\mathbf{G} \cdot \mathbf{r}_j) \quad (3.45)$$

After some mathematical operations the *pdf* of the $|F|$ is,

$$p_c(|F|) \approx \sqrt{\frac{2}{\pi\Sigma}} \exp\left(-\frac{|F|^2}{2\Sigma}\right) \quad (3.46)$$

where p_c represents the probability density function for *centrosymmetric* structures.

By the same way, the *pdf* of the normalized structure factor is calculated, however only the resultant equation (Eq. (3.47)) will be given in this thesis.

$$p_c(|E|) \approx \sqrt{\frac{2}{\pi}} \exp\left(-\frac{|E|^2}{2}\right) \quad (3.47)$$

For *non-centrosymmetric* (or shortly, *acentric*) structures the pdfs of $|F|$ and $|E|$ are,

$$p_a(|F|) \approx \frac{2|F|}{\Sigma} \exp\left(-\frac{|F|^2}{\Sigma}\right) \quad (3.48)$$

$$p_a(|E|) \approx 2|E| \exp(-|E|^2) \quad (3.49)$$

where p_a represents the probability density function for *acentric* structures. Eqns. (3.47) and (3.49) are depicted in Fig. (3.8) that shows how the values of $p(|E|)$ change with increasing values of $|E|$.

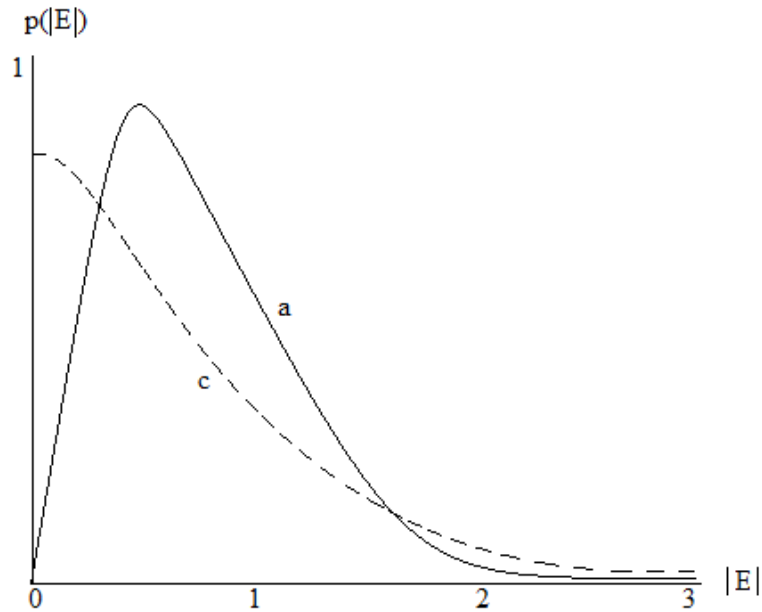


Figure 3.8 The probabilistic density function $p(|E|)$ decreases parabolically while $|E|$ increases. In the graphic, curve-c and curve-a represent the pdfs of centric and acentric structures, respectively.

Table 3.1 Various $|E|$ values depending on the crystal structures with different symmetries.

Average	Acentric	Centric
$\langle E \rangle$	0.886	0.798
$\langle E ^2 \rangle$	1.000	1.000
$\langle E^2 - 1 \rangle$	0.736	0.968

The symmetry group of a crystal structure can be determined by using the numerical values of the normalized structure factors $|E|^2$ that are given in Table 3.1. However, the average of the $|E|^2$ is 1.000 for both of the crystal structures. Therefore, it is not possible to determine the symmetry group of a structure by using $\langle |E|^2 \rangle$ values (Luger, 1980). But $\langle |E^2 - 1| \rangle$ can give information about the symmetry group. If a crystal contains heavy atoms sitting in the special positions (which mean the locations of some symmetry elements of a unit cell are fixed relative to other symmetry elements in the unit cell) or it is a twin crystal, then the value of $\langle |E^2 - 1| \rangle$ decreases.

3.4.2.2 Fundamental Inequalities

As discussed previously, the first inequalities were derived by Harker and Kasper in 1948 and they were convenient for determination of the phases of structure factors from the amplitudes of the highest intensities for centrosymmetric crystal structures. Harker and Kasper had managed this by using *Schwarz inequality* which is given by Eq. (3.50) where a_j and b_j are real or complex numbers.

$$\left| \sum_{j=1}^N a_j b_j \right|^2 \leq \left(\sum_{j=1}^N |a_j|^2 \right) \left(\sum_{j=1}^N |b_j|^2 \right) \quad (3.50)$$

The unitary structure factor $U_{\mathbf{h}}$ can be rewritten as given in Eq. (3.51)

$$U_{\mathbf{h}} = \sum_{j=1}^N u_j \cos(2\pi \mathbf{h} \cdot \mathbf{r}_j) \quad (3.51)$$

where $\sum_{j=1}^N u_j = 1$. Now, assume that $a_j = \sqrt{u_j}$ and $b_j = \sqrt{u_j} \exp(2\pi i \mathbf{G} \cdot \mathbf{r}_j)$. By means of Eq. (3.50) and the assumptions for a_j and b_j we obtain Eq. (3.52) for the unitary structure factor.

$$U_{\mathbf{h}}^2 \leq 1/2 [1 + U_{2\mathbf{h}}^2] \quad (3.52)$$

Eq. (3.52) is true if and only if the $U_{2\mathbf{h}}$ is positive, otherwise the inequality fails (Shmueli, 2007). One can decide where most atoms site in a unit cell by the signs. Thus, the signs can be added into the inequalities of the unitary structure factors as follows:

$$[|U_{\mathbf{h}}| + |U_{\mathbf{k}}|]^2 \leq \frac{1}{2} [1 + s_{\mathbf{h}} s_{\mathbf{k}} s_{\mathbf{h}+\mathbf{k}} |U_{\mathbf{h}+\mathbf{k}}|] [1 + s_{\mathbf{h}} s_{\mathbf{k}} s_{\mathbf{h}-\mathbf{k}} |U_{\mathbf{h}-\mathbf{k}}|] \quad (3.53)$$

In this equation $s_{\mathbf{h}}$ is the sign of $U_{\mathbf{h}}$ or more explanatory, represents the sign of the reflection travelling on \mathbf{h} direction. In case the whole U terms are sufficiently large, we have

$$s_{\mathbf{h}} s_{\mathbf{k}} s_{\mathbf{h}+\mathbf{k}} = +1 \quad (3.54a)$$

$$s_{\mathbf{h}} s_{\mathbf{k}} s_{\mathbf{h}-\mathbf{k}} = +1 \quad (3.54b)$$

Similarly, if $U_{2\mathbf{h}}$ is sufficiently large, then the sign $s_{2\mathbf{h}}$ will be positive. If some unknown phases remain at the further steps of the phase determination process, the below equation can be used.

$$s_{\mathbf{h}} = \sum_{\mathbf{k}} s_{\mathbf{k}} s_{\mathbf{h}-\mathbf{k}} \quad (3.55)$$

Harker-Kasper inequalities were regenerated by Karle and Hauptman in 1950 in order to reduce the limitations of them. Hence, the determinant D in Eq. (3.32), was written for the unitary structure factors as follows:

$$D = \begin{vmatrix} U_0 & U(\mathbf{h}_1) & \cdots & U(\mathbf{h}_n) \\ U(-\mathbf{h}_1) & U_0 & \cdots & U(\mathbf{h}_n - \mathbf{h}_1) \\ U(-\mathbf{h}_2) & U(\mathbf{h}_1 - \mathbf{h}_2) & \cdots & U(\mathbf{h}_n - \mathbf{h}_2) \\ \vdots & \vdots & \ddots & \vdots \\ U(-\mathbf{h}_n) & U(\mathbf{h}_1 - \mathbf{h}_n) & \cdots & U_0 \end{vmatrix} \geq 0 \quad (3.56)$$

When we take $n = 2$ and $\mathbf{h}_2 = 2\mathbf{h}_1$ in Eq. (3.56) for a centrosymmetric crystal structure, Eq. (3.52) is obtained, but the case $n = 2$ and $\mathbf{h}_2 \neq \mathbf{h}_1$ for the same structure, the determinant transforms into Eq. (3.57).

$$U(\mathbf{h}_1)U(\mathbf{h}_2)U(\mathbf{h}_1 - \mathbf{h}_2) \geq \frac{1}{2} [|U(\mathbf{h}_1)|^2 + |U(\mathbf{h}_2)|^2 + |U(\mathbf{h}_1 - \mathbf{h}_2)|^2 - 1] \quad (3.57)$$

In order to shorten Eq. (3.57), let us call the left side of \geq as A and the right side as B . Thus, for a non-centrosymmetric structure the determinant transforms into Eq. (3.58):

$$\cos[\phi(\mathbf{h}_1) - \phi(\mathbf{h}_2) - \phi(\mathbf{h}_1 - \mathbf{h}_2)] \geq \frac{B}{A} \quad (3.58)$$

Eq. (3.58) tells us that there appears a limitation on the combinations of the three phases.

3.4.2.3 Structure Invariants and Semi-invariants

In a unit cell, it is possible to select an origin more than one having the same surroundings. When the selected origin is the center of symmetry, then all the phases will be either 0° or 180° . If the position of the origin is shifted, the phases of the structure factors will change. The phases or their linear combinations that are independent from arbitrary origin selections are known as *structure (or phase) invariants*. However, the phases or their linear combinations that remain invariant with respect to some permissible shifts of the positions of origins are known as *structure semi-invariants* and they can be transformed into structure invariants by adding some symmetry equivalent phases (Giacovazzo et. al., 2002).

When a selected origin is shifted by a vector \mathbf{R} , then the new amplitude ($|F'(\mathbf{h})|$) and the phase ($\phi'(\mathbf{h})$) of the structure factor are given in Eqns. (3.59) and (3.60), respectively.

$$|F'(\mathbf{h})| = |F(\mathbf{h})| \quad (3.59)$$

$$\phi'(\mathbf{h}) = \phi(\mathbf{h}) - 2\pi(\mathbf{h} \cdot \mathbf{R}) \quad (3.60)$$

It is evident from Eq. (3.59) that the amplitude of the structure factor is a structure invariant. According to Eq. (3.60), $\phi(\mathbf{h})$ is a structure invariant only if $\mathbf{h} = 0$. The multiplication of the structure factors is given with Eq. (3.61).

$$\prod_{j=1}^n F'(\mathbf{h}_j) = \left(\prod_{j=1}^n F(\mathbf{h}_j) \right) \exp[-2\pi i(\mathbf{h}_1 + \mathbf{h}_2 + \dots + \mathbf{h}_n) \cdot \mathbf{R}] \quad (3.61)$$

This multiplication is a structure invariant if the below condition is satisfied:

$$\mathbf{h}_1 + \mathbf{h}_2 + \dots + \mathbf{h}_n = 0$$

Table 3.2 shows some structure invariants obtained by means of Eq. (3.61) under required conditions.

Table 3.2 Some structure invariants.

n	<i>Required condition</i>	<i>Structure invariant</i>
1	–	F(000)
2	$\mathbf{h}_1 + \mathbf{h}_2 = 0$	$[F(\mathbf{h})]^2$
3	$\mathbf{h}_1 + \mathbf{h}_2 + \mathbf{h}_3 = 0$	Triplet invariant
4	$\mathbf{h}_1 + \mathbf{h}_2 + \mathbf{h}_3 + \mathbf{h}_4 = 0$	Quartet invariant

The triplet and quartet invariants in Table 3.2 are given by Eqns. (3.62) and (3.63), respectively.

$$F(\mathbf{h}_1)F(\mathbf{h}_2)F(-\mathbf{h}_1 - \mathbf{h}_2) = |F(\mathbf{h}_1)F(\mathbf{h}_2)F(-\mathbf{h}_1 - \mathbf{h}_2)| e^{i[\phi(\mathbf{h}_1)+\phi(\mathbf{h}_2)-\phi(\mathbf{h}_1+\mathbf{h}_2)]} \quad (3.62)$$

$$F(\mathbf{h}_1)F(\mathbf{h}_2)F(\mathbf{h}_3)F(-\mathbf{h}_1 - \mathbf{h}_2 - \mathbf{h}_3) = |F(\mathbf{h}_1)F(\mathbf{h}_2)F(\mathbf{h}_3)F(-\mathbf{h}_1 - \mathbf{h}_2 - \mathbf{h}_3)| e^{i[\phi(\mathbf{h}_1)+\phi(\mathbf{h}_2)+\phi(\mathbf{h}_3)-\phi(\mathbf{h}_1+\mathbf{h}_2+\mathbf{h}_3)]} \quad (3.63)$$

3.4.2.4 Three-Phase Invariant

When we take $\mathbf{h}_1 = 0$, $\mathbf{h}_2 = \mathbf{h}$ and $\mathbf{h}_3 = \mathbf{k}$ in Eq. (3.56) to transform the determinant D into a third-order determinant, we obtain Eq. (3.64),

$$D_3 = \begin{vmatrix} 1 & U(\mathbf{h}) & U(\mathbf{k}) \\ U(-\mathbf{h}) & 1 & U(-\mathbf{h} + \mathbf{k}) \\ U(-\mathbf{k}) & U(-\mathbf{k} + \mathbf{h}) & 1 \end{vmatrix} \geq 0 \quad (3.64)$$

where D_3 represents the third-order determinant. When the above determinant is expanded, we have Eq. (3.65) that is similar to Eq. (3.57).

$$D_3 = 1 - |U_{\mathbf{h}}|^2 - |U_{\mathbf{k}}|^2 - |U_{\mathbf{h}-\mathbf{k}}|^2 + 2|U_{\mathbf{h}}U_{\mathbf{k}}U_{\mathbf{h}-\mathbf{k}}|\cos\phi_{\mathbf{h},\mathbf{k}} \geq 0 \quad (3.65)$$

In this equation $\phi_{\mathbf{h},\mathbf{k}} = \phi_{\mathbf{h}} - \phi_{\mathbf{k}} - \phi_{\mathbf{h}-\mathbf{k}}$ and only the last term on the right side depends on the phase. If the values of the three unitary structure factors approximate to 1, then $\phi_{\mathbf{h},\mathbf{k}}$ must be zero (Eq. (3.66)).

$$\cos(\phi_{\mathbf{h}} - \phi_{\mathbf{k}} - \phi_{\mathbf{h}-\mathbf{k}}) \geq 0 \quad (3.66)$$

The terms in the parentheses must be zero to satisfy the inequality hence, we have Eq. (3.67).

$$\phi_{\mathbf{h}} \approx \phi_{\mathbf{k}} + \phi_{\mathbf{h}-\mathbf{k}} \quad (3.67)$$

3.4.2.5 The Sayre Equation and Tangent Formula

Another method known as *the squaring method* for phase determination was presented by D. Sayre (1952). The method is based on two assumptions:

- *A crystal structure is composed of like atoms with spherical symmetry and identical isotropic displacement parameters.*
- *There is a hypothetical crystal structure that has a squared electron density. The positions of atomic peaks are the same in both structures.*

The first assumption holds for organic crystals that contain C, H, N, O atoms. Fig. (3.9) shows the atomic peaks obtained for such a crystal by Sayre (1952).

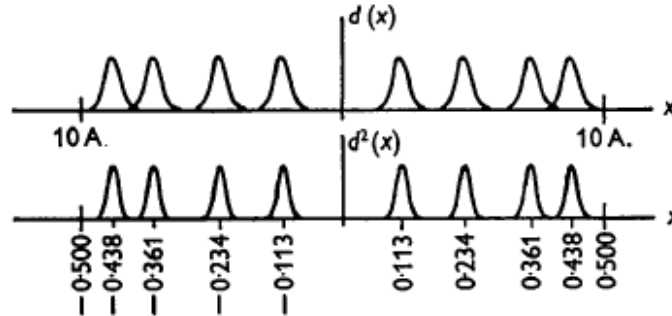


Figure 3.9 The unit cell of a one-dimensional crystal composed of identical and non-overlapping atoms, showing the similarity between $d(x)$ and $d^2(x)$.

According to the assumptions described above, one can write the structure factor of a crystal containing similar atoms as follows:

$$F_{\mathbf{h}} = f_{\mathbf{h}} \sum_{j=1}^N \exp(2\pi i \mathbf{h} \cdot \mathbf{r}_j) \quad (3.68)$$

where $f_{\mathbf{h}}$ is the *general atomic structure factor* that is same for a crystal consisting of similar atoms. One can write the structure factor as given in Eq. (3.69) for a projected structure which assumed to have a squared electron density where $g_{\mathbf{h}}$ is the general atomic structure factor of this structure.

$$F_{\mathbf{h}}^s = g_{\mathbf{h}} \sum_{j=1}^N \exp(2\pi i \mathbf{h} \cdot \mathbf{r}_j) \quad (3.69)$$

The relation between the structure factors in Eqns. (3.68) and (3.69) can be written simply,

$$F_{\mathbf{h}} = \left(\frac{f_{\mathbf{h}}}{g_{\mathbf{h}}} \right) F_{\mathbf{h}}^s \quad (3.70)$$

The electron density function at any \mathbf{r} for the real crystal is described by Eq. (3.71) which we discussed in the previous sections, while the squared electron density function for the hypothetical crystal is given by Eq. (3.72).

$$\rho(\mathbf{r}) = \frac{1}{V} \sum_{h=0}^{\infty} F_{\mathbf{h}} \exp(-2\pi i \mathbf{h} \cdot \mathbf{r}) \quad (3.71)$$

$$\rho^2(\mathbf{r}) = \frac{1}{V^2} \sum_{h=0}^{\infty} \sum_{h'=0}^{\infty} F_{\mathbf{h}} F_{\mathbf{h}'} \exp[-2\pi i (\mathbf{h} + \mathbf{h}') \cdot \mathbf{r}] \quad (3.72)$$

Here, V is the volume of unit cell. By taking $\mathbf{h} + \mathbf{h}' = \mathbf{H}$ and $\mathbf{K} = \mathbf{h}'$ in Eq. (3.72), we obtain Eq. (3.73).

$$\rho^2(\mathbf{r}) = \frac{1}{V^2} \sum_{\mathbf{H}} \sum_{\mathbf{K}} F_{\mathbf{K}} F_{\mathbf{H}-\mathbf{K}} \exp(-2\pi i \mathbf{H} \cdot \mathbf{r}) \quad (3.73)$$

Besides this, Eq. (3.73) can be rewritten in terms of the structure factor of projected structure as follows:

$$\rho^2(\mathbf{r}) = \frac{1}{V} \sum_{\mathbf{H}} F_{\mathbf{H}}^s \exp(-2\pi i \mathbf{H} \cdot \mathbf{r}) \quad (3.74)$$

Equations (3.73) and (3.74) give the same squared electron density thus, when we equate them to each other,

$$\frac{1}{V^2} \sum_{\mathbf{H}} \sum_{\mathbf{K}} F_{\mathbf{K}} F_{\mathbf{H}-\mathbf{K}} \exp(-2\pi i \mathbf{H} \cdot \mathbf{r}) = \frac{1}{V} \sum_{\mathbf{H}} F_{\mathbf{H}}^s \exp(-2\pi i \mathbf{H} \cdot \mathbf{r})$$

$$F_{\mathbf{H}}^s = \frac{1}{V} \sum_{\mathbf{K}} F_{\mathbf{K}} F_{\mathbf{H}-\mathbf{K}}$$

and make use of Eq. (3.70), we finally obtain the *Sayre equation*:

$$F_{\mathbf{H}} = \frac{f_{\mathbf{h}}}{g_{\mathbf{h}} V} \sum_{\mathbf{K}} F_{\mathbf{K}} F_{\mathbf{H}-\mathbf{K}} \quad (3.75)$$

where $f_{\mathbf{h}}/g_{\mathbf{h}}$ represents the factor which states the change in atomic shape also known as *shape factor* (Shmueli, 2007). In one- and two-dimensions the original forms of Eq. (3.75) are given by the following equations:

$$\sum_{\mathbf{p}} F(\mathbf{p}) F(\mathbf{h} - \mathbf{p}) = l S(\mathbf{h}) F(\mathbf{h}) \quad (3.75a)$$

$$\sum_{\mathbf{p}} \sum_{\mathbf{q}} F(\mathbf{p}, \mathbf{q}) F(\mathbf{h} - \mathbf{p}, \mathbf{k} - \mathbf{q}) = a S(\mathbf{h}, \mathbf{k}) F(\mathbf{h}, \mathbf{k}) \quad (3.75b)$$

Here l and a are the length and area of the unit cell of the projected crystal and $S(\mathbf{h})$ and $S(\mathbf{h}, \mathbf{k})$ are the shape factors in one- and two-dimension respectively which are identical to $f_{\mathbf{h}}/g_{\mathbf{h}}$. The equations (3.75a) and (3.75b) are valid whether or not the

crystal structure possesses inversion symmetry (Sayre, 1952). If the real and imaginary parts of the structure factor given in Eq. (3.75) are proportioned, we obtain

$$\tan[\phi(\mathbf{h})] = \frac{\sum_{\mathbf{K}} |F_{\mathbf{K}} F_{\mathbf{H}-\mathbf{K}}| \sin[\phi_{\mathbf{K}} + \phi_{\mathbf{H}-\mathbf{K}}]}{\sum_{\mathbf{K}} |F_{\mathbf{K}} F_{\mathbf{H}-\mathbf{K}}| \cos[\phi_{\mathbf{K}} + \phi_{\mathbf{H}-\mathbf{K}}]} \quad (3.76)$$

In this equation the structure factor F is replaced by the normalized structure factor E in order to obtain the *tangent equation* (Eq. (3.77)) which is another phase determination formula of acentric structures (Karle & Hauptman, 1956).

$$\tan[\phi(\mathbf{h})] = \frac{\sum_{\mathbf{K}} |E_{\mathbf{K}} E_{\mathbf{H}-\mathbf{K}}| \sin[\phi_{\mathbf{K}} + \phi_{\mathbf{H}-\mathbf{K}}]}{\sum_{\mathbf{K}} |E_{\mathbf{K}} E_{\mathbf{H}-\mathbf{K}}| \cos[\phi_{\mathbf{K}} + \phi_{\mathbf{H}-\mathbf{K}}]} \quad (3.77)$$

3.4.2.6 Figures of Merit

At the end of the phase determination process, lots of phase sets are obtained. The correct phase set is determined by comparing the calculated electron density maps (hereafter abbreviated as E-maps) with the expected ones. However, it is a time-consuming and troublesome operation to calculate and comment E-maps for each phase set. For this reason, making use of some proper functions that allow us to estimate the accuracy of the phase sets is more convenient. These functions are referred to as *Figures of Merit (FOM)* and expected to take a minimum or a maximum value for a correct phase set. We can summarize the FOM functions as follows:

- *ABSFOM*: Known as *absolute figure of merit*. This function gives information about the consistency of triplet relations and is given with Eq. (3.78).

$$\text{ABSFOM} = \frac{\sum_{\mathbf{h}} (\alpha_{\mathbf{h}} - \langle \alpha_{\mathbf{h}} \rangle_{\text{ran}})}{\sum_{\mathbf{h}} (\langle \alpha_{\mathbf{h}} \rangle - \langle \alpha_{\mathbf{h}} \rangle_{\text{ran}})} \quad (3.78)$$

In this equation $\alpha_{\mathbf{h}}$ is a parameter of the Karle and Karle (1966) distribution (Eq. (3.79)), $\langle \alpha_{\mathbf{h}} \rangle$ is the expected value of $\alpha_{\mathbf{h}}$ while $\langle \alpha_{\mathbf{h}} \rangle_{ran}$ is the expected value of $\alpha_{\mathbf{h}}$ when the phases are supposed to be randomly distributed (Cascarano, Giacovazzo & Viterbo, 1987).

$$\alpha_{\mathbf{h}} = \left[\left(\sum_{j=1}^n \frac{2|E_{\mathbf{h}}E_{\mathbf{k}}E_{\mathbf{h}+\mathbf{k}}|}{\sqrt{N}} \cos\theta_j \right)^2 + \left(\sum_{j=1}^n \frac{2|E_{\mathbf{h}}E_{\mathbf{k}}E_{\mathbf{h}+\mathbf{k}}|}{\sqrt{N}} \sin\theta_j \right)^2 \right]^{1/2} \quad (3.79)$$

In the equation above, $\theta_j = \theta_{k_j} + \theta_{h-k_j}$. Eq. (3.78) is often reduced to MABS-function given below (Germain, Main & Woolfson, 1970):

$$\text{MABS} = \frac{\sum_{\mathbf{h}} \alpha_{\mathbf{h}}}{\sum_{\mathbf{h}} \langle \alpha_{\mathbf{h}} \rangle} \quad (3.80)$$

For a random phase set the ABSFOM or MABS function must be zero, while it varies between 0.9 and 1.3 for a correct phase set in practice. Thus, the values in this range indicate how well the observed and calculated sets overlap.

- *NQUAL*: Measures the consistency between $\alpha_{\mathbf{h}}$ and $\eta_{\mathbf{h}}$ which is defined in Eq. (3.81) and *NQUAL*-function is given by Eq. (3.82). For a correct phase set the value of the function is expected to be -1 .

$$\eta_{\mathbf{h}} = \frac{1}{N} |E_{\mathbf{h}}| \sum_{\mathbf{k}, \mathbf{l}} E_{\mathbf{k}} E_{\mathbf{l}} E_{\mathbf{h}-\mathbf{k}-\mathbf{l}} \quad (3.81)$$

$$\text{NQUAL} = \frac{\sum_{\mathbf{h}} |\alpha_{\mathbf{h}} \eta_{\mathbf{h}}|}{\sum_{\mathbf{h}} |\alpha_{\mathbf{h}}| |\eta_{\mathbf{h}}|} \quad (3.82)$$

- R_{α} : This function is known as *residual figure of merit* and determines the amount of deviation from the expected value of each triplet (Eq. (3.83)). R_{α} must be small for a correct phase set.

$$R_\alpha = \frac{\sum_h |\alpha_h - \langle \alpha_h \rangle|}{\sum_h \langle \alpha_h \rangle} \quad (3.83)$$

- Ψ_0 : This function is known as *psi-zero figure of merit* and first introduced by Cochran and Douglas (1957).

$$\Psi_0 = \frac{\sum_h |\sum_{h'} E_{h'} E_{h-h'}|}{\sum_h [\sum_{h'} |E_{h'} E_{h-h'}|^2]^{1/2}} \quad (3.84)$$

In Eq. (3.84), the summation over h (Σ_h) includes weak reflections that have small E_h values while the summation over h' (Σ_k) includes strong reflections whose phases have been determined. In case the phase sets of E_h and $E_{h'}$ are correct, then h' tends to be small, otherwise it will be larger.

3.4.2.7 Combined Figures of Merit (CFOM)

Instead of evaluating the FOM functions for each phase set, another function known as CFOM (*combined figures of merit*) produced by combining the coefficients of different FOM functions is used in order to obtain the correct phase set. The function varies based on the software used.

3.5 Electron Density Map (E-map)

The last stage of the structure solution is obtaining a three-dimensional image of the crystal. If the amplitudes and phases of the structure factors are known, one can calculate the electron density function $\rho(x, y, z)$ and thereby plot a map in three-dimension known as electron density map (E-map) by means of the values of ρ . E-maps are calculated by using the phase sets that have the best values of FOM-functions. The maps are obtained by using the normalized structure factors (E_s) instead of F_s . The reason is that the peaks on the map are sharper than those of F_s . For this reason, they are called *E-maps* (Fig. 3.10).

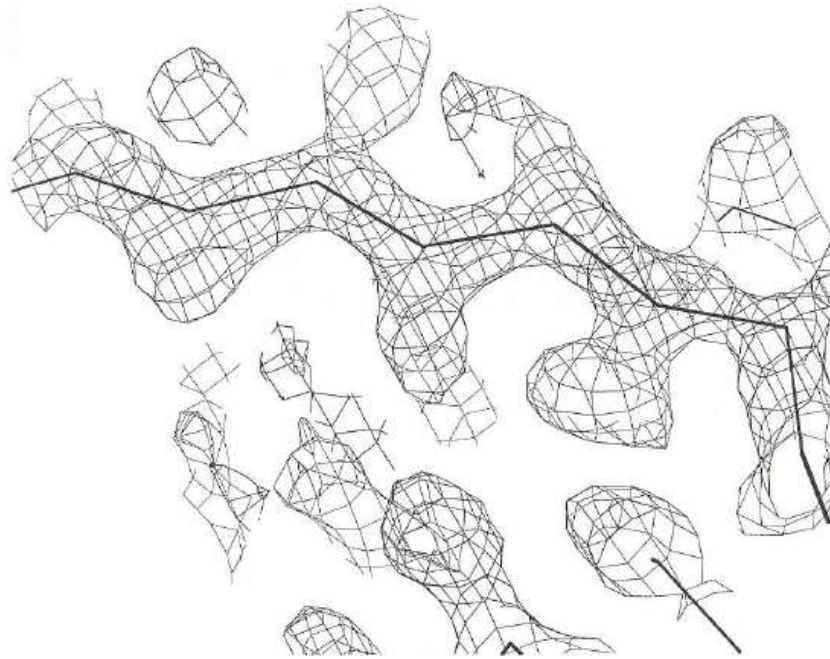


Figure 3.10 E-map presentation.

Each peak on E-maps represents the positions of atoms in a unit cell. The bond lengths and bond angles can be obtained by determining the types of the atoms and calculating the diameters of atoms within the unit cell. But in some cases no peaks are observed where some atoms should be, resulting from the systematic absences that mean additional reciprocal lattice points or some symmetry elements (glide and/or screw symmetry) within a crystal cause some reflected beams to be absent. In such a case, *difference Fourier method* is used in order to find the missing atoms on the map that will be explained in the following chapter.

CHAPTER FOUR

CRYSTAL STRUCTURE REFINEMENT

4.1 Introduction

During the crystal structure solution process the missing phase information is determined in order to obtain the structure accurately. For this reason, some corrections are applied to the diffracted intensity data, E-maps are produced by obtaining the missing phase, thereby the positions of atoms within the crystal lattice are tried to be determined.

After these steps, one has obtained atomic coordinates for all non-hydrogen atoms. However, some of the coordinates can be incorrect or some atom types cannot be assigned at all. Furthermore, structural distortions, positions of lighter atoms have to be determined. Thus, the last but the most important step that a crystallographer obtains an accurate structure is called *refinement*. According to Müller, Herbst-Irmer, Spek, Schneider & Sawaya (2006), “Depending on the structure, this can be a short highway to happiness or a long and rugged road through pain and sorrow” (chap. 2).

During the refinement process, the consistency between the calculated and observed structures is investigated. One can understand whether the model structure has been defined accurately or not by following the changes in the values of some parameters which depend on the molecular structure of the sample crystal.

By refining the structure, one can obtain the locations of hydrogen atoms, the thermal motions and their orientations within the crystal structure.

The most common two methods used in the refinement are:

- *Difference Fourier Method*
- *Least-squares Method*

4.2 Difference Fourier Method

By using the difference Fourier method, the difference between the calculated and observed electron densities is examined. The electron density function (ρ) is calculated by means of Eq. (3.9) as we discussed in chapter three.

$$F_{hkl} = \sum_{j=1}^N f_j e^{i2\pi(hx_j + ky_j + lz_j)} \quad (3.9)$$

Hence, the electron density functions can be rewritten by Eq. (3.26) as follows,

$$\rho_{\text{obs}}(x, y, z) = \frac{1}{V} \sum_h \sum_k \sum_l F_{\text{obs}} \exp(-2\pi i(hx + ky + lz)) \quad (4.1)$$

$$\rho_{\text{cal}}(x, y, z) = \frac{1}{V} \sum_h \sum_k \sum_l F_{\text{cal}} \exp(-2\pi i(hx + ky + lz)) \quad (4.2)$$

where the indices ‘*obs*’ and ‘*cal*’ represent *observed* and *calculated*. When we calculate the difference of Eqns. (4.1) and (4.2) we have

$$\Delta\rho(\mathbf{r}) = \rho_{\text{obs}}(\mathbf{r}) - \rho_{\text{cal}}(\mathbf{r}) \quad (4.3)$$

$$\Delta\rho(x, y, z) = \frac{1}{V} \sum_h \sum_k \sum_l (F_{\text{obs}} - F_{\text{cal}}) \exp[-2\pi i(hx + ky + lz)] \quad (4.4)$$

where $\Delta\rho$ represents the difference of the electron densities. Under the assumption that the phases of the calculated and observed structures are identical, we can rewrite Eq. (4.4) as given below:

$$\Delta\rho(x, y, z) = \frac{1}{V} \sum_h \sum_k \sum_l (F_{\text{obs}} - F_{\text{cal}}) \exp[-2\pi i(hx + ky + lz) + i\phi_{\text{cal}}] \quad (4.5)$$

By the aid of Eq. (4.5) which is known as the *difference Fourier synthesis*, one can plot the E-map of the structure and determine the deficiencies of the calculated model by examining the map.

If there is a missing atom in the calculated model, $\rho_{\text{cal}}(\mathbf{r})$ will be zero and no peak will be observed at the corresponding position, while $\rho_{\text{obs}}(\mathbf{r})$ is maximum and shows a peak. As a result, a peak will be observed at the same position on the E-map of the difference Fourier synthesis ($\Delta\rho$ -map). When the missing atom is placed to the correct position where it stands in the real structure, then $\rho_{\text{cal}}(\mathbf{r}) \approx \rho_{\text{obs}}(\mathbf{r})$ and therefore, $\Delta\rho(\mathbf{r}) \approx 0$, that means no peak will occur in the $\Delta\rho$ -map at that position. Omitting the thermal vibrations of atoms also cause an error in $\Delta\rho$ -map. The peak of the real structure becomes smaller and broader than that of calculated structure and a negative peak will occur in the map (Fig. 4.1-(a)).

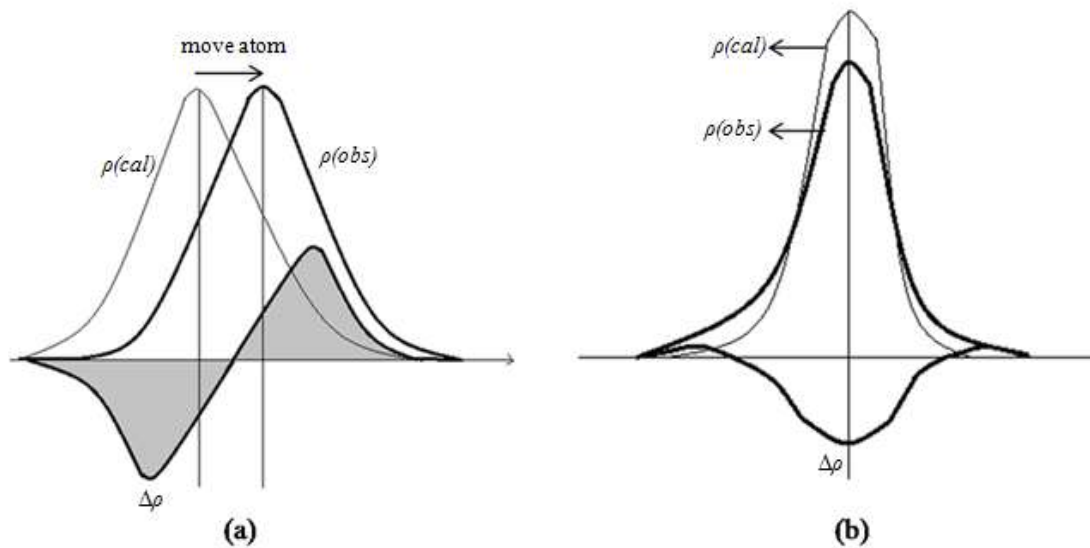


Figure 4.1 The atom, misplaced in the calculated model, is moved to the actual position (a), besides this neglecting the thermal motions causes $\Delta\rho$ to be negative (b).

On the other hand, if the thermal vibration of an atom is given with a value that is higher than normal, then a positive-small peak will occur in the map.

When an atom is misplaced in the calculated model, $\rho_{\text{cal}}(\mathbf{r})$ will be close to a negative minimum value, while $\rho_{\text{obs}}(\mathbf{r})$ is positive maximum in the $\Delta\rho$ -map. For this

reason, the position of the misplaced atom is shifted in order to diminish the difference (Fig. 4.1-(b)). If the calculated model fully matches with the real structure, then the difference synthesis ($\Delta\rho$) will be zero.

4.3 The Method of Least-Squares

The least-squares method that was first created by C. F. Gauss in 1795, is a mathematical approach for finding the best straight line through a given set of points by minimizing the sum of the squares of the remaining points from the curve (Fig. 4.2).

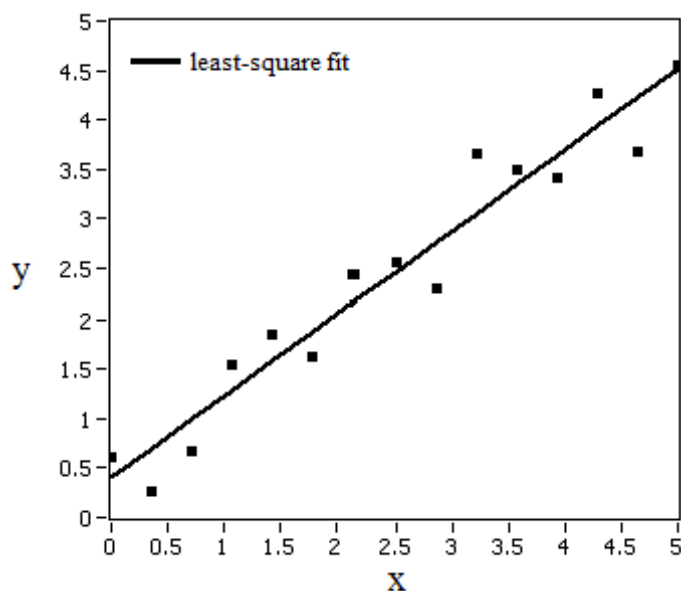


Figure 4.2 The method of least squares gives the best-fitting curve to a given set of points.

In crystallography, the method, first used by Hughes (1941), is applied for increasing the sensitivity of the position and isotropic displacement parameters obtained from structure solution by minimizing the sum of the squares of the structure factors F_{obs} and F_{cal} during the refinement process (Eq. (4.6)).

$$M = \sum w(F_{obs}^2 - F_{cal}^2)^2 \quad (4.6)$$

Eq. (4.6) can be rewritten as the sum of the amplitudes of the structure factors (Eq. (4.7)).

$$\mathbb{M} = \sum w(|F_{\text{obs}}| - |F_{\text{cal}}|)^2 \quad (4.7)$$

In the equations above, w is the weighting factor, presented by Cruickshank, Pilling, Bujosa, Lovell and Truter (1961), equals to $1/\sigma$ where σ is the *standard uncertainty* (or *elasticity*) showing the estimated deviation of a measurement. The calculated model is said to be the best for the real structure, if the function \mathbb{M} approaches to zero. Eq. (4.6) is the refinement against F^2 , while Eq. (4.7) corresponds refinement against $|F|$ that will be explained in the following subsection. Let us rewrite the calculated structure factor for a centrosymmetric crystal structure and assume that the temperature factor is isotropic (Eq. (4.8)),

$$F_{\text{cal}}(hkl) = \sum_{j=1}^{N/2} 2f_j \exp\left(-B_j \frac{\sin^2\theta}{\lambda^2}\right) \cos[2\pi(hx_j + ky_j + lz_j)] \quad (4.8)$$

For j th atom, the correct values of the parameters for observed structure factor are written as follows:

$$F_{\text{obs}}(hkl) = \sum_{j=1}^{N/2} 2f_j \exp\left(-\frac{(B_j + \Delta B_j) \sin^2\theta}{\lambda^2}\right) \times \cos\{2\pi[h(x_j + \Delta x_j) + k(y_j + \Delta y_j) + l(z_j + \Delta z_j)]\} \quad (4.9)$$

The difference between the two structure factors in Eqns. (4.8) and (4.9) is,

$$\Delta F_{hkl} = F_{\text{obs}}(hkl) - F_{\text{cal}}(hkl) \quad (4.10)$$

$$\Delta F_{hkl} = \sum_{j=1}^{N/2} \left(\frac{\partial F_{\text{cal}}}{\partial B_j} \Delta B_j + \frac{\partial F_{\text{cal}}}{\partial x_j} \Delta x_j + \frac{\partial F_{\text{cal}}}{\partial y_j} \Delta y_j + \frac{\partial F_{\text{cal}}}{\partial z_j} \Delta z_j \right) \quad (4.11)$$

Eq. (4.11) can be used for each reflection and the number of equalities is higher than the number of parameters in general.

The anisotropic thermal motions are given by six independent variables: $(U_{11}, U_{22}, U_{33}, U_{12}, U_{23}, U_{13})$ that are obtained from the determinant D which was described before. The first three variable shows the amount of vibration through three ellipsoidal axes perpendicular to each other while the remaining three showing the amount of deviation of the ellipsoidal axis with respect to the crystal axis. One can determine the number of parameters by a simple calculation. Suppose that there exist 10 anisotropically refined atoms in a molecule thus, this molecule will have $10 \times 6 = 60$ parameters. At this point, the least-squares method is activated and the number of the parameters is minimized.

The observed structure factors are adopted to be correct in practice. Hence, in order to ensure the best convergence between the real and calculated structures, Eq. (4.6) must be zero:

$$\mathbb{M} = \sum w(F_{\text{obs}}^2 - F_{\text{cal}}^2)^2 \approx 0 \quad (4.12)$$

The least-squares method is more advantageous than the difference Fourier method. The reason is that one can refine the temperature and scale factors by using this method. In addition, the number of position and isotropic displacement parameters obtained from direct methods or Patterson method are minimized by applying the method (Barut, 2010).

4.3.1 Refinement Against F^2

The refinement against $|F|$ -values causes problems. The reason is that measured intensities are directly related with the square magnitude of the structure factors, thus taking the square root of Eq. (4.7) leads to mathematical problems for weak or negative measured reflections. The only way in order to overcome the problem is setting the negative intensities to zero. But this will lead us lose the weak intensities,

thereby the information about the structure. By taking into account this problem and the relation between the measured intensity and the structure factor ($I \propto |F|^2$), the refinement against F^2 is preferred (Müller, Herbst-Irmer, Spek, Schneider & Sawaya, 2006).

4.4 Constraints and Restraints

“For every atom in the model that is located on a general position in the unit cell, there are three atomic coordinates and one or six atomic displacement parameters (one for isotropic, six for anisotropic models) to be refined” (Müller, Herbst-Irmer, Spek, Schneider & Sawaya, 2006, chap. 2). In order to determine a crystal structure accurately, we need additional parameters defining the position and orientation of a molecule within the crystal structure as well as atomic parameters. The reason of the need for additional information about the structure is the sheer number of parameters. Thus, constraints or restraints must be performed on the parameters to be refined.

In 1960s, performing least-squares method by using the diffraction data obtained had been a problem and it was debated whether to refine crystal structures by using constraints or restraints (Immirzi, 2009). Constraints are the invariable mathematical expressions while the restraints are variable under certain limits.

4.4.1 Constraints

The crystal structures consist of exactly known atom groups can be incorporated to the refinement process as *rigid groups* by fixing the bond lengths and bond angles of them. Thus, the refined parameters can be added into the least-squares equations by performing the required constraints on them.

Instead of refining the three positional parameters for each atom, one can select a *pivot atom* from the group and refine the three position and orientation parameters of that atom which reduces the number of parameters dramatically (Massa, 2004).

Constraints are produced by space-group symmetry relations and generally used for determining the positions of hydrogen atoms and displacement parameters. Resulting from the difficulty of determining the positions of hydrogen atoms from electron density maps, one can refine the structure including hydrogen atoms by constraining them to sit in the actual distances from the atom they will be bound to with isotropic displacement parameters or in other words, by placing the hydrogen atoms on geometrically calculated positions with constant bond lengths and bond angles.

Site occupancy factor is also refined by using constraints. If an atom is present at a certain site in every unit cell, which means there does not exist a disorder, then the factor is fixed to unity (Müller, Herbst-Irmer, Spek, Schneider & Sawaya, 2006).

4.4.2 Restraints

“Soft, flexible constraints (say restraints) may be imposed to some functions of the parameters in order to permit only realistic deviations of their values from fixed standard ones. These functions are used as supplementary observations” (Giacovazzo et. al., 2002, chap. 2). Possible bond lengths and bond angles can be added as additional data which we call *restraints*. Thus, the number of observed data increases. However there does not occur a decrease in the number of refined parameters.

In many cases, restraints are not required. If a crystal structure includes disorder or pseudo-symmetry or one has weak data, then the usage of restraints may be needed. If restraints are used when refining the structure, then the minimization function \mathbb{M} which was given by Eq. (4.6) changes its form and the new equation is written as follows:

$$\mathbb{M} = \sum \frac{1}{\sigma} \left[(F_{\text{obs}}^2 - F_{\text{cal}}^2)^2 + \frac{1}{\sigma} (R_{\text{obs}} - R_{\text{cal}})^2 \right] \quad (4.13)$$

Here, the weighting factor w is taken as $1/\sigma$ and R_{obs} and R_{cal} are the values of the target function calculated from structure parameters. In contrast to constraints, the values of additional data can be changed when using restraints, thereby one can determine the rate of restraints that will contribute the refinement process.

4.5 The Quality of a Refinement: Residual Parameters

There are some parameters which known as *residual parameters* or rather *R-factors* in order to see the consistency between the calculated and observed structures after the refinement process thus, these parameters should converge to minimum values during the refinement.

We can summarize the most commonly used ones as follows:

- *Reliability (R)-factor*: Also known as R_1 -factor and it gives the mean of the standard deviation of the calculated and observed structure factors and also depends on the quality of the collected data. This factor is based on the refinement against $|F|$. For an ideal model the R-factor is zero, but we can never reach to that value because of the random errors thus, for a good set of data, the R-factor must be lower than 0.06.

$$R = \frac{\sum_{\mathbf{h}} |F_{obs}(\mathbf{h})| - |F_{cal}(\mathbf{h})|}{\sum_{\mathbf{h}} |F_{obs}(\mathbf{h})|} \quad (4.14)$$

- *Weighted reliability (wR or wR_2)-factor*: Based on the squares of the structure factors. It is tried to reduce the effects of the data with low reliability on the refinement process. By taking into account the weighting factor w , we can write the equation below,

$$wR = \left\{ \frac{\sum_{\mathbf{h}} w [|F_{obs}(\mathbf{h})|^2 - |F_{cal}(\mathbf{h})|^2]^2}{\sum_{\mathbf{h}} w F_{obs}(\mathbf{h})^2} \right\}^{1/2} \quad (4.15)$$

For a good set of data, the wR -factor must be lower than 0.15.

- *Settlement (S)-factor*: Also known as GooF or GOF which means *goodness of fit*. Based on the number of observed reflections and the refined parameters. The values about 1 indicate a good result. If S is higher than 1, then one can say that the model is better than the collected data which means there is a problem. On the other hand, if S equals to 1, then we observe that the calculated and observed structures fully match as identical twins.

$$S = \text{GooF} = \left\{ \frac{\sum_{\mathbf{h}} w [|F_{\text{obs}}(\mathbf{h})|^2 - |F_{\text{cal}}(\mathbf{h})|^2]^2 }{m - n} \right\}^{1/2} \quad (4.16)$$

In Eq. (4.16) m and n represent the number of independent reflections and refined parameters, respectively.

4.6 Problems in Refinement

The atoms of a crystal structure can be determined from the difference electron density map and can be used in the refinement. Hydrogen atoms within the structure may not be determined by the map thus, they must be added to the correct positions externally. Before adding hydrogen atoms, displacement parameters are refined anisotropically, otherwise they are refined isotropically.

The estimated standard deviation and corrections of the coefficients of refined parameters are performed at the last stage of refinement process.

There are other problems in refinement that should not be overlooked: disorder and twinning. Thus, it must be taken into account whether the structure of sample crystal includes disorder that will be explained further, solvent molecules or twinning in order not to skip any information about the structure.

4.6.1 Disorder

In some cases, more than one molecule occupies the same position in an asymmetric unit of a crystal or the orientations of some atoms differ randomly in different unit cells. This is known as *disorder* which has different types as given below:

- *Substitutional Disorder*: The same position in two unit cells in a crystal is occupied by different atoms. This type of disorder occurs due to extremely large or small displacement parameters.
- *Positional Disorder*: One atom occupies more than one position in a single unit cell (*dynamic disorder*) or in two unit cells (*static disorder*) within a crystal.

In order to overcome the difficulty of disorder during the refinement, the electron density that spreads into a large volume is allocated in two different atomic positions (Sheldrick, 2008). Fig. (4.3) displays the disorder of a crystal atom.

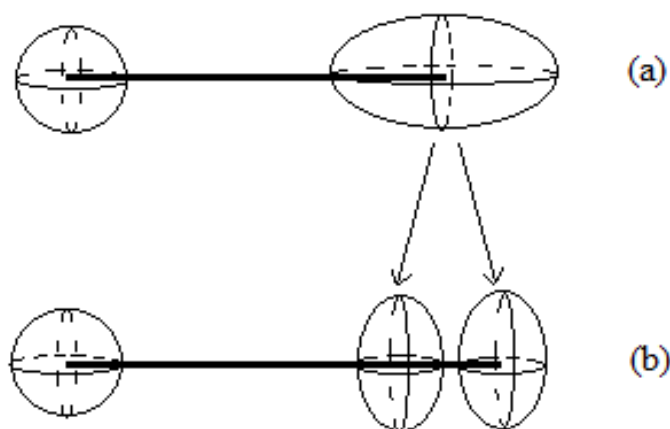


Figure 4.3 Disorder in a crystal structure before (a) and after the refinement (b).

In SHELXL software, one can refine the disordered atoms by using the command 'PART'.

4.6.2 Twinning

As we described in the Subsection 2.3.2, sometimes two or more crystals grow together sharing the same symmetry element which is called twin planes. The crystals that have such formation are called *twin crystals* (Fig. 4.4).

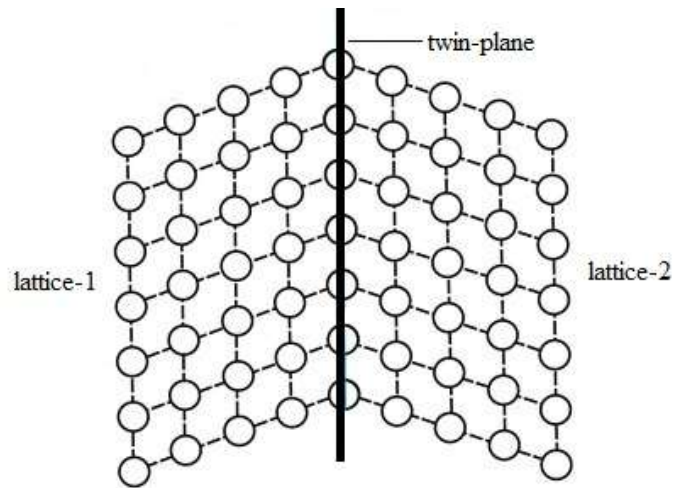


Figure 4.4 Twin crystal and the twinning plane.

One can understand that a crystal is a twin crystal by observing the mean values of variance given by $|E^2 - 1|$ that can be calculated by using the direct methods. For centric crystal structures this value is approximately 0.97 while it is 0.74 for acentric structures. Higher values of variance cause the difference in the collected intensities to become higher. For twin crystals, variance can be lower than what one expects. The reason is that each intensity on the diffraction pattern is the sum of two intensities in practice. Thus, a great care must be taken during the crystal structure solution and refinement processes.

The intensity data is not coherent for twin crystals thus, the whole intensity is the sum of two intensity components as given below:

$$|F_{\text{obs}}|^2 = m_1|F_1|^2 + m_2|F_2|^2 \quad (4.17)$$

where m_1 and m_2 are the parameters, used in the refinement, representing the fractions corresponding to each component.

There are some important signs that give alerts of twinning. For example, $F_{obs} \gg F_{cal}$, inconsistent systematic absences, trigonal or hexagonal space groups can be the signs of twin crystals. Additional information about twins was given in the Subsection 2.3.2 while discussing the selection of a single crystal.

CHAPTER FIVE

RESULTS AND DISCUSSION

A suitable crystal sample of the title compound $[\{\text{Rh}(\text{COD})\text{Cl}\}_2\text{L}]$ where L is 2,6-bis(1-pentamethylbenzyl-1-*H*-benzimidazole-2-yl) pyridine, was chosen for the crystallographic study and then placed on the goniometer head of an Agilent XCalibur X-Ray Diffractometer with EOS CCD detector. All diffraction measurements were performed at room temperature (293°K) within the θ range of $3.0 < \theta < 29.2$ and graphite monochromatized (graphite crystal monochromator $\lambda = 0.71073 \text{ \AA}$) Mo- K_{α} was used as radiation source. Absorption corrections were based on multiple scans. The title compound crystallizes in monoclinic cell setting with space group C12/c1.

The crystal structure was solved by using SHELXS-97 (Sheldrick, 1998). Direct methods using WinGX implementation (Farrugia, 1999) of SHELXS-97 were used to determine the structure. A total of 15,414 reflections were collected for $h_{min} = -36$, $h_{max} = 32$, $k_{min} = -12$, $k_{max} = 12$, and $l_{min} = -18$, $l_{max} = 29$. 6,812 reflections of the total 15,414 are unique while 4,524 of them satisfy the criterion for observed reflections ($I > 2\sigma(I)$).

The refinement of the structure was carried out by full-matrix least-squares techniques on the positional and anisotropic temperature parameters of the non-hydrogen atoms, or equivalently corresponding to 335 parameters using SHELXL-97 (Sheldrick, 1998) software. Hydrogen atoms were placed in the calculated positions and treated as riding atoms with C-H distances in the range 0.93-0.97 Å. The thermal ellipsoid plots were generated by using ORTEP-3 (Farrugia, 1997) and OLEX (Dolomanov, Blake, Champness & Schröder, 2003) softwares. The crystallographic data, the details of data collection and refinement of the title compound are given in Table 5.1. The selected bond distances and angles of the title complex are given in Tables 5.2.

Table 5.1 Crystallographic data, details of data collection and refinement of the title compound.

Chemical formula	$C_{61}H_{73}Cl_6N_5Rh_2$
Formula weight (M_r) (u)	1294.76
Crystal size (mm) / colour	0.127 x 0.328 x 0.409 / yellow
Cell setting / Space group	Monoclinic, C12/c1
Unit cell dimensions	$a = 26.8865(12) \text{ \AA}$ $b = 10.0794(4) \text{ \AA}$ $c = 23.4752(15) \text{ \AA}$ $\alpha = \gamma = 90^\circ, \beta = 110.681(6)^\circ$
Unit cell volume (\AA^3)	5951.8(5)
Number of molecules in units (Z)	4
F(000)	2664
Calculated density (D_x) (Mg.m^{-3})	1.4450(1)
Absorption coefficient (μ) (mm^{-1})	0.866
<i>Reflection Data</i>	
Measured reflections	15,414
Unique reflections	6,812
Observed reflections	4,524
Criterion for observed reflections	$I > 2\sigma(I)$
R_{int}	0.0268
Temperature ($^\circ\text{K}$)	293
$\theta_{\text{min}}/\theta_{\text{max}}$ ($^\circ$)	3.0 / 29.2
h, k, l values (from min. to max.)	$-36 \rightarrow -32, -12 \rightarrow 12, -18 \rightarrow 29$
Radiation used / wavelength (\AA)	$\text{MoK}_\alpha / 0.71073$
No. of reflections/parameters/restraints	6,812 / 335 / 0
<i>Refinement Details</i>	
Goof on F^2	1.031
Final R indices [$I > 2\sigma(I)$]	$R_1 = 0.0458, wR_2 = 0.1045$
R indices (all data)	$R_1 = 0.0830, wR_2 = 0.1195$
$\Delta\rho_{\text{max}}, \Delta\rho_{\text{min}}$ ($\text{e}/\text{\AA}^{-3}$)	0.581, -0.588

In this thesis, the crystal and molecular structure of $\{\text{Rh}(\text{COD})\text{Cl}\}_2\text{L}$ have been determined by single crystal X-ray diffraction method. The title compound is a dimetallic complex consisting of one half molecule and one dichloromethane solvent in the asymmetric unit as shown in Fig. (5.1).

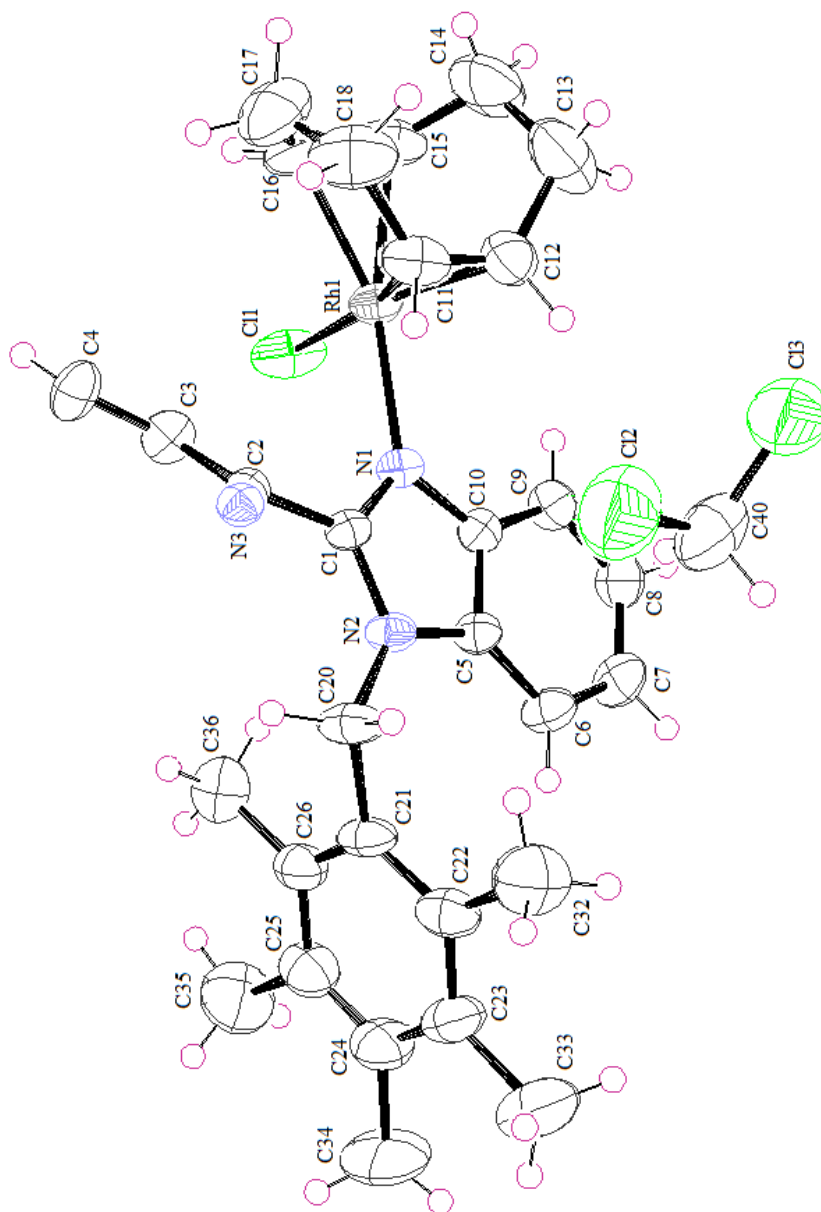


Figure 5.1 ORTEP-3 view of the title compound drawn with 50% probability.

The complete molecular structure is generated by the implementation of the crystallographic two-fold rotation axis that bisects the pyridine ring by crossing midway between N3 and C4 atoms which is illustrated in Fig. (5.2).

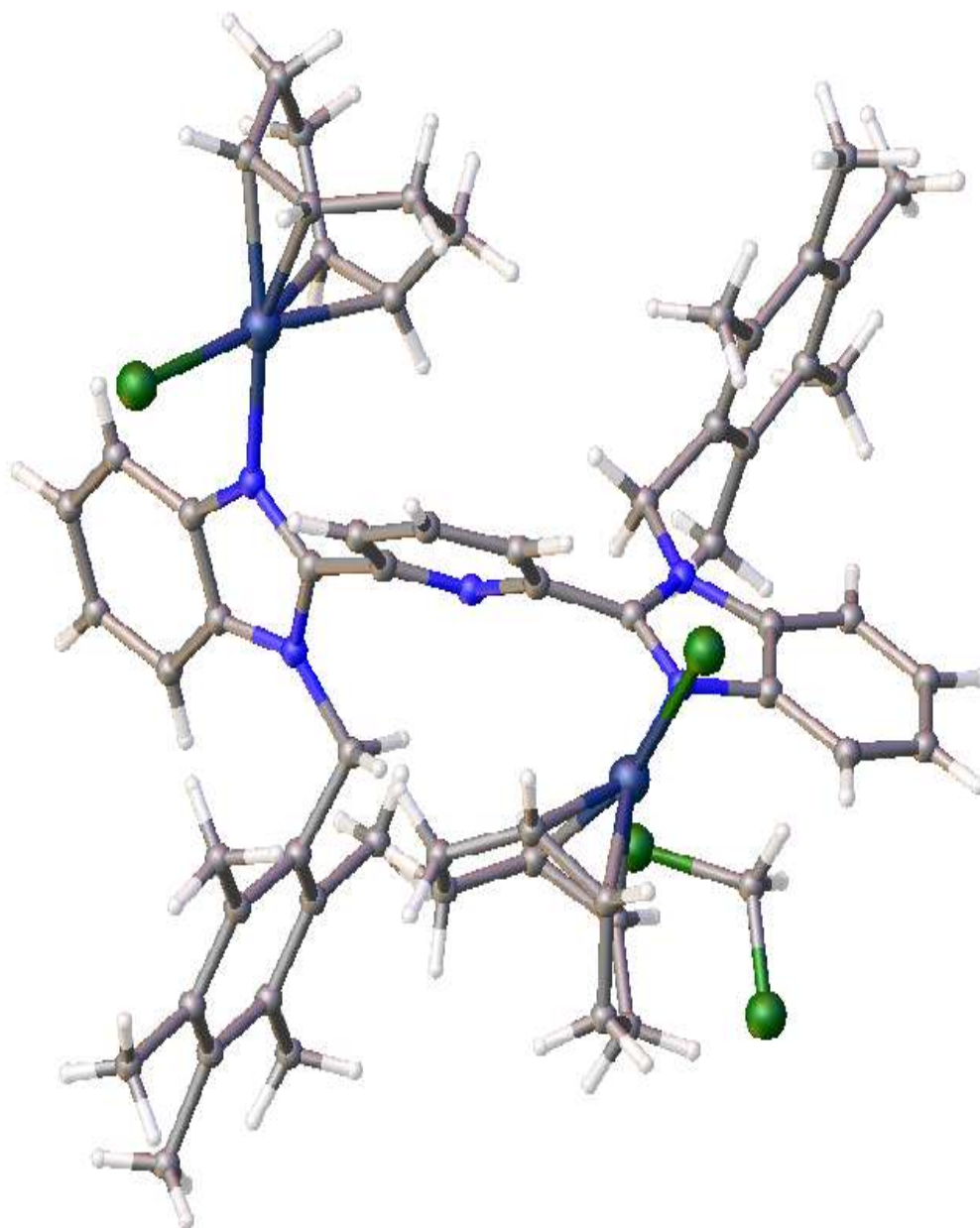


Figure 5.2 The complete view of the title compound in OLEX2 software.

Each benzimidazole ring connects to the [Rh(COD)Cl] units through the nitrogen atoms, thus the terdentate units act as bis-monodentate ligands in the compound (Bénech, Piguet, Bernardinelli, Bünzli & Hopfgartner, 2001). The bond distances and angles of carbene ring are in agreement with standard values (Allen et. al., 1987). The selected bond distances and angles of the title complex are given in Table 5.2.

Table 5.2 Selected bond distances (Å) and angles (°) of the title complex.

Atom label	Value	Atom label	Value
Rh1···Rh1	8.083	Rh1-C11	2.102(4)
Rh1-M1	2.010	Rh1-C12	2.091(4)
Rh1-M2	1.980	Rh1-C16	2.121(4)
Rh1-N1	2.102(3)	Rh1-C15	2.129(4)
Rh1-C11	2.3815(10)	N3-C2	1.338(4)
N1-C1	1.320(4)	C2-C3	1.387(5)
N1-C10	1.390(4)	C2-C1	1.475(4)
N2-C1	1.357(4)	C3-C4	1.376(4)
N2-C5	1.393(4)	C5-C10	1.395(4)
N1-Rh1-M1	175.52	M2-Rh1-N1	91.36
Cl1-Rh1-M2	176.61	M1-Rh1-Cl1	93.49
M1-Rh1-M2	87.53	N1-Rh1-Cl1	87.86(8)
Cl3-C40-Cl2	113.0(3)	C16-Rh1-Cl1	92.78(12)
C12-Rh1-N1	91.60(14)	N1-Rh1-C11	90.97(12)
C12-Rh1-C11	157.44(13)	C11-Rh1-Cl1	164.12(13)
C15-Rh1-Cl1	93.81(12)	N1-C1-C2	121.4(3)
C1-N1-Rh1	126.0(2)	C10-N1-Rh1	127.9(2)
C1-N1-C10	105.7(3)	C1-N2-C5	106.9(3)
N3-C2-C3	123.4(3)	N3-C2-C1	117.8(3)
N1-C1-N2	112.6(3)	N2-C1-C2	125.9(3)
N1-C10-C5	109.4(3)	N2-C5-C10	105.4(3)

In Table 5.2, M1 and M2 represent the midpoints of the olefinic bonds C15-C16 and C11-C12, respectively. N1 atom in the benzimidazole ring directly connects to the Rh metal center in the complex which is an abnormal situation for an NHC-complex. Although both of the C-N bonds in the NHC rings are single bonds, the bond distances of N2-C1 and N1-C1 are different from each other as seen from Table 5.2. The most possible situation that arises here is the presence of π -electron donation from the N1 atom of the imidazole unit into the Rh1, C1 and C10 atoms. But the N2 atom in the imidazole unit that connects with the pentamethylbenzyl ring by C20

atom donates its π -electrons only into the carbon atoms. As a result, the bond distances of N1-C1 and N1-C10 (1.320(4) Å and 1.390(4) Å, respectively) are shorter when compared with the bond distances of N2-C1 and N2-C5 (1.357(4) Å and 1.393(4) Å, respectively). In addition, the bond distance of Rh1-N1 is shorter (2.102(3) Å) due to the π -back bonding when compared with the related studies (Bénech, Piguet, Bernardinelli, Bünzli & Hopfgartner, 2001).

The coordination geometry around Rh1 atom formed by the coordination to the metal of the two olefinic bonds of the cyclooctadiene (COD) ligand, is a slightly distorted square-planar resulting from the difference in the bond angles of trans-trans conformation.

The pyridine framework connects to the Rh(I) metal atoms through the N1-C1 atoms bridge. The pyridine and the benzimidazole rings are approximately coplanar as expected. The Rh-N(NHC) and Rh-Cl bond distances of 2.102(3) Å and 2.3816(12) Å respectively, are within the expected range and in agreement with the related complexes reported previously (Bénech, Piguet, Bernardinelli, Bünzli & Hopfgartner, 2001 and Takenaka & Osakada, 2000).

The geometry of the intra- and inter-molecular interactions of the title compound is tabulated in Table 5.3.

Table 5.3 The intra- and inter-molecular interactions within the title compound (Å, °).

D – H ... A	H ... A	D ... A	\angle D – H ... A
C3 – H3 ... C11	2.82	3.643(4)	148
C40 – H40B ... Cg1	2.39	3.356(6)	173
C34 – H34A ... Cg1 ⁱⁱ	2.79	3.459(7)	127
C14 – H14A ... Cg2 ⁱⁱⁱ	2.90	3.733(6)	144
C18 – H18B ... Cl3 ^{iv}	2.80	3.586(6)	138
C40 – H40A ... Cl1 ^v	2.53	3.496(5)	177

In Table 5.3, the letters D and A represent the donor and acceptor atoms and H is the symbol of hydrogen atom. In the table, Cg1 and Cg2 are the centroids of the C5-C10 and C21-C26 rings, respectively. Symmetry codes are given as follows: (ii) $1/2-x, -1/2+y, 1/2-z$, (iii) $x, 1-y, 1/2+z$, (iv) $-x, 1-y, 1-z$, (v) $x, -1+y, z$.

The intra-molecular interaction of type C3–H3···C11 generates a six-membered S(6) hydrogen ring motif in the compound that is illustrated in Fig. (5.3) (Bernstein, Davis, Shimoni & Chang, 1995).

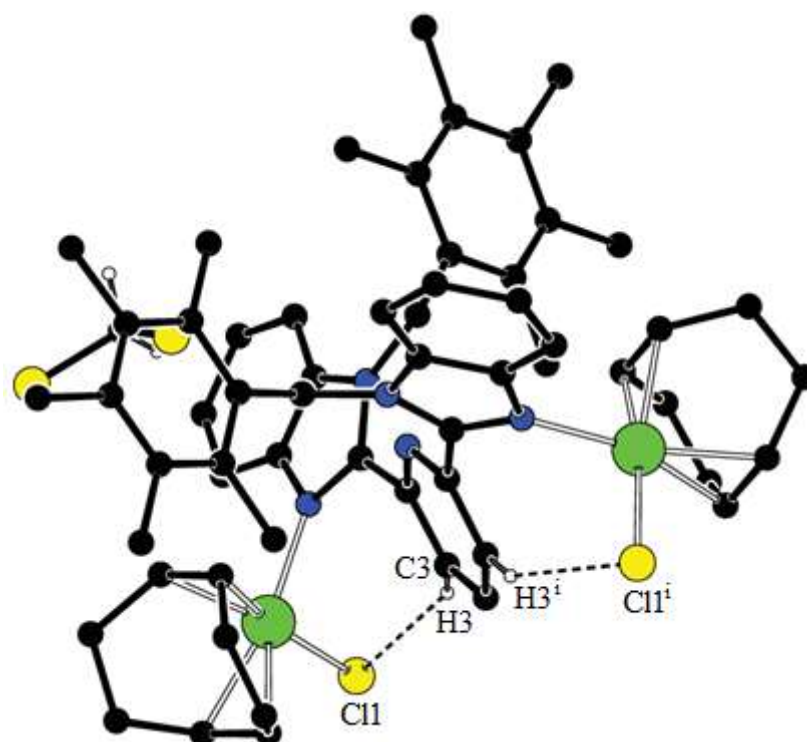


Figure 5.3 Intra-molecular interactions within the structure. The intra-molecular interaction of C3–H3···C11 generates a six-membered ring, producing S(6) hydrogen ring motif.

The pentamethylbenzyl ring connected to the NHC unit by N2–C20 atoms bridge to the benzimidazole framework with the dihedral angle of $89.09(12)^\circ$. The bond distance between the C11–C12 olefinic bond of the COD ligand trans to NHC unit is longer ($1.379(6) \text{ \AA}$) when compared with the distance between the metal atom and the midpoint of the C15–C16 olefinic bond ($1.376(6) \text{ \AA}$) that is trans to the chloride

atom. This type of binding of COD unit reveals the larger trans influence of the NHC ligand when compared with chloride (Gülcemal, Gökçe & Çetinkaya, 2013).

The dihedral angle between the least-squares planes of the five- and six-membered ring components of the benzimidazole framework is 0.55(19) with maximum deviation from the least-squares plane of -0.013(3) Å for N1 atom. The 5,6-dimethyl arms of the pentamethylbenzyl ring are slightly deviated from planarity. The interplanar angle occurs between the pyridine ring and the benzimidazole side arms is 48.75(13)°. The COD ring exhibits a boat conformation with the Rh-C(COD) bond distances ranging from 2.091(4) to 2.121(4) Å.

There exist three inter-molecular interactions of type C-H... π and C-H...Cl in the crystal structure of the title compound. The first interaction occurs between a carbon atom of the solvent molecule and a six-membered ring component of the benzimidazole ring system (Fig. 5.4).

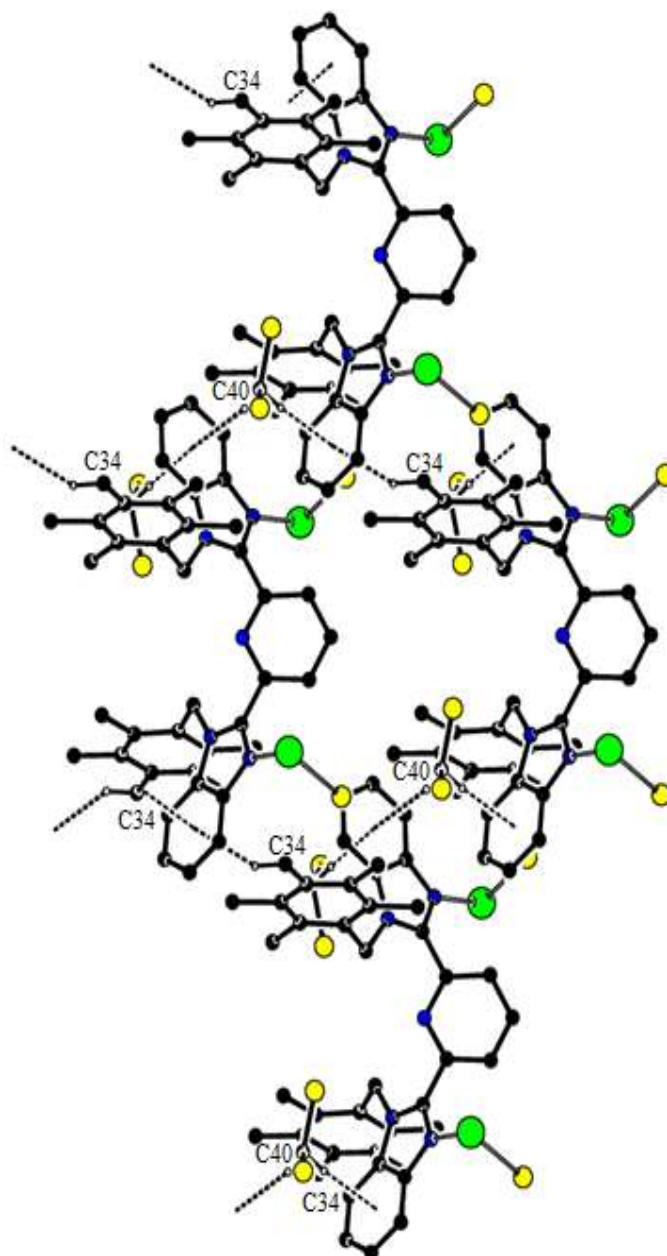


Figure 5.4 Inter-molecular interaction of type C40–H40B...Cg1 and C34–H34A...Cg1ⁱⁱ.

The second one occurs by means of C34 atom in the molecule at position (x, y, z) acting as a C–H... π hydrogen bond donor to C5–C10 ring component of the benzimidazole framework (Fig. 5.4). The last interaction is observed between C14 atom of the COD ring at (x, y, z) and the pentamethylbenzyl ring (C21–C26) in the molecule at $(x, 1 - y, \frac{1}{2} + z)$ as shown in Fig. (5.5).

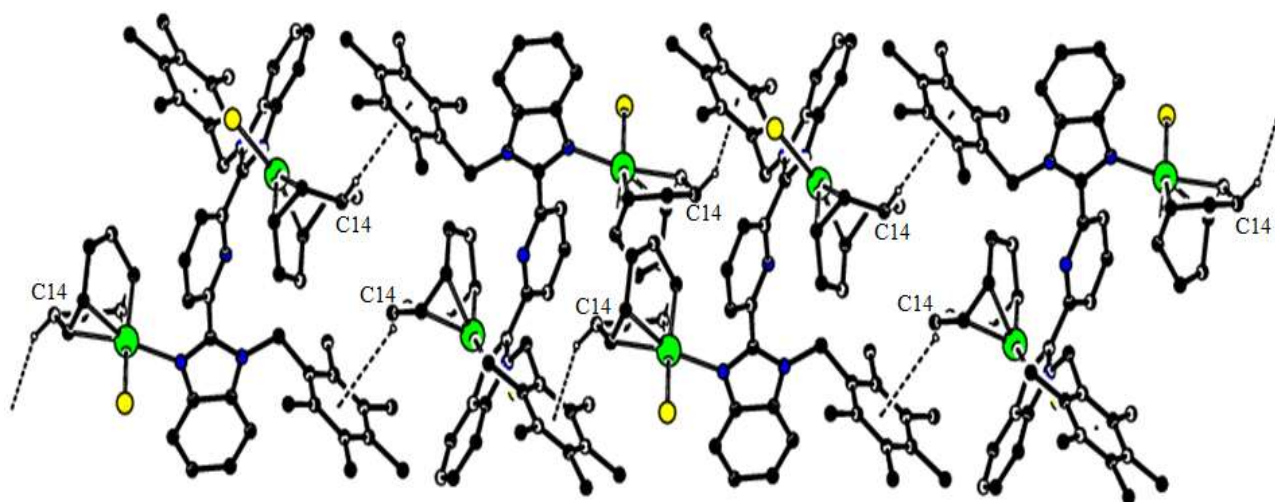


Figure 5.5 Inter-molecular interaction of type C14 – H14A ... Cg2ⁱⁱⁱ.

In addition, the title compound possesses inter-molecular interactions of type C–H...Cl. C18 and C40 atoms at (x, y, z) position act as C–H...Cl bond donors to the Cl3 atom in the molecule at $(-x, 1 - y, 1 - z)$ and the Cl1 atom in the molecule at $(x, -1 + y, z)$ respectively, leading to a centrosymmetric $R_4^4(16)$ dimer (Bernstein, Davis, Shimoni & Chang, 1995) as shown in Fig. (5.6).

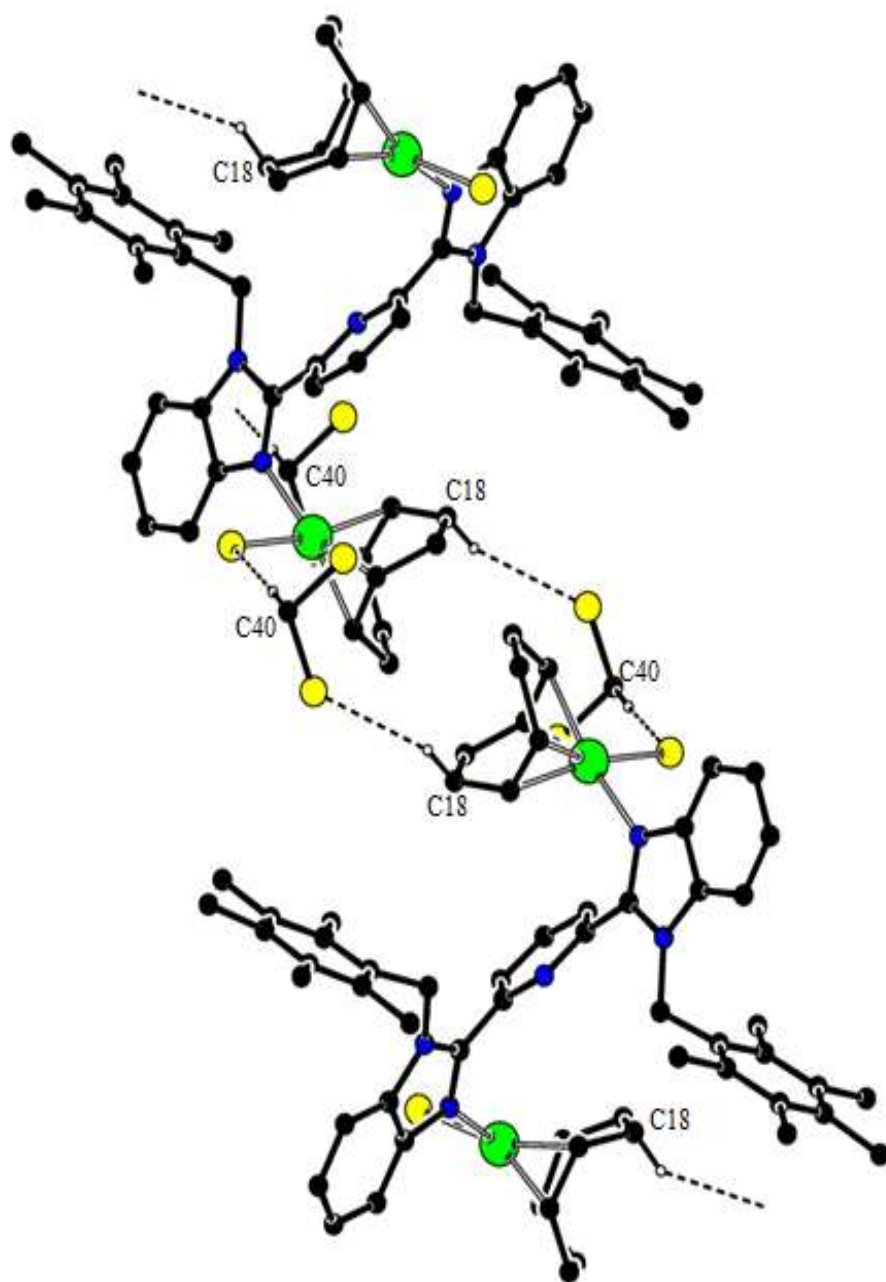


Figure 5.6 Inter-molecular interaction of type C18 – H18B ... C13^{iv} and C40 – H40A ... C11^v.

REFERENCES

- Allen, F. H., Kennard, O., Watson, D. G., Brammer, L., Orpen, A. G. & Taylor, R. (1987). Tables of bond lengths determined by X-ray and neutron diffraction. Part 1. Bond lengths in organic compounds. *Journal of the Chemical Society, Perkin Transactions, 2*, 1-19.
- Ansari, K. F. & Lal, C. (2009). Synthesis and biological activity of some heterocyclic compounds containing benzimidazole and beta-lactam moiety. *Journal of Chemical Sciences, 121* (6), 1017-1025.
- Ateş-Alagöz, Z., Kuş, C. & Çoban, T. (2005). Synthesis and antioxidant properties of novel benzimidazoles containing substituted indole or 1,1,4,4-tetramethyl-1,2,3,4-tetrahydro-naphthalene fragments. *Journal of Enzyme Inhibition and Medicinal Chemistry, 20* (4), 325-331.
- Barber, B. & Best, C. (n. d.). *Atomic scale structure of materials*. Retrieved June 22, 2013, from <http://www.doitpoms.ac.uk/tlplib/atomic-scale-structure/printall.php>
- Bariwal, J. B., Shah, A. K., Kathiravan, M. K., Somani, R. S., Jagtap, J. R. & Jain, K. S. (2008). Synthesis and antiulcer activity of novel pyrimidylthiomethyl-and pyrimidylsulfinylmenthyl benzimidazoles as potential reversible proton pump inhibitors. *Indian Journal of Pharmaceutical Education and Research, 42* (3), 235-243.
- Barkla, C. G. (1905). Polarised Röntgen radiation. *Philosophical Transactions of the Royal Society of London, Series A, 204*, 467-479.
- Barut, D. (2010). *Bazı oksalamid ve karbazol türevlerinin moleküler ve kristal yapı analizi*. Dokuz Eylül University-Graduate School of Natural and Applied Sciences, Izmir: Thesis for the degree of Master of Science.

- Bénech, J. –M., Piguet, C., Bernardinelli, G., Bünzli, J. –C. G. & Hopfgartner, G. (2001). Square-planar rhodium(I) complexes with aromatic bent terdentate nitrogen ligands as candidates for rod-like extended materials. *Journal of the Chemical Society, Dalton Transactions*, 5, 684-689.
- Bennett, D. W. (2010). Systematic Error. In *Understanding single-crystal X-ray crystallography* (378-465). Federal Republic of Germany: Wiley-VCH.
- Bernstein, J., Davis, R. E., Shimoni, L. & Chang, N. L. (1995). Patterns in hydrogen bonding: functionality and graph set analysis in crystals. *Angewandte Chemie International Edition in English*, 34 (15), 1555-1573.
- Blake, A. J., Clegg, W., Cole, J. M., Evans, J. S. O., Main, P., Parsons, S. & Watkin, D. J. (2009). Crystal growth and evaluation. W. Clegg (Ed.). In *Crystal structure analysis: principles and practice* (2nd ed.) (27-40). New York: Oxford University Press.
- Bragg, W. H. & Bragg, W. L. (1913). The reflection of X-rays by crystals. *Proceedings of the Royal Society of London, Series A*, 89 (605), 428-438.
- Bragg, W. H. (1915). Bakerian Lecture - X-rays and crystal structure. *Philosophical Transactions of the Royal Society of London, Series A*, 215, 253-274.
- Cascarano, G., Giacovazzo, C. & Viterbo, D. (1987). Figures of merit in direct methods: a new point of view. *Acta Crystallographica A*, 43, 22-29.
- Cochran, W. & Douglas, A. S. (1957). The use of a high-speed digital computer for the direct determination of crystal structures. II. *Proceedings of the Royal Society of London, Series A*, 243 (1233), 281-288.
- Cockcroft, J. K. (n. d.). *Instrument X-ray optics: I. Reflection geometry*. Retrieved July 14, 2013, from <http://pd.chem.ucl.ac.uk/pdnn/inst1/optics1.htm>

- Connolly, J. R. (2012). *Introduction quantitative X-ray diffraction methods*. Retrieved July 2, 2013, from <http://epswww.unm.edu/xrd/xrdclass/09-quant-intro.pdf>
- Cruickshank, D.W.J., Pilling, D.E., Bujosa, A., Lovell, F.M. & Truter, M.R. (1961). *Computing methods and the phase problem in X-ray crystal analysis*. Oxford: Pergamon.
- Deshmukh, M. B., Suryavanshi, A. W., Jagtap, S. S. & Deshmukh, S. A. (2009). Microwave assisted synthesis of 2,3,4-trisubstituted 1,2 dihydropyrimido- [1,2-a] benzimidazole. *Journal of The Indian Chemical Society*, 86, 302-305.
- Devivar, R. V., Kawashima, E., Revankar, G. R., Breitenbach, J. M., Kreske, E. D., Drach J. C. & Townsend L. B. (1994). Benzimidazole ribonucleosides: design, synthesis, and antiviral activity of certain 2-(alkylthio)- and 2-(benzylthio)-5,6-dichloro-1-(beta-D-ribofuranosyl)benzimidazoles. *Journal of Medicinal Chemistry*, 37 (18), 2942-9.
- Dolomanov, O. V., Blake, A. J., Champness, N. R. & Schröder, M. (2003). OLEX: new software for visualization and analysis of extended crystal structures. *Journal of Applied Crystallography*, 36, 1283-1284.
- Ewald, P. P. (1913). Zur theorie der interferenzen der röntgenstrahlen in kristallen. *Physikalische Zeitschrift*, 14 (11), 465-472.
- Ewald, P. P. (Ed.). (1962). *Fifty years of crystallography*. Utrecht: N. V. A. Oosthoek's Uitgevers Maatschappij.
- Farrugia, L.J. (1997). Ortep-3 for Windows. *Journal of Applied Crystallography*, 30, 565.
- Farrugia, L.J. (1999). WinGX. *Journal of Applied Crystallography*, 32, 837-838.

- Gellis, A., Kovacic, H., Boufatah, N. & Vanelle, P. (2008). Synthesis and cytotoxicity evaluation of some benzimidazole-4,7-diones as bioreductive anticancer agents. *European Journal of Medicinal Chemistry*, 43 (9), 1858-64.
- Germain, G., Main, P. & Woolfson, M. M. (1970). On the application of phase relationships to complex structures II. Getting a good start. *Acta Crystallographica B*, 26 (3), 274-285.
- Giacovazzo, C., Monaco, H. L., Artioli, G., Viterbo, D., Milanesio, M., Ferraris, G., Gilli, G., Gilli, P., Zanotti, G. & Catti, M. (2002). Crystallographic computing. C. Giacovazzo, (Ed.). In *Fundamentals of crystallography* (3rd ed.) (83-87). Oxford: Oxford University Press.
- Gökçe, A. G. (2008). *Bazı Paladyum(II) N-heterosiklik karben komplekslerinin kristalografik ve kuantum mekaniksel yöntemlerle incelenmesi*. Dokuz Eylül University-Graduate School of Natural and Applied Sciences, Izmir: Thesis for the degree of Doctor of Philosophy.
- Gülcemal, S., Gökçe, A. G. & Çetinkaya, B. (2013). Iridium(I) N-heterocyclic carbene complexes of benzimidazol-2-ylidene: effect of electron donating groups on the catalytic transfer hydrogenation reaction. *Dalton Transactions*, 42, 7305-7311.
- Harker, D. & Kasper, J. S. (1948). Phases of Fourier coefficient directly from crystal diffraction data. *Acta Crystallographica*, 1, 70-75.
- Hauptman, H. (1986). The direct methods of X-ray crystallography. *Science*, 233, 178-183.
- Hughes, E. W. (1941). The crystal structure of melamine. *Journal of the American Chemical Society*, 63 (6), 1737-1752.

- Immirzi, A. (2009). Constraints and restraints in crystal structure analysis. *Journal of Applied Crystallography*, 42, 362-364.
- Karabıyık, H. (2008). *Bazı rodyum(I) N-heterosiklik karben komplekslerinin kristalografik ve kuantum mekaniksel yöntemlerle incelenmesi*. Dokuz Eylül University-Graduate School of Natural and Applied Sciences, Izmir: Thesis for the degree of Doctor of Philosophy.
- Karle, J. & Hauptman, H. A. (1950). The phases and magnitudes of the structure factors. *Acta Crystallographica*, 3, 258-261.
- Karle, J. & Hauptman, H. A. (1956). A theory of phase determination for the four types of non-centrosymmetric space groups $1P222$, $2P22$, $3P12$, $3P22$. *Acta Crystallographica*, 9 (8), 635-651.
- Karle, J. & Karle, I. L. (1966). The symbolic addition procedure for phase determination for centrosymmetric and noncentrosymmetric crystals. *Acta Crystallographica*, 21, 849-859.
- Kittel, C. (2005). *Introduction to solid state physics* (8th ed.). USA: John Wiley & Sons Publication.
- Kuş, C., Ayhan-Kılıcıgil, G., Can-Eke, B. & İşcan, M. (2004). Synthesis and antioxidant properties of some novel benzimidazole derivatives on lipid peroxidation in the rat liver. *Archives of Pharmacal Research*, 27, 156-163.
- Ladd, M. F. C. & Palmer, R. A. (2003). *Structure determination by X-ray crystallography* (4th ed.). New York: Kluwer Academic/Plenum Publishers.

- Leonard, J. T., Rajesh, O. S., Jeyaseeli, L., Muruges, K., Sivakumar, R., & Gunasekaran, V. (2007). Synthesis, antiinflammatory and antibacterial activities of substituted phenyl benzimidazoles. *Asian Journal of Chemistry*, 19 (1), 116-120.
- Lipson, H., Langford, J. I. & Hu, H.-C. (2004). Trigonometric intensity factors. Prince, E. (Ed.). In *International tables for crystallography (vol. C): mathematical, physical and chemical tables* (3rd ed.) (596-599). Dordrecht: Kluwer Academic Publishers.
- Lonsdale, K. (1947). Extinction in X-ray crystallography. *Mineralogical Magazine*, 28 (196), 14-25.
- Luger, P. (1980). *Modern X-ray analysis on single crystals*. Berlin: Walter de Gruyter.
- Massa, W. (2004). *Crystal structure determination* (2nd ed.). Heidelberg: Springer-Verlag.
- Müller, P., Herbst-Irmer, R., Spek, A. L., Schneider, T. R. & Sawaya, M. R. (2006). Twinning. P. Müller, (Ed.). *Crystal structure refinement: A crystallographer's guide to SHELXL* (106-150). New York: Oxford University Press.
- Omar, M. A. (1975). *Elementary solid state physics: principles and applications*. Massachusetts: Addison-Wesley Publishing.
- Ott, H. (1927). Zur methodik der strukturanalyses, *Zeitschrift für Kristallographie*, 66, 136-153.
- Öfele, K. (1968). 1,3 Dimethyl-4-imidazolinylyliden-(2)-pentacarbonylchrom ein neuer übergangsmetall-carben-komplex. *Journal of Organometallic Chemistry*, 12 (3), 42-43.

- Patterson, A. L. (1934). A Fourier series method for the determination of the components of interatomic distances in crystals. *Physical Review*, 46, 372-376.
- Pickworth-Glusker, J., & Trueblood, K. N. (2010). *Crystal structure analysis: a primer* (3rd ed.). New York: Oxford University Press.
- Ripoll, M. M., & Cano, F. H. (n. d.). *Crystallography*. Retrieved June 27, 2013, from <http://www.xtal.iqfr.csic.es/Cristalografia/welcome-en.html>
- Rivas, M., Flores, W., Rivera, J., Sergiyenko, O., Hernández-Balbuena, D. & Sánchez-Bueno, A. (2013). A method and electronic device to detect the optoelectronic scanning signal energy centre. S. L. Pyshkin & J. M. Ballato, (Ed.). In *Optoelectronics - Advanced Materials and Devices* (401-404). Croatia: InTech.
- Sayre, D. (1952). The squaring method: a new method for phase determination. *Acta Crystallographica*, 5 (1), 60-65.
- Sayre, D. (2002). X-ray crystallography: The past and present of the phase problem. *Structural Chemistry*, 13 (1), 81-96.
- Sevinçek, R. (2006). *Bazı azlakton türevlerinin biçimlenimsel ve kristalografik incelemeleri*. Dokuz Eylül University-Graduate School of Natural and Applied Sciences, Izmir: Thesis for the degree of Master of Science.
- Sheldrick, G.M. (1998). SHELXL-97 University of Göttingen, Germany.
- Sheldrick, G.M. (1998). SHELXS-97 Universty of Göttingen, Germany.
- Sheldrick, G. M. (2008). A history of SHELX. *Acta Crystallographica A*, 64 (1), 112-122.

- Shmueli, U. (2007). *Theories and techniques of crystal structure determination*. New York: Oxford University Press.
- Spek, A.L. (1990). Platon/Pluton. *Acta Crystallographica A*46, C34.
- Takenaka, Y. & Osakada, K. (2000). Preparation and structure of [RhCl(nbd)(dmap)] (nbd = bicyclo[2.2.1]hepta-2,5-diene; dmap = 4-(*N,N*-dimethylamino)pyridine. *Bulletin of the Chemical Society of Japan*, 73 (1), 129.
- Tilley, R. J. D. (2006). The temperature factor. In *Crystals and crystal structures* (130-132). Great Britain: John Wiley & Sons Publications.
- Wanzlick, H. -W., & Schönherr, H. -J. (1968). Direct synthesis of a mercury salt-carbene complex. *Angewandte Chemie International Edition in English*, 7 (2), 141-142.
- Weaver, M. L. (n. d.). *Class 18-Structure factor*. Retrieved July 1, 2013, from http://bama.ua.edu/~mweaver/courses/MTE583/MTE%20583_Class_18.pdf
- Wilson, A. J. C. (1942). Imperfections in the structure of cobalt II. mathematical treatment of proposed structure. *Proceedings of The Royal Society A*, 180 (982), 277-285.
- Wilson, A. J. C. (1949). The probability distribution of X-ray intensities. *Acta Crystallographica*, 2, 318-320.

APPENDICES

1. The Fractional Coordinates & Equivalent Isotropic Temperature Parameters

The full set of the fractional coordinates (x, y, z) and equivalent isotropic temperature parameters (U_{eq}) of the atoms is given in the following table.

Atom label	x	y	z	$U_{eq}(\text{\AA}^2)$
Rh(1)	0.091860(10)	0.75085(3)	0.428410(10)	0.03521(9)
Cl(1)	0.15494(4)	0.90385(11)	0.41640(6)	0.0596(4)
N(1)	0.11709(10)	0.6151(3)	0.37624(12)	0.0310(9)
N(2)	0.11386(10)	0.4813(3)	0.29953(12)	0.0316(9)
N(3)	0	0.5886(4)	1/4	0.0279(12)
C(1)	0.09100(12)	0.5834(3)	0.31885(14)	0.0290(10)
C(2)	0.04350(12)	0.6579(3)	0.28141(14)	0.0292(10)
C(3)	0.04558(14)	0.7954(3)	0.28173(17)	0.0394(11)
C(4)	0	0.8643(5)	1/4	0.0453(17)
C(5)	0.15851(12)	0.4434(3)	0.34866(15)	0.0312(10)
C(6)	0.19730(14)	0.3470(4)	0.35669(17)	0.0430(12)
C(7)	0.23645(14)	0.3392(4)	0.41306(18)	0.0492(14)
C(8)	0.23845(14)	0.4255(4)	0.46034(17)	0.0462(12)
C(9)	0.20089(14)	0.5217(4)	0.45301(16)	0.0405(11)
C(10)	0.16031(12)	0.5294(3)	0.39592(15)	0.0313(10)
C(11)	0.02295(15)	0.6384(4)	0.41585(19)	0.0475(12)
C(12)	0.06295(18)	0.5978(4)	0.46825(19)	0.0554(16)
C(13)	0.0663(3)	0.6317(6)	0.5319(2)	0.090(2)
C(14)	0.0641(3)	0.7753(5)	0.5427(2)	0.088(3)
C(15)	0.08021(19)	0.8607(4)	0.5001(2)	0.0589(17)
C(16)	0.04468(17)	0.9039(4)	0.4452(2)	0.0561(16)
C(17)	-0.01297(18)	0.8668(5)	0.4194(3)	0.079(2)
C(18)	-0.02354(18)	0.7226(5)	0.4136(3)	0.077(2)
C(20)	0.09215(14)	0.4205(4)	0.23853(16)	0.0468(14)

Atom label	x	y	z	$U_{eq}(\text{\AA}^2)$
C(21)	0.13367(13)	0.3637(4)	0.21594(15)	0.0405(11)
C(22)	0.13839(16)	0.2248(4)	0.21152(18)	0.0480(14)
C(23)	0.17408(17)	0.1755(4)	0.18528(19)	0.0551(17)
C(24)	0.20421(17)	0.2622(5)	0.1647(2)	0.0593(16)
C(25)	0.20122(16)	0.3980(5)	0.17120(19)	0.0566(14)
C(26)	0.16500(15)	0.4490(4)	0.19625(17)	0.0462(14)
C(32)	0.1058(2)	0.1315(5)	0.2344(2)	0.077(2)
C(33)	0.1776(2)	0.0251(5)	0.1767(3)	0.093(3)
C(34)	0.2409(3)	0.2061(6)	0.1334(3)	0.104(3)
C(35)	0.2340(2)	0.4924(6)	0.1481(3)	0.089(3)
C(36)	0.1611(2)	0.5977(5)	0.2021(2)	0.0717(17)
C(40)	0.1143(2)	0.2252(5)	0.4353(3)	0.092(3)
Cl(2)	0.05193(8)	0.26085(16)	0.38099(10)	0.1137(8)
Cl(3)	0.11548(7)	0.23742(16)	0.50812(9)	0.1020(7)

2. Anisotropic Displacement Parameters

The anisotropic displacement parameters of the title compound are given in the table below in \AA^2 units.

Atom label	U_{11}	U_{22}	U_{33}	U_{23}	U_{13}	U_{12}
Rh(1)	0.03314(16)	0.03460(16)	0.03940(16)	-0.01030(12)	0.01469(11)	-0.00388(13)
Cl(1)	0.0494(6)	0.0514(6)	0.0898(8)	-0.0321(6)	0.0391(6)	-0.0238(5)
N(1)	0.0290(15)	0.0314(15)	0.0341(15)	-0.0053(12)	0.0129(12)	-0.0006(12)
N(2)	0.0238(14)	0.0389(16)	0.0320(15)	-0.0076(12)	0.0099(11)	0.0006(13)
N(3)	0.025(2)	0.030(2)	0.032(2)	0.00000	0.0141(16)	0.00000
C(1)	0.0243(16)	0.0295(17)	0.0352(18)	-0.0028(13)	0.0131(14)	-0.0012(14)
C(2)	0.0264(18)	0.0318(17)	0.0321(17)	0.0002(13)	0.0136(14)	-0.0014(15)
C(3)	0.036(2)	0.0346(18)	0.045(2)	-0.0050(15)	0.0112(17)	-0.0085(17)
C(4)	0.051(3)	0.024(3)	0.056(3)	0.00000	0.013(3)	0.00000

Atom label	U ₁₁	U ₂₂	U ₃₃	U ₂₃	U ₁₃	U ₁₂
C(5)	0.0238(17)	0.0357(19)	0.0349(18)	-0.0026(14)	0.0113(14)	0.0003(15)
C(6)	0.036(2)	0.045(2)	0.048(2)	-0.0066(17)	0.0149(17)	0.0070(18)
C(7)	0.031(2)	0.052(2)	0.058(3)	0.0020(19)	0.0077(18)	0.0111(19)
C(8)	0.036(2)	0.052(2)	0.042(2)	0.0042(18)	0.0032(17)	0.0034(19)
C(9)	0.037(2)	0.044(2)	0.0358(19)	-0.0028(16)	0.0072(16)	-0.0021(18)
C(10)	0.0273(17)	0.0310(18)	0.0362(18)	0.0003(14)	0.0119(14)	-0.0036(15)
C(11)	0.047(2)	0.047(2)	0.057(2)	-0.0208(19)	0.029(2)	-0.021(2)
C(12)	0.075(3)	0.047(2)	0.054(3)	0.003(2)	0.035(2)	-0.003(2)
C(13)	0.132(5)	0.095(4)	0.053(3)	0.003(3)	0.044(3)	-0.015(4)
C(14)	0.126(5)	0.096(5)	0.050(3)	-0.018(3)	0.042(3)	-0.002(4)
C(15)	0.068(3)	0.057(3)	0.060(3)	-0.031(2)	0.033(2)	-0.015(2)
C(16)	0.062(3)	0.038(2)	0.081(3)	-0.013(2)	0.041(3)	0.003(2)
C(17)	0.054(3)	0.078(4)	0.112(4)	0.007(3)	0.037(3)	0.016(3)
C(18)	0.046(3)	0.101(5)	0.088(4)	-0.026(3)	0.030(3)	-0.011(3)
C(20)	0.034(2)	0.065(3)	0.039(2)	-0.0210(19)	0.0101(16)	0.0050(19)
C(21)	0.0284(19)	0.057(2)	0.0324(18)	-0.0130(17)	0.0062(15)	0.0102(18)
C(22)	0.042(2)	0.060(3)	0.041(2)	-0.0129(18)	0.0135(17)	-0.001(2)
C(23)	0.055(3)	0.056(3)	0.054(3)	-0.014(2)	0.019(2)	0.013(2)
C(24)	0.049(2)	0.076(3)	0.062(3)	-0.002(2)	0.031(2)	0.016(2)
C(25)	0.045(2)	0.076(3)	0.052(2)	0.002(2)	0.021(2)	0.007(2)
C(26)	0.042(2)	0.058(3)	0.038(2)	-0.0028(18)	0.0134(17)	0.011(2)
C(32)	0.082(4)	0.071(4)	0.087(4)	-0.012(3)	0.040(3)	-0.015(3)
C(33)	0.113(5)	0.070(4)	0.106(5)	-0.020(3)	0.053(4)	0.016(3)
C(34)	0.105(5)	0.119(5)	0.122(5)	-0.015(4)	0.084(4)	0.030(4)
C(35)	0.078(4)	0.106(5)	0.102(4)	0.014(4)	0.056(3)	-0.002(3)
C(36)	0.080(3)	0.062(3)	0.073(3)	0.010(2)	0.027(3)	0.008(3)
C(40)	0.087(4)	0.048(3)	0.168(7)	0.016(3)	0.080(4)	0.001(3)
Cl(2)	0.1149(14)	0.0963(12)	0.1330(16)	0.0170(10)	0.0477(12)	0.0057(10)
Cl(3)	0.0887(11)	0.1019(12)	0.1336(14)	0.0144(10)	0.0620(10)	0.0120(9)

3. Bond Distances

The bond distances of the title complex are given in the following table in Å units.

Atom label	Bond length	Atom label	Bond length
Rh(1) – Cl(1)	2.3816(12)	C(9) – C(10)	1.400(5)
Rh(1) – N(1)	2.102(3)	C(11) > C(12)	1.379(6)
Rh(1) – C(11)	2.102(4)	C(11) – C(18)	1.496(7)
Rh(1) – C(12)	2.091(4)	C(12) – C(13)	1.504(7)
Rh(1) – C(15)	2.128(5)	C(13) – C(14)	1.474(8)
Rh(1) – C(16)	2.121(4)	C(14) – C(15)	1.495(7)
N(1) – C(1)	1.320(4)	C(15) > C(16)	1.376(6)
N(1) – C(10)	1.390(4)	C(16) – C(17)	1.499(7)
N(2) – C(1)	1.356(4)	C(17) – C(18)	1.478(7)
N(2) – C(5)	1.393(4)	C(20) – C(21)	1.508(5)
N(2) – C(20)	1.475(5)	C(21) – C(22)	1.413(6)
N(3) – C(2)	1.338(4)	C(21) – C(26)	1.392(6)
N(3) – C(2)a	1.338(4)	C(22) – C(23)	1.402(6)
C(1) > C(2)	1.475(5)	C(22) – C(32)	1.508(7)
C(2) – C(3)	1.387(4)	C(23) – C(24)	1.389(7)
C(3) – C(4)	1.376(5)	C(23) – C(33)	1.537(6)
C(5) – C(6)	1.389(5)	C(24) – C(25)	1.383(7)
C(5) – C(10)	1.395(5)	C(24) – C(34)	1.531(9)
C(6) – C(7)	1.372(5)	C(25) – C(26)	1.401(6)
C(7) – C(8)	1.396(6)	C(25) – C(35)	1.521(8)
C(8) – C(9)	1.366(6)	C(26) – C(36)	1.512(6)

4. Bond Angles

The complete set of the bond angles (°) of the title complex is given with the table below.

Atom label	Angle	Atom label	Angle
Cl(1)-Rh(1)-N(1)	87.86(9)	C(3)-C(4)-C(3)a	119.4(4)
Cl(1)-Rh(1)-C(15)	93.82(13)	N(2)-C(5)-C(6)	133.7(3)
N(1)-Rh(1)-C(12)	91.59(14)	C(5)-C(6)-C(7)	117.1(3)
C(11)-Rh(1)-C(12)	38.41(17)	C(8)-C(9)-C(10)	116.8(3)
C(12)-Rh(1)-C(15)	81.28(17)	C(5)-C(10)-C(9)	121.6(3)
Rh(1)-N(1)-C(1)	126.0(2)	C(12)-C(11)-C(18)	125.3(4)
C(1)-N(2)-C(5)	106.9(3)	C(11)-C(12)-C(13)	124.9(5)
C(2)-N(3)-C(2)a	117.1(3)	Rh(1)-C(15)-C(14)	112.8(3)
N(2)-C(1)-C(2)	125.9(3)	Rh(1)-C(16)-C(15)	71.4(3)
C(1)-C(2)-C(3)	118.7(3)	C(16)-C(17)-C(18)	114.9(4)
Cl(1)-Rh(1)-C(11)	164.12(12)	C(20)-C(21)-C(22)	119.9(4)
Cl(1)-Rh(1)-C(16)	92.79(13)	C(21)-C(22)-C(23)	118.5(4)
N(1)-Rh(1)-C(15)	165.31(14)	C(22)-C(23)-C(24)	120.2(4)
C(11)-Rh(1)-C(15)	91.31(18)	C(23)-C(24)-C(25)	121.4(4)
C(12)-Rh(1)-C(16)	96.45(17)	C(24)-C(25)-C(26)	119.1(4)
Rh(1)-N(1)-C(10)	128.0(2)	C(21)-C(26)-C(25)	120.3(4)
C(1)-N(2)-C(20)	124.7(3)	N(2)-C(5)-C(10)	105.4(3)
N(1)-C(1)-N(2)	112.6(3)	C(6)-C(7)-C(8)	122.2(4)
N(3)-C(2)-C(1)	117.9(3)	N(1)-C(10)-C(5)	109.4(3)
C(2)-C(3)-C(4)	118.4(3)	Rh(1)-C(11)-C(12)	70.4(3)
Cl(1)-Rh(1)-C(12)	157.44(13)	Rh(1)-C(12)-C(11)	71.2(2)
N(1)-Rh(1)-C(11)	90.98(14)	C(12)-C(13)-C(14)	113.7(4)
N(1)-Rh(1)-C(16)	156.78(14)	Rh(1)-C(15)-C(16)	70.8(3)
C(11)-Rh(1)-C(16)	82.12(17)	Rh(1)-C(16)-C(17)	110.2(3)
C(15)-Rh(1)-C(16)	37.79(17)	C(11)-C(18)-C(17)	115.1(4)
C(1)-N(1)-C(10)	105.6(3)	C(20)-C(21)-C(26)	119.5(4)
C(5)-N(2)-C(20)	128.3(3)	C(21)-C(22)-C(32)	120.9(4)
N(1)-C(1)-C(2)	121.4(3)	C(22)-C(23)-C(33)	119.4(4)
N(3)-C(2)-C(3)	123.4(3)	C(23)-C(24)-C(34)	119.2(5)
C(24)-C(25)-C(35)	121.1(4)	C(15)-C(16)-C(17)	125.2(4)

Atom label	Angle	Atom label	Angle
C(21)-C(26)-C(36)	120.8(4)	N(2)-C(20)-C(21)	114.3(3)
C(6)-C(5)-C(10)	120.9(3)	C(22)-C(21)-C(26)	120.5(4)
C(7)-C(8)-C(9)	121.5(4)	C(23)-C(22)-C(32)	120.6(4)
N(1)-C(10)-C(9)	129.1(3)	C(24)-C(23)-C(33)	120.3(4)
Rh(1)-C(11)-C(18)	112.5(3)	C(25)-C(24)-C(34)	119.4(4)
Rh(1)-C(12)-C(13)	112.1(3)	C(26)-C(25)-C(35)	119.8(4)
C(13)-C(14)-C(15)	114.3(5)	C(25)-C(26)-C(36)	118.9(4)
C(14)-C(15)-C(16)	122.7(5)		

5. Torsion Angles

The following table provides information about the whole set of the torsion angles (°) of the title complex.

Atom label	Angle	Atom label	Angle
Cl(1)-Rh(1)-N(1)-C(1)	-104.5(3)	C(8)-C(9)-C(10)-C(5)	-0.4(5)
C(11)-Rh(1)-N(1)-C(10)	-111.8(3)	C(9)-C(10)-N(1)-Rh(1)	-7.8(5)
Cl(1)-Rh(1)-N(1)-C(10)	84.0(3)	C(12)-C(11)-Rh(1)-C(15)	-74.2(3)
C(12)-Rh(1)-N(1)-C(1)	98.1(3)	C(18)-C(11)-Rh(1)-C(12)	121.1(5)
C(11)-Rh(1)-N(1)-C(1)	59.7(3)	Rh(1)-C(11)-C(12)-C(13)	104.3(5)
C(12)-Rh(1)-N(1)-C(10)	-73.4(3)	Rh(1)-C(11)-C(18)-C(17)	1.0(6)
C(16)-Rh(1)-N(1)-C(1)	-12.4(5)	C(11)-C(12)-Rh(1)-N(1)	-89.6(2)
N(2)-C(1)-N(1)-C(10)	0.7(4)	C(13)-C(12)-Rh(1)-Cl(1)	61.2(6)
N(1)-C(1)-N(2)-C(5)	0.2(4)	C(13)-C(12)-Rh(1)-C(15)	-17.7(4)
C(2)-C(1)-N(2)-C(20)	-5.2(5)	C(11)-C(12)-C(13)-C(14)	-54.7(8)
N(2)-C(1)-C(2)-N(3)	51.8(4)	C(13)-C(14)-C(15)-C(16)	88.8(7)
C(3)-C(2)-N(3)-C(2)a	-1.3(4)	C(14)-C(15)-Rh(1)-C(12)	5.7(4)
C(2)-C(3)-C(4)-C(3)a	-1.2(4)	C(16)-C(15)-Rh(1)-C(11)	-75.3(3)
C(10)-C(5)-N(2)-C(1)	-0.9(4)	C(14)-C(15)-C(16)-Rh(1)	-105.4(4)

Atom label	Angle	Atom label	Angle
C(10)-C(5)-C(6)-C(7)	1.1(5)	C(15)-C(16)-Rh(1)-N(1)	176.3(3)
C(6)-C(5)-C(10)-N(1)	-179.7(3)	C(17)-C(16)-Rh(1)-Cl(1)	145.8(3)
C(6)-C(7)-C(8)-C(9)	0.8(6)	C(17)-C(16)-Rh(1)-C(12)	-54.9(4)
C(15)-C(16)-C(17)-C(18)	-55.5(7)	C(13)-C(12)-Rh(1)-C(16)	-52.4(4)
C(21)-C(20)-N(2)-C(5)	-33.6(5)	C(12)-C(13)-C(14)-C(15)	-22.8(9)
C(20)-C(21)-C(22)-C(23)	174.4(3)	C(14)-C(15)-Rh(1)-Cl(1)	-152.1(4)
C(26)-C(21)-C(22)-C(32)	178.2(4)	C(14)-C(15)-Rh(1)-C(16)	118.3(5)
C(22)-C(21)-C(26)-C(25)	0.7(6)	C(16)-C(15)-Rh(1)-C(12)	-112.5(3)
C(21)-C(22)-C(23)-C(33)	-176.6(4)	C(14)-C(15)-C(16)-C(17)	-3.4(7)
C(22)-C(23)-C(24)-C(25)	2.1(7)	C(15)-C(16)-Rh(1)-C(11)	102.5(3)
C(33)-C(23)-C(24)-C(34)	0.0(7)	C(17)-C(16)-Rh(1)-N(1)	54.7(6)
C(34)-C(24)-C(25)-C(26)	175.8(4)	C(17)-C(16)-Rh(1)-C(15)	-121.6(5)
C(24)-C(25)-C(26)-C(36)	-178.8(4)	C(16)-C(17)-C(18)-C(11)	-17.8(8)
C(16)-Rh(1)-N(1)-C(10)	176.1(4)	N(2)-C(20)-C(21)-C(22)	109.4(4)
C(2)-C(1)-N(1)-Rh(1)	9.7(5)	C(20)-C(21)-C(22)-C(32)	-5.6(5)
N(1)-C(1)-N(2)-C(20)	177.0(3)	C(20)-C(21)-C(26)-C(25)	-175.6(3)
N(1)-C(1)-C(2)-N(3)	-130.6(3)	C(22)-C(21)-C(26)-C(36)	-178.6(4)
N(2)-C(1)-C(2)-C(3)	-129.9(4)	C(32)-C(22)-C(23)-C(24)	-179.6(4)
N(3)-C(2)-C(3)-C(4)	2.6(5)	C(22)-C(23)-C(24)-C(34)	-177.0(5)
C(6)-C(5)-N(2)-C(1)	-179.6(4)	C(23)-C(24)-C(25)-C(26)	-3.3(7)
C(10)-C(5)-N(2)-C(20)	-177.6(3)	C(34)-C(24)-C(25)-C(35)	-0.4(7)
N(2)-C(5)-C(10)-N(1)	1.4(4)	C(35)-C(25)-C(26)-C(21)	178.2(4)
C(6)-C(5)-C(10)-C(9)	-0.3(5)	N(2)-C(1)-N(1)-Rh(1)	-172.4(2)
C(7)-C(8)-C(9)-C(10)	0.1(6)	C(2)-C(1)-N(1)-C(10)	-177.2(3)
C(5)-C(10)-N(1)-Rh(1)	171.6(2)	C(2)-C(1)-N(2)-C(5)	177.9(3)
C(9)-C(10)-N(1)-C(1)	179.3(4)	N(1)-C(1)-C(2)-C(3)	47.7(5)
C(12)-C(11)-Rh(1)-C(16)	-110.9(3)	C(1)-C(2)-N(3)-C(2)a	176.9(3)
C(18)-C(11)-Rh(1)-C(15)	47.0(4)	C(1)-C(2)-C(3)-C(4)	-175.6(3)
C(18)-C(11)-C(12)-Rh(1)	-104.2(4)	C(6)-C(5)-N(2)-C(20)	3.7(6)
C(12)-C(11)-C(18)-C(17)	82.3(7)	N(2)-C(5)-C(6)-C(7)	179.7(4)

Atom label	Angle	Atom label	Angle
C(11)-C(12)-Rh(1)-C(15)	103.3(3)	N(2)-C(5)-C(10)-C(9)	-179.2(3)
C(13)-C(12)-Rh(1)-N(1)	149.4(4)	C(5)-C(6)-C(7)-C(8)	-1.4(6)
C(8)-C(9)-C(10)-N(1)	179.0(4)	C(15)-C(16)-Rh(1)-Cl(1)	-92.6(3)
C(5)-C(10)-N(1)-C(1)	-1.3(4)	C(15)-C(16)-Rh(1)-C(12)	66.8(3)
C(12)-C(11)-Rh(1)-N(1)	91.3(3)	C(17)-C(16)-Rh(1)-C(11)	-19.1(3)
C(18)-C(11)-Rh(1)-N(1)	-147.6(4)	Rh(1)-C(16)-C(17)-C(18)	25.5(6)
C(18)-C(11)-Rh(1)-C(16)	10.2(4)	C(21)-C(20)-N(2)-C(1)	150.3(3)
C(18)-C(11)-C(12)-C(13)	0.0(8)	N(2)-C(20)-C(21)-C(26)	-74.3(4)
C(11)-C(12)-Rh(1)-Cl(1)	-177.8(2)	C(26)-C(21)-C(22)-C(23)	-1.9(6)
C(11)-C(12)-Rh(1)-C(16)	68.6(3)	C(20)-C(21)-C(26)-C(36)	5.1(5)
C(13)-C(12)-Rh(1)-C(11)	-121.0(5)	C(21)-C(22)-C(23)-C(24)	0.5(6)
Rh(1)-C(12)-C(13)-C(14)	27.3(7)	C(32)-C(22)-C(23)-C(33)	3.4(6)
C(13)-C(14)-C(15)-Rh(1)	7.7(7)	C(33)-C(23)-C(24)-C(25)	179.2(5)
C(14)-C(15)-Rh(1)-C(11)	42.9(4)	C(23)-C(24)-C(25)-C(35)	-179.5(5)
C(16)-C(15)-Rh(1)-Cl(1)	89.6(3)	C(24)-C(25)-C(26)-C(21)	1.9(6)
Rh(1)-C(15)-C(16)-C(17)	102.0(4)	C(35)-C(25)-C(26)-C(36)	-2.5(6)